COMPUTATIONAL ANALYSIS OF MIXING IN MICROCHANNELS

By

Param Adhikari

Submitted in Partial Fulfillment of the Requirements

for the Degree of

Master of Science

in the

Mechanical Engineering

Program

YOUNGSTOWN STATE UNIVERSITY

May, 2013

COMPUTATIONAL ANALYSIS OF MIXING IN MICROCHANNELS

Param Adhikari

I hereby release this thesis to the public. I understand that this thesis will be made available from the Ohio LINK ETD Center and the Maag Library Circulation Desk for public access. I also authorize the University or other individuals to make copies of this thesis as needed for scholarly research.

Signature:

Param Adhikari, Student Date

Approvals:

Dr. Yogen M. Panta, Thesis Advisor Date

Dr. H.W. Kim, Committee Member Date

Dr. Ganesh V. Kudav, Committee Member Date

Bryan DePoy, Interim Dean of School of Graduate Studies and Research Date

ABSTRACT

Not only due to its versatility and inexpensive availability, lab-on-a-chip integrates multi-tasks for a complete μTAS. Due to easy portability in micro-devices, microfluidics has potential to revolutionize in many applications that include food, pharmaceutical, biomedical and chemical industries, etc. Mixing is inevitable for the analysis of trace chemicals, drugs, bio-molecules, fluidic controls in microfluidics, etc. Such miniaturized microfluidics had already proven better over bulky instrumentations, because of time and transportation required in handling.

In this work, both active and passive were computationally studied. Passive mixing is considered with the mass fraction at different velocities of various mixer models when the fluids are in contact with each other. A two dimensional comparative analysis was performed to see the degree of mixing on two standard geometries including T and Y for general purposes. Along with standard geometries including T & Y, combinatory models with more than two inlet ports were also investigated using ANSYS Fluent, finite volume software. The engulfment flow was the major reason responsible for the mixing process. The engulfment flow was one of the major reasons responsible for the mixing process. Diffusion is a dominant phenomenon in passive mixing at the junction where various inlets meet and convective process becomes prevalent. Identification of geometrical correlation with the flow field variables and mixing parameters are crucial for better mixing design. The active mixing would be mathematically modeled with additional body force in the momentum equation. Thus, active mixers are externally activated for

better mixing possibilities than the time consuming and possible complex geometries in passive mixing.

Concentration variances over time at the outlet were simultaneously compared in all models for mixing. Also average concentration was tracked over time so as to confirm uniformity in mixing. Active circular mixers were observed to work effectively with four electrode pairs at frequency of 8 Hz and potential of 0.1 volt. Parametric analysis on various geometries, mixing obstacles and electrode positions in the mixing zone showed that circular mixer with converging inlet and diverging outlet promises for better mixing efficiency and effectiveness.

ACKNOWLEDGEMENTS

I would like to express my sincere appreciation to my advisor, Dr. Yogen M. Panta, for the incessant support in my studies and research as a graduate student. His guidance, patience, ideas, and opinions helped me immensely throughout this thesis work. In addition, my special thanks go to Dr. Ganesh V. Kudav and Dr. H.W. Kim for having accepted the task of serving on my thesis committee, helping me in proofreading and providing important suggestions. I would also like to acknowledge Dr. Elvin Shields for his continuous support for my graduate studies. My classmates and dear friends Sanket Aryal, Sai Ram Atmuri and Upendra Dawadi are appreciated for their unforgettable friendly support and help.

Last of all I want to convey my appreciation to the YSU-Department of Mechanical and Industrial Engineering for providing resources to accomplish this research. This thesis work was supported by YSU URC Grant & RP Award for partial funding and providing research release hours.

I would also like to give my endless thanks to my family for their encouragement and support. Without their love and support, none of this work would have ever been possible.

TABLE OF CONTENTS

PAGE

PAGE

LIST OF FIGURES

PAGE

PAGE

LIST OF TABLES

PAGE

CHAPTER 1
INTRODUCTION

1.1 History of Micro Total Analysis Systems

The portability in small space, massive parallelization, controlled and well defined laminar flow pattern attracts using microfluidics for various applications. It has potential to revolutionize food, pharmaceutical, biomedical and chemical industries. There is a dramatically increasing literature on microfluidics by several published materials. Numerous patents referring to microfluidics have been issued. It is evident that microfluidics is well established. Academia and industry are currently collaborating to develop new techniques and products. Commercial applications of microfluidic technology has been implemented on various useful technologies including inkjet technology (Le, 1998). Other include high pressure liquid chromatography (Manz, et al., 1990) and several microfluidic structures such as microvalves (Shoji, et al., 1988) and micropumps (Lintel, et al., 1988), (Gass, et al., 1994) using silicon micromachining. This has provided a basis for automation in microfluidics leading to micro total analysis systems, also named as lab on a chip. Pregnancy test strips, drug abuse test strips and cardiac markers are the commercially used analysis systems that utilize capillary based liquid transport. Fabrications of microfluidic chip are not yet commercially successful. Electrokinetics is one of the flexible and versatile microfluidic platforms where the microfluidic flow control is gained by electric fields (Mark, et al., 2010). Microfluid domain offers high surface to volume ratio for laminar fluid flow. In lab on a chip, diffusion is the primary mixing process in this micro regime as the Reynolds number is quite low.

1.2 Micromixing

Mixing is inevitable for the analysis of chemical components, drug manipulation and fluidic controls in many fluid systems. With miniaturization, everything micro-technology is being more popular. Small disposable devices are proved better than bulky analysis systems because of time, transportation, portability and small volume economics. Micro total analysis systems (μTAS) incorporates the concept of lab on a chip. However, the challenges involved are multifarious. Fluid flow manipulation, chemical detection, electrical and magnetic interaction in a micro environment is complicated. Bio-MEMS is one of the applications of μTAS, where micro-mixing is the one of the fundamental steps required for micro biochemical analysis, protein folding, polymer chain reaction, DNA hybridization, and so on. Microfluidic devices have had a considerable impact in biomedical fields, clinical diagnostics, drug development, and are extensively applied in the food and chemical industries (Mark, et al., 2010). One such device used for laboratory testing is shown in **Figure 1.1**.

Figure 1.1 Various microchannels as shown in a testing device (www.thinxxs.com, 2012)

The fluid flow in microfluidic devices is basically very laminar where the mixing is primarily by diffusion. In micro dimensions, there is low Reynolds number(Re) and high Peclet number(Pe) which signify the long mixing length and extended retention time to ensure satisfactory mixing results. Interfacial contact area can be increased by folding the mixing species multiple times along the flow line. Then with the increased contact area, samples can be mixed within 55-300 milliseconds and thus, high throughput can be achieved. Alternatively, the mixing time can be increased for better mixing performance. However, mixing efficiency was not improved (Mark, et al., 2010). Although mixing time can be increased, it is not practical for applications in lab on a chip and μTAS. As this passive mixing does not prove practical enough for the analysis of large scale molecules, active mixing has evolved. Apart from micro mechanical means to improve the active mixing process by using moving parts, an efficient design is currently researched upon by using electric fields and magnetic fields to optimize the mixing process. A low voltage operated electro-osmotic mixer, consequently, holds a promising solution for this purpose.

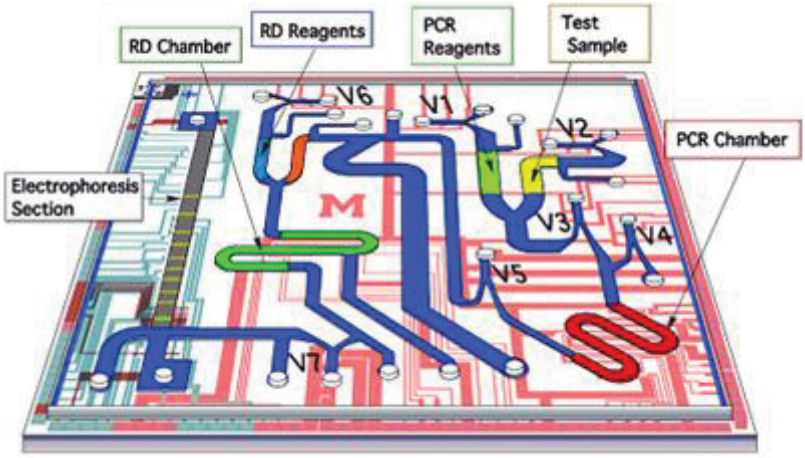

Figure 1.2 Lab on a chip showing various laboratory processes (www.azonano.com, 2013)

The dream of microfluidics researchers has been to build a single lab-on-a-chip for over decades (Knight, 2002). The active field of academic research offers great — perhaps even revolutionary — new capabilities for the future (Whitesides, 2006). The technological breakthroughs in academic laboratories around the world are happening and being bridged commercially for practical use (Blow, 2009) (Mark, et al., 2010). The microfluidic mixing enhancement, therefore, is the key in setting the milestone for the development of lab-on-a-chip. One such microfluidic lab on a chip showing various laboratory processes is shown in **Figure 1.2**. The electrochemical detection of analytes using electric and/or magneto hydrodynamic effects were investigated (Panta, et al., 2009). It would be interesting to develop such detection techniques in a miniaturized chip. Microfluidic mixing is an inevitable process to realize this technology. Several passive mixer include various micro-channel designs such as the T-design (Gobby, et al., 2001), L-design (Bau & Yi, 2000), serpentine pipe design (Liu, et al., 2000) (Kim, et al., 2005), (Beebe, et al., 2001), flow splitting design (deMello, et al., 1999), ridged-floor mixer design (Stroock, et al., 2002), staggered herringbone mixer design (SHM)

(Stroock, et al., 2002), (Camesasca, et al., 2006), (Stroock, et al., 2002), zigzag/wave-like configuration mixer design (Mengeaud, et al., 2002), (Chen & Cho, 2007), etc. The split-up of the liquid streams into lamellae and subsequent recombination, so-called multilamination, has also been reported (Hessel, et al., 2003), (Hardt & Schönfeld, 2003). Majority of the microfluidic devices utilize secondary transverse flows to induce chaotic stirring (Meisel & Ehrhard, 2006). Secondary transverse flows do no significantly improve mixing, and need to be fabricated delicately too (Chen, et al., 2003). These micro mixers enhance the analyte species mixing process by using specific channel geometries to increase the interfacial contact area between the mixing species (Chen & Cho, 2008).

1.3 Processes and types

Active mixing

An active micro mixer comprising of a main channel and multiple pairs of side channels generates chaotic mixing effects by pulsating electric inputs (Niu & Lee, 2003). Active micromixers are being developed to cope the unmet results from passive mixers (**Figure 1.3**). A mixing chamber mimicking a source/sink system (Evans, et al., 1997) is designed to stir fluids effectively using micro fabricated valves and phase-change liquid micro pumps. Pressure disturbances from side channels were also utilized in micro channel flows to enhance micromixing (Lee, et al., 2001), (Volpert, et al., 1999). The mixing of two reagents by time-pulsing their respective flow rates in the two inlet channels was already reported (Glasgow & Aubry, 2003). Recently, effect of various dimensionless parameters for better mixing efficiency in pulse-flow was examined to optimize the mixing performance (Glasgow, et al., 2004). Electro-osmotically driven mixing process

for two aqueous solutions via the application of periodically varying electric fields at the two inlet channels was further developed. Published data indicates that mixing could be significantly enhanced at a selective appropriate Strouhal number. The efficient mixing of two species via electrokinetic instability effects induced by a time-periodic electric field was reported (Shin, et al., 2005) (Lin, et al., 2004) (Fu, et al., 2005). Pulsating electric fields further excite secondary flows around internal obstacles in a micro channel or flowing along meandering micro channels was also experimented (Meisel & Ehrhard, 2006). Experimental results confirmed that these secondary flows greatly enhanced the mixing efficiency within the micro channel. Coupling of magnetic and electric fields (Bau, et al., 2001) as well as micro-magnetic stir-bar by the application of external rotating bar (Lu, et al., 2002), (Ryu, et al., 2004) were also found in the publications. It has been noted that a microchannel specific geometry can be used to further enhance the mixing process (Brian, 2010). Many different shapes of microchannels were modeled and studied parametrically for electrode pairs, mixing channel width, frequency of the applied voltage and analyte concentration to investigate and optimize the mixing process in COMSOL 4.2a, a finite element multiphysics package (COMSOL, 2011). An improvement in mixing process was seen while placing several circular obstacles in the mixing zone of circular electro osmotic mixer, named as control model.

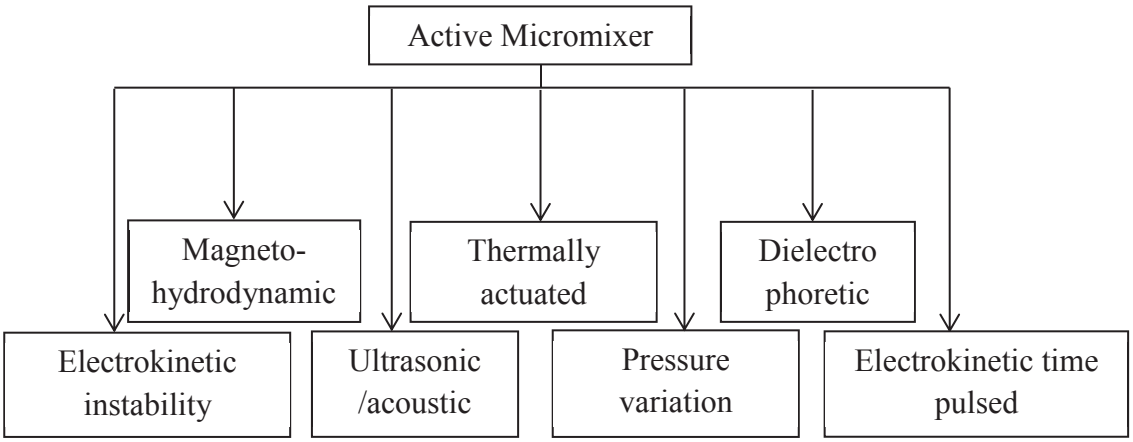

Figure 1.3 Categories of active mixer

Passive mixing

In contrast to active mixers, passive micromixers do not have a forced mixing from external sources (**Figure 1.4**). However, a mixing reagent could be added in the solution which could accelerate the diffusive or convective mixing process. Due to laminar flow regime, mixing process relies on chaotic advection effects that can be realized by molecular diffusion process with increased contact area and/or larger mixing time.

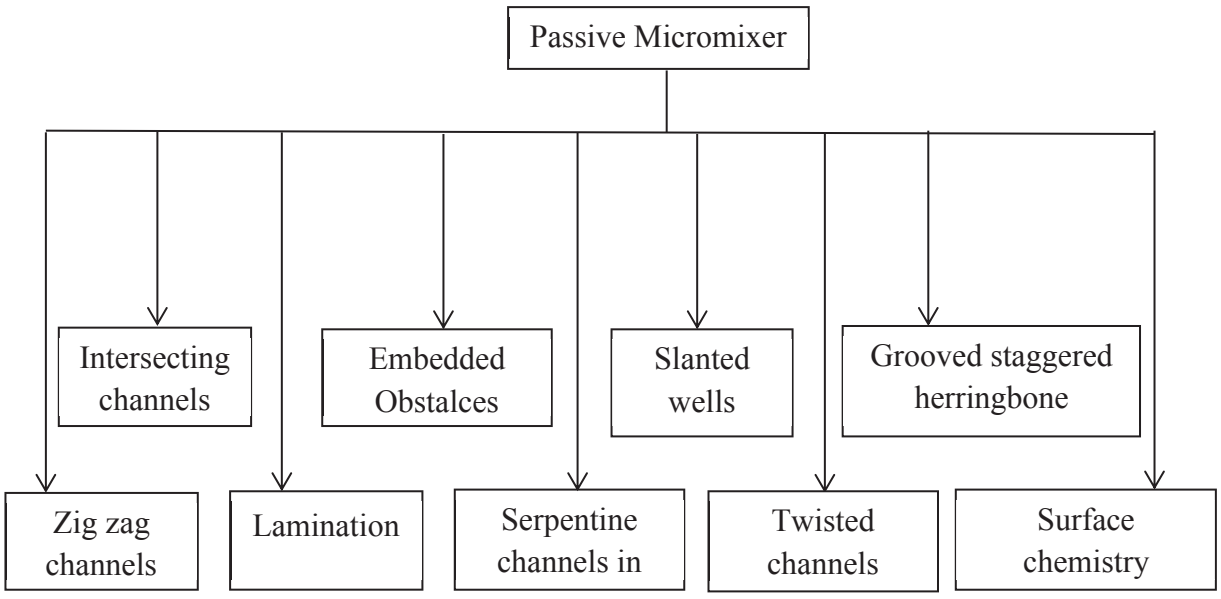

Figure 1.4 Categories of passive micromixers

At low Reynolds number of 2 to 100, flow segmentation appears through inertial effects or shear forces in the channel. The method to split, rearrange and combine fluid flows can be used to enhance the mixing effect. Passive mixing can be induced by microchannel designs. Some of which include lamination, intersecting channels, zigzag channels, 3-D serpentine structures, embedded barriers, slanted wells, twisted channels, grooved staggered herringbone channel designs. One of the other techniques for passive mixers includes surface chemistry technology. Passive mixing techniques utilize either diffusive or convective mixing.

1.4 Optimization of micromixing

Mechanism of passive mixing process is described by convection-diffusion equation for fluids. Despite the mixing difficulty due to low Reynolds number and high Peclet number, the micro domain in the microchannels enable the laminar flow controlling techniques. Fick's law provides the fundamental understanding for approximate solution when the species are merely at same temperature in a dilute solution. Furthermore, the chaotic mixing at higher velocities is best described by 'Poincare maps' and 'Lyapunov exponents' (Brian, 2010). The latter one characterizes the time rate of flow separation of very small fluid trajectories. The maximum Lyapunov exponent being positive implies chaotic system. The electro-osmotic mixer presented in this thesis has a positive maximum Lyapunov exponent (Chen, et al., 2003). Passive micro mixers were not found to be analyzed on the light of this exponent in the literature. Out of several mixing techniques available in the micro domain, electric mixing is widely used. Direct application of electric field at the inlet and outlet of micro channel induces plug like flow (Zhang, et al., 2004). However, care should be given as high voltage could impart

corrosion on electrodes and as a result, water bubbles may be formed leading to possible hindrance for qualitative as well as quantitative analysis of mixing results. Multiphysics phenomenon involving sample solutions containing analyte species depends on many parameters such as permittivity, dielectric constant, potential difference, ionic species, etc.

1.5 Electrokinetic mixing: (EDL)

When an electric field is applied at electrically conducting channel walls, there will be an interaction between the charged wall and the ions present in the solution. This was described as first approximate theory for the prediction of formation of double layer at the interface (**Figure 1.5**) (Gouy, 1910) (Chapman, 1913). Later on, Gouy-Chapman-Stern model was reported (Lyklema, 1995). The opposite charges get accumulated right next to the electrically conducting wall. The Columbic force forms a layer named as electric double layer (EDL). The net effect is the variation of electric potential near the surface of the electrode and also the formation of differential capacitance. The first layer is firmly attracted to the electrode while the second layer is loosely attracted. EDL has become crucial since microfluidics work in large surface to volume ratio as discussed earlier. The formation of this parallel double layer is also referred to as Debye layer and resultant thickness as Debye length (**Figure 1.6**). This thickness results in slipping plane at the surface that separates the surface of the significant double layer with the rest of the fluid flow. The electric potential at this plane is also referred as zeta potential or simply the electrokinetic potential (Knight, 2002). The schematic of electric double layer formed along the wall is shown below (**Figure 1.5 and 1.6**).

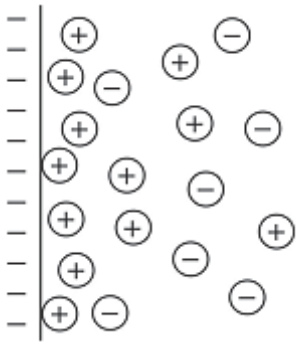

Figure 1.5 Electric Double Layer (Lyklema, 1995)

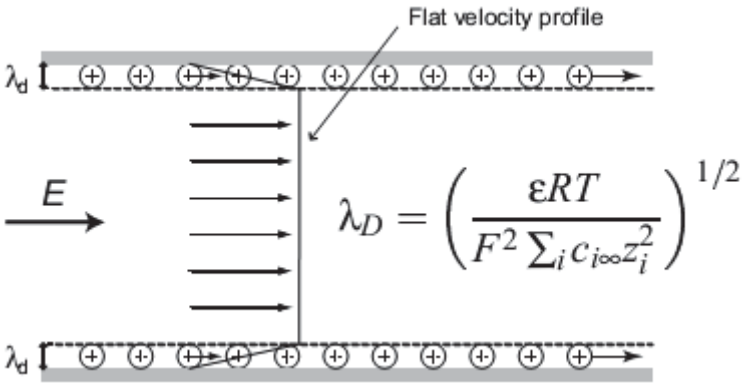

Figure 1.6 Flat velocity profile due to slip velocity showing Debye layer

1.6 Objective of thesis

The thesis work is focused on study and optimization of active and passive mixing processes using microchannels. Using commercially available simulation packages – ANSYS Fluent 13 and COMSOL Multiphysics 4.2a, microchannel models were parametrically studied for optimization of mixing process.

The specific objectives of this research are as follows:

a) Study the effects of a combination of several basic geometries for *passive mixing* in the light of mixing length and standard deviation of the mass fraction at outlet
b) Parametric study to optimize the mixing process for *active mixing*

1.7 Organization of thesis

The thesis materials are presented with introductory contents in **Chapter 1**. **Chapter 2** provides the description of microchannel geometry including mathematical modeling, numerical modeling, model validation, and analysis tools used to study as well as optimize the micro mixing process. **Chapter** presents passive micromixing and **Chapter 4** reports active micromixing. **Chapter 5** concludes the thesis work with suggestions to future work.

CHAPTER 2
ANALYSIS OF FLUID FLOW IN MICROFLUIDIC SYSTEMS

Fluid flow in microfluidic systems is laminar and most of the previous work was about active mixing made of rectangular microchannels. Microchannel models include shapes of T, Y, Y4, Y5 used for passive mixing. Similarly, varieties of electroosmotic micro-mixers were modeled to study the active mixing as well.

2.1 Geometric modeling

Here, T and Y micro-mixers were named two main control models to analyze the passive mixing. The dimensions of the geometries are as shown below (**Figure 2.1**). The channel width was fixed as 0.05mm for both models.

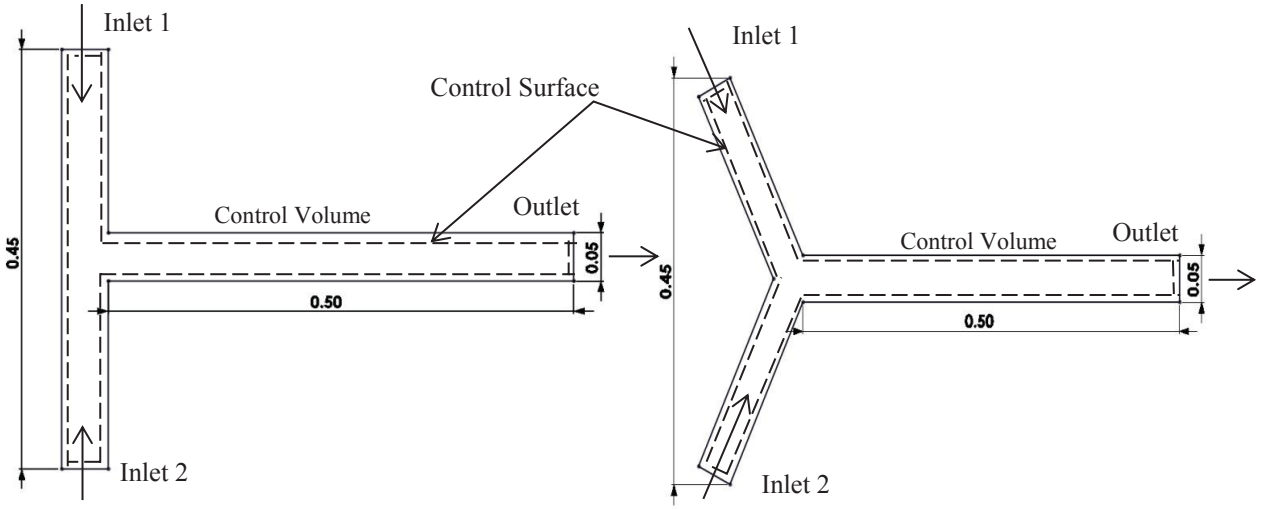

(a) T-micromixer 'control model -1' (b) Y-micromixer 'control model -2'

Figure 2.1 Micromixers used as main 'control models' (Dimensions in mm)

The major control models used to analyze the active electro osmotic mixing are given below.

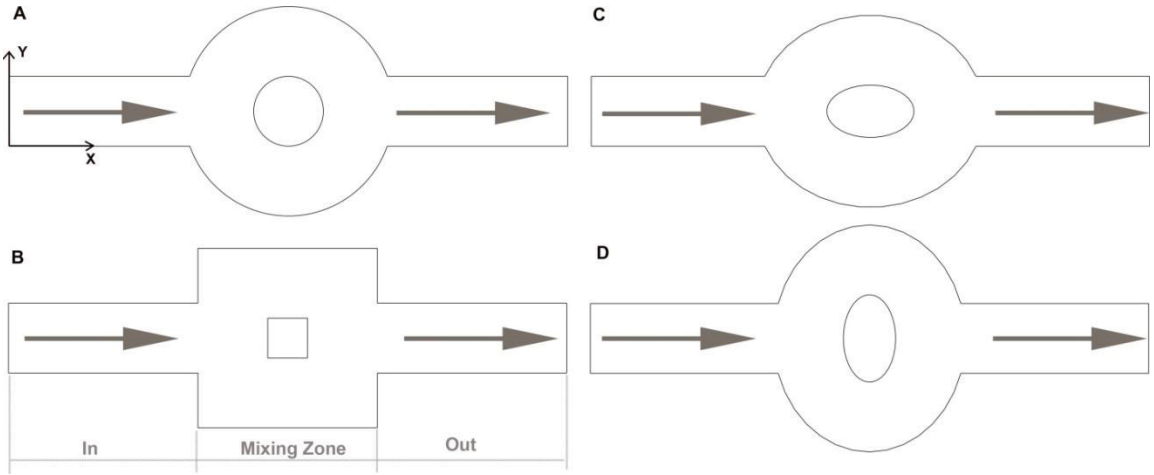

Figure 2.2 Designs of geometries for electroosmostic active mixers

The primary circular electro osmotic mixer (**Figure 2.2 A**) contains an area enclosed within the 5µm and 15µm radius connecting inlet to outlet. The distance between the inlet and outlet extremities is 80µm. Inlet, outlet and mixing channel width are maintained to be 10µm (Chen, et al., 2003), (COMSOL, 2011). All other shape modifications were obtained by taking the same mixing width and mixing area (**Figure. 2.2**).

2.2 Mathematical modeling

The mathematical modeling of passive micromixing in microchannels for T, Y and other models involve physics of fluid flow, and physics of mass transport including diffusion and connective transfer modes. However, in active electroosmotic mixing an electrokinetic force in the electric double layer exists. Since the fluid is incompressible,

steady state and Newtonian in nature, fluid flow follows the continuity and momentum conservation along with convection-diffusion equation for mass transport.

Physics of Fluid Flow

Continuity Equation

The rate of fluid mass leaving a control volume is equal to the rate of mass entering the control volume. Mass remains conserved in a control volume.

Mathematically,

$$\frac{\partial \rho}{\partial t} + \nabla \cdot \left(\rho \vec{V}\right) = 0 \qquad \text{……..(2.1)}$$

Where,

$\frac{\partial \rho}{\partial t} \equiv$ rate of change of density within the control volume

$\nabla \equiv$ vector operator in Cartesian coordinates $= \frac{\partial}{\partial x}\hat{i} + \frac{\partial}{\partial y}\hat{j} + \frac{\partial}{\partial z}\hat{k}$

$\nabla.(\rho\overrightarrow{V}) \equiv$ net flow across boundaries of the control volume

For incompressible and steady flow, the continuity equation reduces to:

$$\nabla \cdot \left(\rho \vec{V}\right) = 0 \qquad \text{…… …(2.2)}$$

Momentum Equation

Newton's second law can be applied to the fluid domain. It states that the net force acting on an element is equal to the time rate of change of its linear momentum. This law, being

applied for x-, y- and z– directions in three dimensions holds true for fluid. The equations can be formulated as;

$$\frac{\partial(\rho u)}{\partial t} + \nabla \cdot \rho \vec{V} u = dF_{Bx} + \frac{\partial \sigma_{xx}}{\partial x} + \frac{\partial \tau_{yx}}{\partial y} + \frac{\partial \tau_{zx}}{\partial z} + S_{Mx} \qquad \text{……(2.3)}$$

$$\frac{\partial(\rho v)}{\partial t} + \nabla \cdot \rho \vec{V} v = dF_{By} + \frac{\partial \tau_{xy}}{\partial x} + \frac{\partial \sigma_{yy}}{\partial y} + \frac{\partial \tau_{zy}}{\partial z} + S_{My} \qquad \text{……(2.4)}$$

$$\frac{\partial(\rho w)}{\partial t} + \nabla \cdot \rho \vec{V} w = dF_{Bz} + \frac{\partial \tau_{xz}}{\partial x} + \frac{\partial \tau_{yz}}{\partial y} + \frac{\partial \sigma_{zz}}{\partial z} + S_{Mz} \qquad \text{……(2.5)}$$

Where,

$\vec{V} \equiv$ total velocity vector of the fluid

$u, v, w \equiv$ x-, y-, and z-components of the velocity, respectively

$\sigma_{ii} \equiv$ normal viscous stress terms

$\tau_{ij} \equiv$ shear viscous stress terms

$dF_{Bi} \equiv$ differential body force component

$S_{Mi} \equiv$ momentum source term component

The rate of shearing strain is proportional to the viscous stress or vice-versa. For fluid domain in the control volume, the viscous stress can be expressed in terms of velocity gradients.

$$\tau_{xy} = \tau_{yx} = \mu\left(\frac{\partial v}{\partial x} + \frac{\partial u}{\partial y}\right) \qquad \text{……(2.6)}$$

$$\tau_{yz} = \tau_{zy} = \mu\left(\frac{\partial w}{\partial y} + \frac{\partial v}{\partial z}\right) \qquad \text{…..…(2.7)}$$

$$\sigma_{xx} = -p - \frac{2}{3}\mu\nabla\cdot\vec{V} + 2\mu\frac{\partial u}{\partial x} \qquad \text{……..(2.8)}$$

$$\sigma_{yy} = -p - \frac{2}{3}\mu\nabla\cdot\vec{V} + 2\mu\frac{\partial v}{\partial y} \qquad \text{…….(2.9)}$$

$$\sigma_{zz} = -p - \frac{2}{3}\mu\nabla\cdot\vec{V} + 2\mu\frac{\partial w}{\partial z} \qquad \text{….(2.10)}$$

Where, $p \equiv$ local pressure

$\mu \equiv$ dynamic or absolute viscosity of the fluid

It should also be noted that the kinematic viscosity, υ , can be substituted for μ, the ratio of the dynamic viscosity of the fluid by its density, ρ.

The kinematic viscosity equation is shown in the following equation.

$$\upsilon = \frac{\mu}{\rho} \qquad \text{……..(2.11)}$$

The equations of viscous stresses formulated above when substituted in equations of motion yields the Navier-Stokes equation for x, y, z –components.

$$\rho\frac{Du}{Dt} = \rho g_x - \frac{\partial p}{\partial x} + \frac{\partial}{\partial x}\left[\mu\left(2\frac{\partial u}{\partial x} - \frac{2}{3}\nabla\cdot\vec{V}\right)\right] + \frac{\partial}{\partial y}\left[\mu\left(\frac{\partial u}{\partial y} + \frac{\partial v}{\partial x}\right)\right] + \frac{\partial}{\partial z}\left[\mu\left(\frac{\partial w}{\partial x} + \frac{\partial u}{\partial z}\right)\right] \qquad \text{…(2.12)}$$

$$\rho\frac{Dv}{Dt} = \rho g_y - \frac{\partial p}{\partial y} + \frac{\partial}{\partial x}\left[\mu\left(\frac{\partial u}{\partial y} + \frac{\partial v}{\partial x}\right)\right] + \frac{\partial}{\partial y}\left[\mu\left(2\frac{\partial v}{\partial y} - \frac{2}{3}\nabla\cdot\vec{V}\right)\right] + \frac{\partial}{\partial z}\left[\mu\left(\frac{\partial v}{\partial z} + \frac{\partial w}{\partial y}\right)\right] \qquad \text{…(2.13)}$$

$$\rho\frac{Dw}{Dt} = \rho g_z - \frac{\partial p}{\partial z} + \frac{\partial}{\partial x}\left[\mu\left(\frac{\partial w}{\partial x} + \frac{\partial u}{\partial z}\right)\right] + \frac{\partial}{\partial y}\left[\mu\left(\frac{\partial v}{\partial z} + \frac{\partial w}{\partial y}\right)\right] + \frac{\partial}{\partial z}\left[\mu\left(2\frac{\partial w}{\partial z} - \frac{2}{3}\nabla\cdot\vec{V}\right)\right] \qquad \text{…(2.14)}$$

Under incompressible and constant velocity assumption, the above equations further reduce to the most general form as expressed below.

$$\rho\left(\frac{\partial u}{\partial t}+u\frac{\partial u}{\partial x}+v\frac{\partial u}{\partial y}+w\frac{\partial u}{\partial z}\right)=-\frac{\partial p}{\partial x}+\mu\left(\frac{\partial^2 u}{\partial x^2}+\frac{\partial^2 u}{\partial y^2}+\frac{\partial^2 u}{\partial z^2}\right)+\rho g_x \qquad \ldots(2.15)$$

$$\rho\left(\frac{\partial v}{\partial t}+u\frac{\partial v}{\partial x}+v\frac{\partial v}{\partial y}+w\frac{\partial v}{\partial z}\right)=-\frac{\partial p}{\partial y}+\mu\left(\frac{\partial^2 v}{\partial x^2}+\frac{\partial^2 v}{\partial y^2}+\frac{\partial^2 v}{\partial z^2}\right)+\rho g_y \qquad \ldots(2.16)$$

$$\rho\left(\frac{\partial w}{\partial t}+u\frac{\partial w}{\partial x}+v\frac{\partial w}{\partial y}+w\frac{\partial w}{\partial z}\right)=-\frac{\partial p}{\partial z}+\mu\left(\frac{\partial^2 w}{\partial x^2}+\frac{\partial^2 w}{\partial y^2}+\frac{\partial^2 w}{\partial z^2}\right)+\rho g_z \qquad \ldots(2.17)$$

The two dimensional analysis of fluid flow yields the following expressions neglecting gravity terms.

$$\rho\left(u\frac{\partial u}{\partial x}+v\frac{\partial u}{\partial y}\right)=-\frac{\partial p}{\partial x}+\mu\left(\frac{\partial^2 u}{\partial x^2}+\frac{\partial^2 u}{\partial y^2}\right) \qquad \ldots(2.18)$$

$$\rho\left(u\frac{\partial v}{\partial x}+v\frac{\partial v}{\partial y}\right)=-\frac{\partial p}{\partial y}+\mu\left(\frac{\partial^2 v}{\partial x^2}+\frac{\partial^2 v}{\partial y^2}\right) \qquad \ldots(2.19)$$

In vector form, it can be again reformed as:

$$\rho\,\mathbf{v}\bullet\nabla\mathbf{v} = -\nabla p + \mu\nabla^2\mathbf{v} + S \qquad \ldots\ldots\ldots\ldots\ldots\ldots\ldots\ldots\ldots\ldots\ldots\ldots\ldots\ldots\ldots\ldots(2.20)$$

Where S is body force which is neglected in passive mixing whereas electric forces take over inside the electric double layer in electroosmotic mixing.

In active electroosmotic mixing:

Inside the electric double layer (EDL), the fluid motion is governed by

$$\rho\left[\frac{\partial \mathbf{V}}{\partial t}+(\nabla.\mathbf{V})\mathbf{V}\right]=-\nabla p+\mu\nabla^2\mathbf{V}+\rho_e\mathbf{E} \qquad \text{……(2.21)}$$

Where ρ_e is the charge density, **E** is the electric field intensity and μ is the dynamic viscosity.

The slip velocity at the edge of the electric double layer is given by

$$U_{slip}=-\frac{\varepsilon\zeta\mathbf{E}_x}{\mu} \qquad \text{…(2.22)}$$

Where ε is permittivity of the medium, ζ is the potential(0.1V), $\mathbf{E}_x$ is the electric field intensity in the x-direction.

In the bulk of the fluid (outside the 'electric double layer'), the fluid motion is governed by the Navier Stokes equation,

$$\rho\left[\frac{\partial \mathbf{V}}{\partial t}+(\nabla.\mathbf{V})\mathbf{V}\right]=-\nabla p+\mu\nabla^2\mathbf{V} \qquad \text{……..(2.23)}$$

Physics of Mass Transport

Convection-Diffusion Equation

The species transport is described by the diffusion-convection equation which is:

$$\frac{dc}{dt}+(\nabla.\boldsymbol{V})c=D\nabla^2c \qquad \text{Where } c=\rho\omega \text{ ……..…(2.24)}$$

Where c, ω and D are concentration, mass fraction and diffusion coefficient of the species.

2.3 Numerical modeling

ANSYS Fluent

The computational power of a software is utilized in numerical modeling to solve for the given set of conditions in microchannel geometries. This utilizes the diligent processors to solve the iterative process of calculations. ANSYS Fluent was used in this analysis of several passive mixers. The geometries were solved in the fluid domain. The present version of ANSYS Package contains its own designing tool, ANSYS Design Modeler. However, models were drawn in Solidworks and then meshed. Mesh has a high influence in determining the accuracy of the solution. ANSYS Mesh is used nowadays to create meshes as required in the domain. Mesh needs to be refined to capture the phenomenon where there is rapid change in flow field variables. Finer mesh leads to more accuracy with a price of high computational power and time. The complete numerical modeling in computer completes basically in three steps- preprocessing, mesh generation and post processing. ANSYS Fluent has the capability to couple several multiple physics where it actually uses the results from a set of physics to another set of physics in the same or another domain. ANSYS Fluent utilized two different solvers namely pressure based and density based solvers. It is of our choice to select the solver which best mimics the real working of the model.

CFD Methodology: ANSYS Fluent

The procedures to get successful results in ANSYS Fluent for a given fluid flow problem is summarized below.

1. Geometric construction of fluid flow domain in any CAD software or the given ANSYS Design Modeler. All models used in this analysis of passive micromixers were designed in SolidWorks.
2. ANSYS Meshing was used to mesh the whole fluid domain into discrete volumes with appropriate mesh parameters and techniques for the given fluid flow. The regions of particular interest were meshed with smaller volumes to capture the ongoing phenomenon.
3. Selection of the type of solvers, materials and models for the given type of problem under study.
4. Setting of boundary conditions, fluid properties, convergence criteria and maximum number of iterations for post- processing and result visualization.

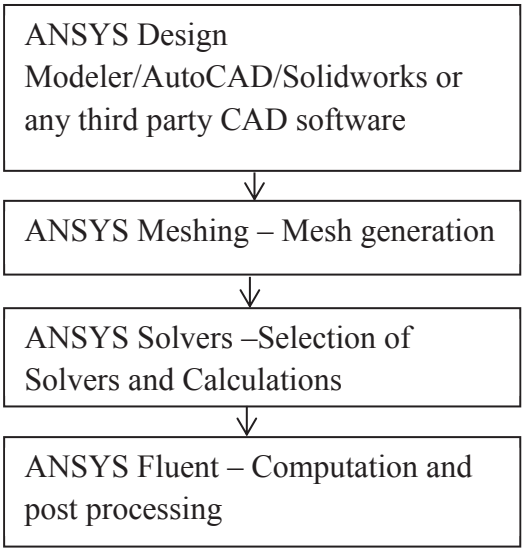

Figure 2.3 CFD Methodology

The procedures listed above can be categorized under preprocessing, solver and post-processing (**Figure 2.3**). preprocessing involves the basic steps of geometry creation and meshing of the given model. This could be accomplished by either any of the commercial CFD software or by the built in ANSYS Design Modeler. Then after, meshing is done using Gambit. It has been replaced by ANSYS Meshing for its user friendliness. The solver and post-processing part is done in ANSYS Fluent. However, newer stand-alone software has emerged in recent versions of ANSYS package called ANSYS Post-processing which is particularly useful for the analysis of results from the solver itself. It allows the user get visual impressions of various plots to better understand the physics of fluid flow in that domain in terms of various variables.

The computational modeling begins from the pre-processing as the first step. The geometry can be either created in the given ANSYS Design Modeler or by any other commercially available CAD facilities such as AutoCAD or Solidworks. All passive mixer models were created in Solidworks and transferred to ANSYS Mesh for meshing of these models. Each model was meshed using various elements. T-shaped microchannel was meshed with 1250 quadrilateral elements while Y shaped microchannel was meshed with 3300 triangular elements with finer meshes in the mixing channel for better results. The Y3 micro channel with three inlets was meshed with 3759 triangular elements with coarse mesh at inlets while finer mesh at the mixing channel and outlet. The YT and Y5 were meshed

with 4648 and 5087 triangular mesh elements with a finer mesh in the area of interest in the mixing channel.

The CFD package ANSYS Fluent 12.0 was used as solver for the scenarios of different inlet velocities. The same aqueous solution of water was chosen as inlet fluid from all the ports. A pressure based solver was used for the solution of two dimensional fluid transport phenomena with no slip boundary condition at walls and atmospheric gauge pressure as zero at outlet. A SIMPLEC algorithm was chosen for pressure velocity coupling and first order upwind for the computation of momentum terms and diffusion convection equations in the laminar mixing flow problem.

The post-processing of results includes the visualization of the converged results. A pressure, velocity and mass fractions of different species from various ports were observed at the outlet and the extent of mixing were determined.

COMSOL Multiphysics

COMSOL Multiphysics 4.2a is another numerical modeling software to simulate a flow field on a finite element basis. This has been utilized to analyze the various electro-osmotic mixers in Chapter 4. The complexities of fluid flow domain are merged with electric field being applied on the electrode to get a transient solution over time. It allows the user to model the ongoing phenomenon based on partial differential equations and features a user friendly intuitive work environment for modeling several scientific and engineering problems. The powerful interactive work environment is well facilitated for coupling multiple physics and solving it simultaneously. Geometry definition, meshing,

physics specifications, solutions and visualizations are packed in a single screen desktop. Modeling is highly simplified in terms of predefined physics interfaces for applications that diversify from fluid flow to structural mechanics. The flexibility allows the user to set material properties, boundary conditions and source terms to be any arbitrary functions of the dependent variables. It offers several predefined or convenient multiphysics application templates for common types of problems. The attractive features of this package are that the partial differential equations can be self-defined and linked with other equations. The complexity of our current problem allowed us to choose COMSOL for its ease in handling multiphysics based on finite element analysis. The preprocessing, solving and post processing of the meshed model were done in COMSOL.

The working of COMSOL Multiphysics involves a number of algorithms and programs that are used to study the electroosmotic mixing in the microchannels. The mathematical equations are discretised in model. The different types of solvers available for the partial differentiation equation based problems are summarized below in **Table 2.1**.

Table 2. 1 COMSOL Multiphysics solver types and their usage

Solver Type	**Usage**
Stationary	For stationary PDE problems (linear or nonlinear)
Time-dependent	For time-dependent PDE problems (linear or nonlinear)
Eigen value	For eigenvalue PDE problems
Parametric	For parameterized sets of stationary PDE problems (linear or nonlinear)

Stationary segregated	For stationary multiphysics PDE problems (linear or nonlinear)
Parametric segregated	For parameterized sets of stationary multiphysics PDE problems (linear or nonlinear)
Adaptive	For stationary (linear or nonlinear) or eigenvalue PDE problems using adaptive mesh refinement

Multiphysics Methodology: COMSOL

There are series of steps before getting the results in COMSOL Multiphysics. It starts all from geometry creation, subdomain setup, boundary setup, mesh generation, simulation to post processing of results. The steps have been categorized under pre-processing, processing and post-processing which have been structured in the following chart (**Figure 2.4**).

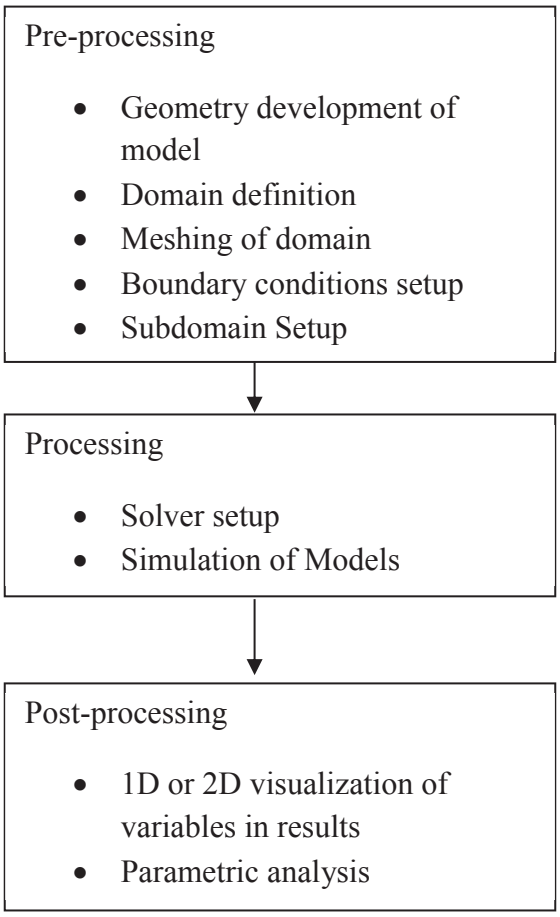

Figure 2.4 Steps in computational modeling in COMSOL 4.2a

The construction of geometry was done in COMSOL 4.2a in 2D with the application of two different modules coupled with each other to determine the extent of the mixing phenomenon. The modules are: Laminar fluid flow and Transport of Dilute species. The fluid domain was discretized using appropriate meshing parameters. 2D triangular mesh elements were generated. Physics controlled mesh was used for the domain with finer elemental growth at the electrode regions and sharp corners. Mesh boundaries, edges and vertices correspond to geometric boundaries, edges and vertices. Automatic meshing is optimized according to the geometry and physics involved in the modeling. Boundary conditions set the interfaces between the geometric model and its surroundings. The

subdomain limits the physics on a model's main domain. The governing equations set the main idea behind the solution of the model. The continuity and momentum equation is set by Navier-Stokes equation. The electric field applied becomes the source term over Navier Stokes equation. The convective and diffusive mixing uses the flow field from laminar flows and solves the problem. After the problem is solved, several visualizations and data interpretations are done to analyze the solution in the post-processing part.

Multiphysics Solver Techniques: COMSOL

Laminar fluid flow is chosen and transient solver is used to solve the fluid flow domain. The selection is of utmost importance since it can simplify results with fewer errors in comparison to the experimental ones.

Stationary Segregated Algorithm

Stationary segregated solver is used for linear or nonlinear stationary PDE problems to split the solution steps into substeps. The different substeps are defined by grouping solution components' names together. In a solution step for a substep, the segregated solver uses the damped Newton method and computes only the Jacobian related to the solution components, a procedure that can save both memory and assembly time. Also, it is possible to choose which linear system solver to use in a substep independently from other substeps. For problems where a full Newton approach does not converge, a segregated solution approach can sometimes work well. On the other hand, in the vicinity of a solution where the Newton approach converges quadratically, the segregated solver approach often converges more slowly.

For the segregated solver there is a possibility to directly—i.e., without any regards to the equations—impose a restriction on the degrees of freedoms. To use this feature, the value of freedom edit field is edited and a space-separated list is entered whose entries alternate between component names (the names of the degrees of freedom) and limiting values, for example c1 0 c2 1e-3. For these pairs, the solution vector is modified after each sub step in such a way that

$$U_j = \max(U_j, U^L) \qquad \text{……(.2.25)}$$

Where, *Uj's are* the corresponding degrees if freedoms and U_L denotes the limiting value. Note that if either *Uj* or *UL* is complex valued the real part of that quantity is used in the above equation.

PARDISO Direct Solver

The parallel sparse direct linear solver PARDISO works on general systems of the form $Ax = b$. In order to improve sequential and parallel sparse numerical factorization performance, the solver algorithms are based on a Level-3 BLAS update, and they exploit pipelining parallelism with a combination of left-looking and right-looking supernode techniques. The code is written in C and FORTRAN. COMSOL Multiphysics uses the PARDISO version developed by Olaf Schenk and collaborators, which is included with Intel MKL (Intel Math Kernel Library).

In the Linear System Solver Settings dialog box, following preordering algorithms can be chosen:

- Minimum degree

• Nested dissection (the default algorithm)

It can also specify if the solver should use a maximum weight matching strategy by choosing row preordering on (default) or off. For symmetric matrices there is a choice between using 2-by-2 Bunch-Kaufmann pivoting (default) or not. In the case of positive definite matrices, row preordering and 2-by-2 Bunch-Kaufmann pivoting are not needed. The solution time is usually reduced if you deselect these features.

To avoid pivoting, PARDISO uses a pivot perturbation strategy that tests the magnitude of the potential pivot against a constant threshold of

$$\varepsilon = \alpha \left| PP_{\mathrm{MPS}} D_r A D_c P \right|_{\infty} \qquad \ldots\ldots(.2.26)$$

Where *P* and *P*MPS are permutation matrices, *Dr* and *Dc* are diagonal scaling matrices, and is the infinity norm (maximum norm). If the solver encounters a tiny pivot during elimination, it sets it to

$$\mathrm{sign}(l_{ii})\varepsilon \left| PP_{\mathrm{MPS}} D_r A D_c P \right|_{\infty} \qquad \ldots\ldots(.2.27)$$

The pivot threshold ε can be specified as required. The perturbation strategy is not as robust as ordinary pivoting. In order to improve the solution PARDISO uses iterative refinements. PARDISO also includes out-of-core capabilities. The PARDISO out-of-core solver stores the LU factors on the hard drive. This minimizes the internal memory usage. The price is longer solution times because it takes longer time to read and write to disk than using the internal memory. COMSOL Multiphysics can optionally estimate and check the error after the solution phase. Error checking is at least done for problems where pivot perturbation or iterative improvement has been used.

Convergence Criteria

The segregated solver terminates if a convergence criterion is fulfilled or if the number of segregated iterations exceeds the number in the Maximum number of segregated iterations edit field (in the Stationary page settings). The value in the Tolerance (default = 10−3) edit field for each group in the General page settings gives the convergence criterion. The segregated-solver iterations stop when for all groups the relative error estimate is smaller than the corresponding tolerance.

When termination of the segregated solver is based on the estimated error, it terminates if, for the entire group's *j*, the error estimate is smaller than the corresponding tolerance,

$$\mathrm{err}_{j,k} < \mathrm{tol}_j, \qquad \ldots\ldots(.2.28)$$

Where, the error estimate in segregated iteration *k* is

$$\mathrm{err}_{j,k} = \max(\mathrm{e}^N_{j,k}, \mathrm{e}^S_{j,k}) \qquad \ldots\ldots(.2.29)$$

The number tol_j is taken from the Relative tolerance edit field for the corresponding group settings for the Stationary segregated solver on the General page of the Solver Parameters dialog box. Furthermore,

$$\mathrm{e}^N_{j,k} = \max_l(1-\alpha_l)\left[\frac{1}{N_j}\sum_{i=1}^{N_j}\left(\frac{\left|(\Delta U^{l,j,k})_i\right|}{W^j{}_i}\right)^2\right]^{1/2} \qquad \ldots\ldots(.2.30)$$

This is an estimate of the largest damped Newton error. Here l is taken for all iterations in all substeps solving for the group j, αl is the damping factor, $\Delta U^{l,j,k}$ is the Newton

increment vector, and N*j* is the number of DOFs. The weight factor W*ji* is described below.

$$e^{S}_{j,k} = \left[\frac{1}{N_j} \sum_{i=1}^{N_j} \left(\left| \frac{(U^{j,k} - U^{j,k-1})_i}{W^j_i} \right| \right)^2 \right]^{1/2}, \qquad \ldots\ldots(.2.31)$$

Where, $e^{S}_{j,k}$ is the relative increment over one complete iteration k. In this expression, U*j,k* is the segregated solution vector for the group j, and W*ji* = max(|U*ji*|, S*i*), where S*i* is a scale factor that the solver determines from the settings in the Scaling of variables area.

The selection in the Matrix symmetry list applies to all the segregated solver groups. For the Automatic choice, the solver can detect and make use of symmetry for the group Jacobian independently of other groups.

The selection in the linearity list on the stationary page applies to all the segregated solver groups. This selection is not as important as it is for the standard stationary solver because the stationary segregated solver uses the same iterative procedure both for linear and nonlinear problems and always checks the error criteria. The associated settings do affect which group Jacobians that are reassembled, and an incorrect selection can therefore result in suboptimal convergence.

2.4 Solver Validation

The two dimensional microfluidic systems were solved to study the active and passive mixing. 64-bit system architecture with a RAM size of 16GB on Intel Xeon processor was used to solve for the numerical setup. The mesh specifications used in the study of

passive mixing is given in **Chapter 3** whereas for the active mixing is given in **Chapter 4**. Solutions obtained for different mesh sizes were compared to ensure that the numerical solutions are convergent, independent of the size of the finite elements, and satisfy the governing laws for fluid flow and species diffusion. To verify the code, the numerical predictions with solutions available in the literature were compared and studied.

Validation for passive mixing

The qualitative validation was done in a T-shaped micromixer (Bothe, et al., 2006). The tracer distribution on a cross section of 0.1 mm X 0.2 mm inside the mixing zone, obtained by laser induced fluorescence and micro resolution confocal microscopy were well portrayed by the numerical results obtained from FLUENT 6.1. Several gometric variations in passive mixing were studied in microfluidic systems using FLUENT 6.1 (Jeon & Shin, 2009). The experiments with gold nanoparticles and copper sulphate II solutions showed good agreement of mixing tendencies with simulation results. Computer numerical simulations were utilized to support the unique mixing performances as observed from the optical microscope (Wong, et al., 2004). Mixing in a split and recombine micromixer with tapered microchannels was also done (Sheu, et al., 2012). The comparison between the experimental data and numerical results showed a very similar trend. The variation in experimental and computational mixing index was found to be as large as 0.035 in one of their designs. A MEMS-based multilaminated flow micromixer was studied numerically and experimentally (Adeosun & Lawal, 2009). The simulation results were in good agreement with the experimental data, especially in the low flow-rate range (Reynolds number <13 in their study).The experimental and numerical studies of sidewall profile effects on flow and heat transfer inside micro-

channels (Wei & Joshi, 2007) showed that the results from micro-particle image velocimetry closely agreed with numerical simulation. It was found that channels with larger aspect ratio with even 0.5° slope in channel sidewall had 20% deviation on the location of maximum velocity. Fluent 6.0 was ulitized in the study of a passive microfludic device to achieve submillisecond mixing. The unique mixing geometry employed two T-type premixers and four butterfly-shaped in-channel mixing elements. The experimental results were consistent with the simulation data.

Validation for active mixing

Active mixing has been attained by electrokinetic instability, ultrasonic vibration, and magneto hydrodynamics. The current work is focused in the utilization of electrokinetic time pulsed variations which induces the instabilities within the solution for mixing. The slip velocity profile was studied by using AC electroosmosis in microchannel (Wang, et al., 2009). An excellent agreement between experimental and numerical calculation was seen on the slip velocity profile. Triple layer assumption consisting of Stern layer, inner layer and middle (or buffer) layer was experimentally validated by the measure of slip velocity using the micro-PIV technique. In another numerical studies using FLUENT, it was concluded that any electroosmotic flow driven system could incorporate mixing by just varying the voltage with time. The velocity gradient in the Debye layer was neglected and replaced by the slip velocity as in this work (Glasgow, et al., 2004).

The particular application of the boundary conditions at the walls of all micromixers modeled here is validated only when the electric field would be at least quasi-steady to neglect the transient effects. That is, the time scale of the transient flow must be much lesser than that of the unsteady electric field. The boundary condition applied at the walls

is also referred to as 'Helmholtz-Smoluchowski' equation. The main model with circular mixing zone (**Figure 2.1.2 A**) was validated (Chen, et al., 2003). The actual fabrication of a similar circular mixing model was done by using SOI (Silicon on Insulator) processing techniques (Zhang, et al., 2004).

2.5 Analysis Tools

The following tools and methods used to analyze the mixing extent has been discussed in this section of this chapter.

Passive Mixing

The plots used to describe the passive mixing phenomenon are briefed hereunder.

a) Reynolds number Vs. Inlet Velocity: The Reynolds number at the outlet versus the mean inlet velocity is plotted for various passive micromixers. A straight line fitting was obtained for each of the so studied micromixers. The Reynolds number is given by

   $Re=\rho Vd/\mu$ ……(.2.32)

   Where ρ is the density, V is the velocity, d is the hydraulic diameter and μ is dynamic viscosity of fluid.

   A low Reynold's number signifies the laminar flow in the domain.

b) Peclet number Vs. Mean Inlet Velocity: The Peclet numbers at the outlet have been shown for each of the mean inlet velocities for each micromixer. A straight line fitting was obtained. A Peclet number is calculated by the following relation,

$$Pe = Vd/D \qquad \ldots\ldots(.2.33)$$

Where D is the mass diffusion coefficient.

A higher Peclet number signifies convective mixing rather than the diffusive one.

c) Standard Deviation of Mass fraction vs. Inlet velocities: Here standard deviation of mass fraction of the species at outlet vs. inlet velocities was seen.

d) Mixing length vs. Inlet velocity in mixing channel

   The mixing length was qualitatively observed and plotted from the contour of mass fractions.

e) Comparison of mixing trends of each micromixer at inlet as well as mid-section and outlet of the mixing channel: Mass fraction of each species has been plotted at inlet as well as mid-section and outlet of mixing channel. The trends show the distribution of mass fraction of species at those sections for 0.001m/s and 8m/s velocity.

Active (Electroosmotic) Mixing

The concentration variance at outlet over time was observed for various models under study. The fall of concentration variance over time is taken as a major determinant for evaluating the various models of micromixers.

CHAPTER 3
STUDY OF PASSIVE MIXING OF FLUIDS IN MICROCHANNELS

Micro mixers are generally used to mix a number of fluids in micro channels, in a few milliseconds of time. An extensive review was made on effective mixing processes in regard to mass fractions of the species at different mixing velocities when the fluids contact each other. Mixing effectiveness of various micro mixers was compared based on their geometric structures at same velocities from inlets. This has been demonstrated by using numerical simulation for micro channels of rectangular cross-section at a low Reynolds number flow. The widths of micro mixers are maintained 50μm and exit boundary is maintained at atmospheric pressure. Mixing fluids were taken with same fluid properties such as density, viscosity, concentration, temperature, etc. The computational results were obtained by numerical simulations using ANSYS FLUENT, commercial fluid dynamic software. The results have thus revealed to better understand the mixing parameters in various designs.

Keywords: Passive mixing, T micro channel, Y micro channel, ANSYS FLUENT

3.1 Introduction

Micromixers are basic components in microfluidic analysis for more than a decade as they have proven to be essential units for reaction technology. The large area-to-volume ratio of micro-reactors gives prospect of better yield and selectivity than conventional designs (Bothe, et al., 2006). The term 'micromixing' is generally used to describe the degree of mixing on a molecular scale. A micromixer is an integrated part of a microfluidic system where sample preparation, injection, manipulation, reaction, separation, and detection may be involved. Modern day micromixers have attracted greater attention in many application areas of physics, chemistry, biology, medicine, engineering, etc. It is useful where small amounts of reagents are required, thus resulting in ample saving on expensive reagents in chemical engineering at the laboratory scale (Wong, et al., 2004). Moreover, their low production cost, reduced reaction time, portability and the multiplicity of design are the general advantages of micro-scale applications (Nguyen & Wu, 2005). There are many types of micromixers for wide range of application. A regular credit-card-sized fluidic chip is used with micromixer elements as parts of the integrated system; this is used for sample preparation of chemicals with very low flow rate in sub-ml/hr. Glass micromixer of checkcard size is an example for this type of device where the typical flow rate is like 10-1000ml/hr. At production level, microstructured mixers are surrounded by a large housing where the flow rate ranges from 100-1000 l/hr (Hessel, et al., 2005). However the design of micromixers is largely a trial-and-error process resulting from inefficiencies and suboptimal designs (Falk & Commenge, 2010).

Micromixers are used for a number of chemical biology applications including protein folding, enzyme reaction, protein-ligand interaction, cell activation, polymerase chain reaction, DNA separation, DNA sequencing, other clinical diagnostics and biological analysis (Auroux, et al., 2002). Due to high demand in biochemical analyses to uniformly mix two or more reagents before the desired reaction, micromixing has been applied to propel liquid reactions. An example of organic metallic synthesis or speeding up gas phase reactions includes the ethylene oxide formation (Hessel, et al., 2004). In addition, micromixers can be used as micro reactors for homogenous liquid phase reactions. The mixing time is counted in sub-milliseconds which is very essential in processes such as protein folding process used to detect causes of a certain disease conditions. In order to optimize micromixers for such applications capable of mixing two reagents, the shortest span of time is considered to achieve desired ratio. In general, micro devices offer fundamental advantages compared with conventional macro scale systems due to their small characteristic dimensions. Apparent advantages of micro reactors are highly efficient micromixing, a high area-to-volume ratio, efficient heat transfer ability, the avoidance of hot spots by effective temperature control, and high operational safety (Ehlers, et al., 2000). Lastly, the mixing in small volumes bears the safety aspect, both for thermal and mechanistic reasons (Vesser, 2001). Therefore, micro structured mixers were placed upstream of reaction zones which were fed with unsafe substances (Haas-Santo, et al., 2002).

However, efficient fluidic mixing is not an easy task to achieve because of the laminar flow of fluids in microfluidic channels, a low Reynolds number of an order of unity and slow flow rates of the fluids due to small dimensions of the channels. Such problems are

more prominent in biological applications where large biomolecules having significantly smaller diffusion coefficients are mixed within microchannels. This normally requires longer time and bigger channel length to bring different biomolecules together for pure diffusion (Zhang, et al., 2008). To overcome these limitations, micromixers are basically classified into active and passive (static) mixers. An active mixer uses external power, e.g. - an electric supply to stir the sample in microchannel. External power may be any or combined of integrated micropumps, ultrasonic vibrations, bubble induced vibrations, electro kinetic instabilities, dielectrophoresis, electro hydrodynamics, electro osmosis, piezoelectric vibrating membranes, small impellers and magneto hydrodynamics. This approach is used in problems which are associated with ineffective mixing in micromixers. On the other hand, passive mixers have small protrusions in microchannels or rough surfaces on microchannel or fluid pumping energy or hydrostatic potential which results in fine and fast mixing without the use of external power supply. The mixing of two fluids in passive mixers may also be because of diffusion in a small span of time. These components are relatively easy and inexpensive to fabricate and package with other devices. Passive mixing can be improved by modifying the geometries. They are further classified into two types- lamination micromixers and injection micromixers. In a lamination micromixer, the fluid streams are split into several small streams and are later joined in mixing channel. On the other side, an injection micromixer differs from lamination micromixer. It splits one stream into several substreams in the form of microplumes which increases the contact surface and decreases the mixing path (Hossain, et al., 2009). Relying on the above applications,various micromixers were developed on various principles over the decade and investigated. Each of the micromixers has

different mixing capacity, mixing speed and operating requirements. Some micromixers are more suitable for a certain application than others. Multilaminated mixers use the principle of minimizing diffusional distance between fluids by splitting and arranging the streams into a single multilaminated channel (deMello, et al., 1999). So the thickness of each fluid layer is greatly reduced, allowing fast mixing. In other category of micromixers, a transversal component of velocity is generated to increase the interfacial area across which diffusion takes place. This flow is achieved using helical channels (Liu, et al., 2000), bas-relief structure on the channel (Stroock, et al., 2002), or electrokinetic instability (Oddy, et al., 2001). A comprehensive overview of micromixers with different working principles were reported by Hessel et al. (2005). Micromixer elements typically have flows in the sub-ml/hr, ml/hr-l/hr and 10-10,000 l/hr ranges respectively covering the whole range up to the conventional static mixers. The higher flow rates in microstructured mixers can act as process-intensification tools.

Extensive research has been done to cope with the mixing in micro domain. Seck Hoe Wong computationally studied the mixing characteristics of two liquids in a micro T-mixer with asymmetrical flow at inlets. Different pressures applications at inlets were studied by an experimental approach (Hossain, et al., 2009). Gobby et al studied the mixing characteristics of two gases in a micro T-mixer through the use of a computational approach. The influence of flow speed, aspect ratio, and angle between two inlets were reported in this study. Bokenkamp et al worked on micro T-mixer that used turbulence as its mechanism for fast mixing between two fluids (Bökenkamp, et al., 1998). The study showed that turbulence was realized with the use of large microchannels of 500 μm wide and the mixing time was as short as 110 μs. Kockmann

et al carried out numerical studies on mixing in a micro T-mixer with rectangular cross section. Kockmann showed the three regimes of flow in a micro channel namely laminar flow, vortex flow and engulfment flow depending on Reynolds number of flow in the microchannel. It showed that the engulfment flow has an improved mixing over the other two (Kockmann, et al., 2006). Arnaud Goullet studied mixing in various micromixers at different inflow rates of 48nl/s to 4.8µl/s in the form of pulsed flow. It was found that mixing was more efficient when both secondary flows induced by the channel geometry features and pulsing flow were combined (Goullet, et al., 2006). A study was done by Tsung-Han Tsai on a Y-type semi- active micromixer which used magnet for mixing. The magnet was placed at the bottom of the mixer for mixing of water and ferro-nanofluid with Fe_3O_4 nanoparticles. Three different volumetric flow rates of 3L/min, 6 L/min, and 10 L/min were used, and the results showed that a rapid mixing between ferro-nanofluid and water could be achieved immediately downstream of the permanent magnet for all volumetric flow rates and all channel widths tested (Tsai, et al., 2009). Magnetohydrodynamic flow was extensively used for mixing, pumping and also detection of trace metals (Panta, et al., 2009).

3.2 Mathematical modeling

The fluid motion in the micro-channel is modeled by the Navier Stokes equation and continuity equation; assuming the fluid is incompressible.

Physics of Fluid flow:

Conservation of mass: Continuity equation

$$\nabla.\mathbf{V} = 0 \qquad \ldots\ldots\ldots\ldots\ldots\ldots\ldots\ldots\ldots\ldots (3.1)$$

Conservation of momentum: Navier Stokes equation

$$\rho\left[\frac{\partial \mathbf{V}}{\partial t}+(\nabla.\mathbf{V})\mathbf{V}\right]=-\nabla p+\mu\nabla^2\mathbf{V} \qquad \text{..... (3.2)}$$

Where ρ represents the fluid's density (kg/m^3), μ is the dynamic viscosity (m^2/s), and **V** is the velocity (mm/s), and p is the pressure (Pa).

Physics of Mass Transport:

Similarly, species transport is described by the diffusion-convection equation:

$$\frac{dc}{dt}+(\nabla.\boldsymbol{V})c=D\nabla^2 c \qquad \text{..... (3.3)}$$

Where, $c = \rho\omega$

c, ω and D are concentration, mass fraction and diffusion coefficient of the species.

According to basic laws of fluid dynamics flow of fluid also depends on the dimensionless parameter which is known as Reynolds number (Re).

$$\mathrm{Re}=\frac{\rho\bar{u}d}{\mu} \qquad \text{..... (3.4)}$$

Where ū is the mean velocity and d is the characteristic length.

Similarly, Peclet number is given by

$$Pe=\frac{\bar{u}d}{D} \qquad \text{..... (3.5)}$$

Where ū is the mean velocity, d is the characteristic length and D is the diffusion coefficient of the species.

For fluid flow in a closed microchannel the characteristic length is the hydraulic diameter of the channel for computing the Reynolds number. Depending on the Reynolds number, the flow is characterized into three regimes. The flow in which the Reynolds number is less than 2300 is often considered as laminar flow. For the flow in which Reynolds number more than 4000 falls into to turbulence flow. If the Reynolds number of the flow is between 2300 and 4000, the flow is in a transitional regime between laminar and turbulent flow. For a microchannel the occurrence of turbulent flow is rare, and the flow is highly laminar and the Reynolds number rarely exceeds 2000 due to the fact that the characteristic length of the microchannel is smaller, so rapid mixing of fluid in a micromixer is hard to achieve. For larger macro sized pipes, a Reynolds number of 4000 and more can be easily achieved, so rapid mixing is often easy.

Rapid fluid mixing in laminar regimes is usually challenging to achieve. Laminar flow is further classified into three different flow regimes. At low velocities, there is a stratified flow regime in which the streamlines are scarcely bent to form a secondary flow and follow the channel walls.. At medium velocities, vortex flow regime is obtained where vortices are built up inside the channel. The mixing process is still diffusion for both the cases. However, the mixing phenomenon becomes better due to the higher fluid velocity and therefore shorter residence time for the fluid particles to diffuse. The effect is, to some extent, compensated by the swirling fluid flow which gives a slightly improved mixing quality by dragging fluid streams from the middle to the top and bottom side of the mixing channel. The third regime flow occurs at high velocity which is

engulfment flow regime in which axial symmetry of the model breaks up. Here the flow streamlines break at the middle of the channel but tries to reach the opposite side of the wall. This engulfment of the streamlines leads improvement of the mixing degree.

The designing or modeling of micromixers was done by using a pre-processor Solid-Works, a CAD software. The models from Solid-Works were then exported to another pre-processor ANSYS Meshing where meshing of these models was done. All models were of same width of 50μm before and after confluence of rectangular cross section. **Figure 3.1** and **Figure 3.2** show the different geometric cross sections of models that were evaluated.

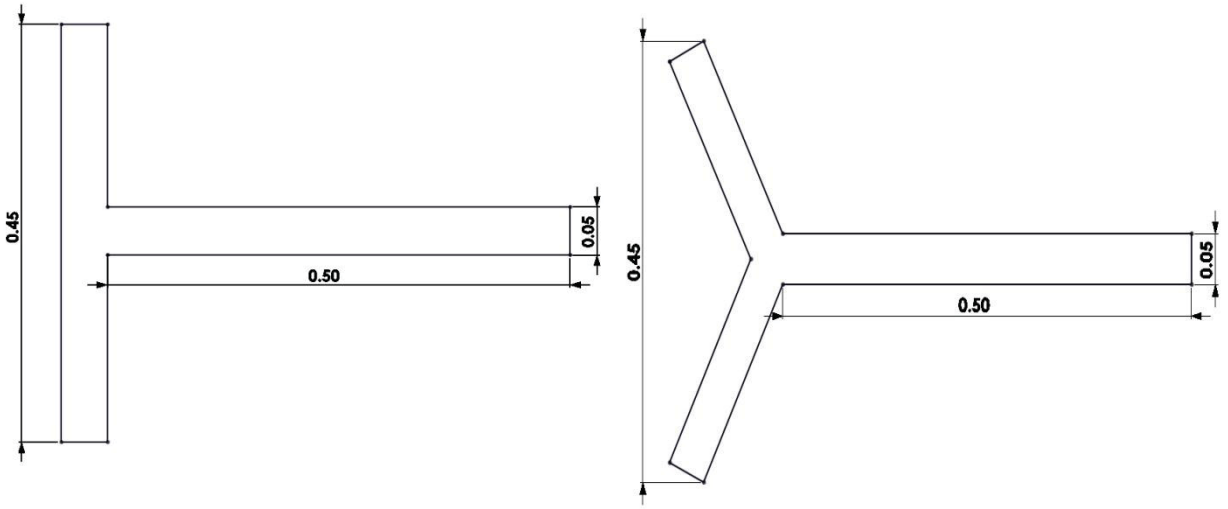

(a) (b)

Figure 3.1 Micromixer models with two inlets named as (a) T and (b) Y

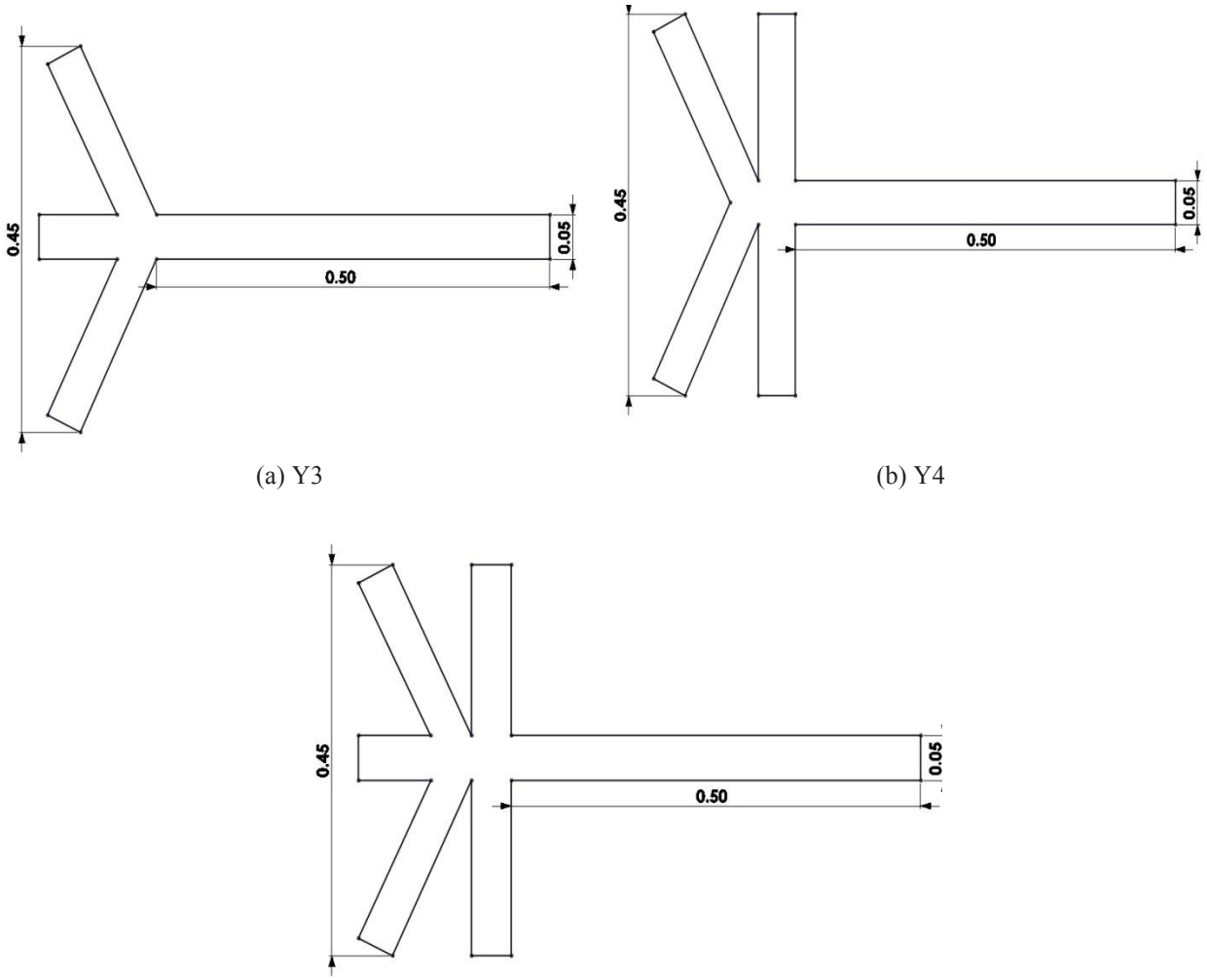

(a) Y3

(b) Y4

(c) Y5

Figure 3.2 Micromixer models with (a) three inlets named Y3, (b) four inlets named Y4 and (c) five inlets named Y5 (All dimensions in mm)

These models were meshed in ANSYS Meshing. T-shaped micromixer was meshed using 1250 quadrilateral elements since it had only two inlets and one outlet. The Y-micromixer was meshed with 3300 triangular elements of finer mesh elements in the mixing channel. Likewise, Y3 model was meshed using 3759 triangular cells with a little coarser mesh near inlets and finer mesh at mixing channel and outlet. The Y4 model was meshed using 4648 triangular elements and the mesh area of interest is made finer than that of inlets. Y5 model was meshed with 5087 triangular cells of finer quality mesh.

For consistency of comparisons, same aqueous solution was used in all inlets. The aqueous solution here was water with dynamic viscosity of 0.001003 kg/m-s and density of 998.2 kg/m^3 at standard temperature of 27°C. Equal concentrations were used. No chemical changes were expected to occur in the solution. Since, this is a passive mixer, there were no other external forces to force the mixing inside the microchannel.

A pressure based solver technique was used for the simulation of the two-dimensional fluid transport phenomena along with appropriate boundary conditions in ANSYS FLUENT. No-slip conditions at the walls, mass flow rate and the species mass fractions at inlet zone and a gauge pressure of zero at the outlet zone were applied as boundary conditions. Discretization schemes such as SIMPLEC algorithm for pressure-velocity coupling and first order upwind for the computation of Navier -Stokes and diffusion-convection equations were chosen to solve the laminar mixing flow problem. Six cases of these models at different inlet velocities were solved and tabulated.

3.3 Results and discussions

The results shown in **Table 3.1** (Scenario I) indicate that the mixing was not effective in Y3, Y4 and Y5 models.. This is illustrated in the tabulated of mass fraction at the exit of the microchannels. For the micro Y-mixer with three inlets the mass fraction of species "a", "b"& "c" were 0.26, 0.475& 0.26 respectively. The result indicate that the mixing was done in a very limited scale. This is the same case for other two models. **Figure A1.1** & **Figure A1.2** show the fluid trajectory plots, which show the mixing of the fluid species was mainly in the inlet zone but not in the mixing zone. This is due to the fact

that the mixing is completely due to diffusion and is a stratified flow regime in which the species streamlines were scarcely seem to be converted to a secondary flow.

Table 3.1 Mass fraction of species at outlet for inlet velocities of 0.001 m/s (Scenario I)

Model	Boundary conditions at inlet					Mass fraction of species at outlet					Maximum velocity at outlet m/s	Reynolds number at outlet
	1	2	3	4	5							
						a	b	c	d	e		
T	x	x				0.5	0.5				0.00294	0.09665
Y	x	x				0.5	0.5				0.00297	0.10196
Y3	x	x	x			0.26	0.475	0.26			0.00447	0.1527
Y4	x	x	x	x		0.26	0.23	0.23	0.26		0.00597	0.20107
Y5	x	x	x	x	x	0.25	0.13	0.237	0.13	0.25	0.00746	0.255

The results in **Table 3.2** (Scenario II) were almost similar to the results of first scenario for four models in terms of mass fractions at exit. There was a slight change in mass fractions of species “a” and “b” in micro Y4 model when compared with scenario I. The mass fraction of species “a” changed from 0.26 (**Table 3.1**) to 0.295 (**Table 3.2**) and mass fraction of species “b” from 0.23 (**Table 3.1**) to 0.2 (**Table 3.2**). This indicates slight improvement in mixing of species “a” and decrease in mixing of species “b” . The Reynolds number of fluid flow was slightly higher than the previous case and the species transport and diffusion speeded up beyond the centerline of mixing channel shown by fluid streamlines of species in **Figure A1.3 & Figure A1.4**. Mixing is completely due to diffusion and the flow is still stratified flow regime in which the species flow streamlines were scarcely bent to form a secondary flow and follow along the channel walls.

Table 3. 2 Mass fraction of species at outlet for inlet velocities of 0.01 m/s (Scenario II)

Model	Boundary conditions at inlet					Mass fraction of species at outlet					Max velocity at outlet m/s	Reynolds number at outlet
	1	2	3	4	5							
						a	b	c	d	e		
T	x	x				0.5	0.5				0.02935	0.9665
Y	x	x				0.5	0.5				0.02972	1.01959
Y3	x	x	x			0.262	0.473	0.262			0.04466	1.527
Y4	x	x	x	x		0.295	0.2	0.2	0.295		0.05969	2.0112
Y5	x	x	x	x	x	0.25	0.13	0.237	0.131	0.25	0.07458	2.5502

In **Table 3.3** (Scenario III), a marginal improvement in mixing of species was seen when velocity at inlets were multiplied by 10 compared to scenario II (0.1 m/s compared to 0.01 m/s). The mass fractions of species “a”& “b” at microchannel exits were similar for first two models. In the rest three models (Y3,Y4 & Y5), there was a slight improvement in the mixing of all species. The mass fraction of species in scenario II and scenario III were seen more consistent and even which indicates mere improvement in mixing. **Figure A1.5 & Figure A1.6** show the fluid trajectory plots in terms of mass fraction. The Reynolds number of the flow was increased compared to the previous scenarios and still the mixing is only due to diffusion and the flow is still stratified flow regime where the streamlines are scarcely bent to form a secondary flow and follow at channel walls.

Table 3.3 Mass fraction of species at outlet for inlet velocities of 0.1 m/s (Scenario III)

Model	Boundary conditions at inlet					Mass fraction of species at outlet					Maximum velocity at outlet m/s	Reynolds number at outlet
	1	2	3	4	5							
						a	b	c	d	e		
T	x	x				0.5	0.5				0.2935	9.6726
Y	x	x				0.5	0.5				0.2971	10.1959
Y3	x	x	x			0.28	0.44	0.28			0.4462	15.27
Y4	x	x	x	x		0.28	0.21	0.21	0.28		0.5964	20.112
Y5	x	x	x	x	x	0.231	0.15	0.236	0.15	0.231	0.7449	25.502

In **Table 3.4** (Scenario IV) the velocity at inlets were maintained at 1 m/s. The Reynolds number is now higher and the species from inlets were able to reach beyond the top and bottom of mixing channel as shown by fluid trajectory plots of species in **Figure A1.7 & Figure A1.8**. The mass fractions tabulated indicate the betterment in mixing in all the five models when compared to previous Scenario II. In Y3 micromixer model the mass fraction of all species was approximately 0.33 promising for almost complete, consistent and even mixing. Here the mixing is completely due to diffusion.

Table 3.4 Mass fraction of species at outlet for inlet velocity of 1 m/s (Scenario IV)

Model	Boundary conditions at inlet					Mass fraction of species at outlet					Maximum velocity at outlet m/s	Reynolds number at outlet
	1	2	3	4	5							
						a	b	c	d	e		
T	x	x				0.5	0.5				2.941	97.2517
Y	x	x				0.5	0.5				2.956	101.959
Y3	x	x	x			0.331	0.337	0.331			4.423	152.783
Y4	x	x	x	x		0.25	0.25	0.25	0.25		5.927	201.12
Y5	x	x	x	x	x	0.2	0.198	0.2	0.198	0.2	7.392	255.02

In **Table 3.5** (Scenario V) the velocity was maintained at 2 m/s. It is twice as the previous scenario. As a result of high velocity the Reynolds number of flow is high. Here mixing of species is done adjacent to the mixing channel and one species was unable to travel into other inlets of different species. Due to this we have an improved mixing which can be seen from the fluid trajectories from **Figure A1.9 & Figure A1.10**. The fluid trajectories for models Y4 and Y5 show that the mass fractions of species were trying to be equal which is an improved mixing.

Table 3.5 Mass fraction of species at outlet for inlet velocities of 2 m/s (Scenario V)

Models	Boundary conditions at inlets					Mass fraction of species at outlet					Maximum velocity m/s	Reynolds number At outlet
	1	2	3	4	5							
						a	b	c	d	e		
T	x	x				0.5	0.5				5.892	195.244
Y	x	x				0.5	0.5				5.896	201.007
Y3	x	x	x			0.33	0.33	0.33			8.818	305.573
Y4	x	x	x	x		0.25	0.25	0.25	0.25		11.795	401.64
Y5	x	x	x	x	x	0.2	0.2	0.2	0.2	0.2	14.695	509.627

In scenario VI (**Table 3.6**) and VII (**Table 3.7**) the Reynolds number in mixing channel was even higher while the flow velocity at inlets was maintained at 4 m/s and 8 m/s respectively. As a result of high flow velocities, there is an improvement in mixing of species. This is illustrated by the flow trajectory plots in **Figures A1.11, A1.12, A1.13, & A1.14**. The tabulated mass fractions indicate the ratios of species at outlet. The ratios were equal for all the species which indicates fine mixing. For the last two models, the mixing was still continued even though it seemed to get normalized for the tenth place value.

Table 3.6 Mass fraction of species at outlet for inlet velocities of 4 m/s (Scenario VI)

Models	Boundary conditions at inlets					Mass fraction of species at outlet					Maximum velocity m/s	Reynolds number At outlet
	1	2	3	4	5							
						a	b	c	d	e		
T	x	x				0.5	0.5				11.804	392.23
Y	x	x				0.5	0.5				11.733	401.751
Y3	x	x	x			0.33	0.33	0.33			17.525	610.962
Y4	x	x	x	x		0.25	0.25	0.25	0.25		23.403	802.557
Y5	x	x	x	x	x	0.2	0.2	0.2	0.2	0.2	29.124	1018.04

Table 3.7 Mass fraction of species at outlet for inlet velocities of 8 m/s (Scenario VII)

Models	Boundary conditions at inlets					Mass fraction of species at outlet					Maximum velocity m/s	Reynolds number At outlet
	1	2	3	4	5							
						a	b	c	d	e		
T	x	x				0.5	0.5				23.554	787.743
Y	x	x				0.5	0.5				23.044	802.681
Y3	x	x	x			0.33	0.33	0.33			34.783	1220.66
Y4	x	x	x	x		0.25	0.25	0.25	0.25		46.402	1603.21
Y5	x	x	x	x	x	0.2	0.2	0.2	0.2	0.2	57.735	2031.88

In laminar fluid flow keeping the same incompressible flow, Reynolds number in rectangular ducts varies linearly with increasing velocity. An ideal case is assumed with no head losses in the micro mixer at its inlet, junction and outlet in all scenarios I-VII. According to Prandtl's first kind the secondary flow is due to the centrifugal force when fluid flows in a curved path. Due to this the flow with higher flow velocity tend to flow outwards while the slower flow at top and bottom tends to move inwards towards the bend (Gulliver & Halverson, 1987). In a micromixer, this gives rise to a secondary flow phenomenon at the junction where the streams of liquid from the inlets change the direction of flow in the mixing channel. Flow separation occurs at the top of the junction where the two inlet fluid streams change direction. Vortices are formed at the junction resulting mixing between the inlet species in that region. The mixing process was just started. The partially mixed solution is swept away by the secondary flow toward the side walls of the mixing channel. It could be observed from the related figures of scenarios V, VI and VII. The mass fraction of the liquid around the bend showed some mixing there due to cross flow. Cross flow at the junction assists in the mixing process by creating a larger area of contact for mixing. All applied boundary conditions were symmetrical. In real life however, perfect symmetrical condition is rarely obtained. This is due to factors such as the presence of some waves on the surface of the microchannel caused by some imperfect etching during fabrication, small protrusion in the microchannel, etc. Slight difference in the speed of flow can occur in the mixing experiments due to slightly different paths taken by the fluids before entering the microchannel, viscosity of the liquids might also be slightly different.

Computational passive mixing studies of various microchannels for the seven scenarios showed that the enhanced mixing performance was mainly affected by increasing the incoming velocity at the inlets. When the velocity at the inlets is in between the range 0.001-0.1 m/s the mixing of species is done at the inlets rather than at the junction of the mixing channel. For T and Y- mixers, almost complete mixing was be achieved at these velocities because a small vertical velocity component is assumed to be sufficient to have significant effect on the mixing species from one inlet cross the center line and mixes with other species in its inlet channel. This indicates that complete mixing cannot be achieved at the junction and outlet.

Using mass fraction data, a standard deviation of the mass fractions of the species was plotted with inlet velocities for each mixer. At lower inlet velocities, the value of standard deviation is significantly higher than that of higher velocities. This shows that the ideal mass fraction for mixing could be obtained at higher velocities. This is illustrated in the **Figure 3.3**.

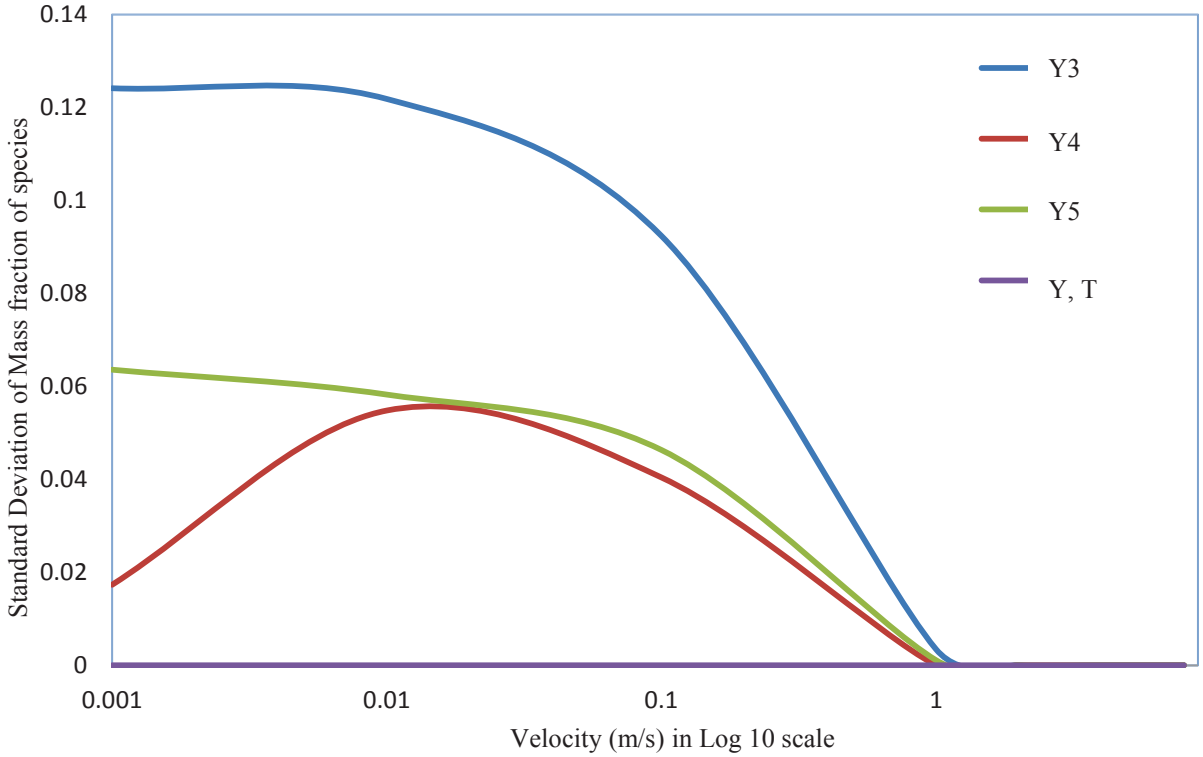

Figure 3.3 Standard deviation of mass fraction vs. inlet velocities

The mixing length was determined for each scenario. The plot of mixing length varying with inlet velocity in mixing channel is shown in **Figure A1.15**. At low inlet velocities of 0.001m/s, 0.01m/s and 0.1m/s in Y, T and Y3 type mixers, the mixing was seen in the respective inlet channels before the mixing channel itself. As the velocity was increased from 1m/s to 8m/s, the mixing length gradually increases to show linear characteristics. However, in case of Y4 and Y5 mixers, the mixing processes were different. The Y4 mixer showed the unusual decrease in mixing length when the velocity was 0.1m/s and increased drastically at 1m/s inlet velocity. The Y5 mixer did not show proper mixing in the entire mixing channel along the length neither in the inlet channels at 0.001m/s. When observed from 0.01m/s to 0.1m/s, the mixing length decreased unusually and again

increased drastically at 1m/s inlet velocity. At inlet velocities of 2, 4 and 8 m/s the mixing channel did not provide adequate length for the equal mixing of the species.

Table 3.8 Mixing length of given models at respective velocities obtained from concentration contours

Velocity	**Mixing length (µm)**				
m/s	**T**	**Y**	**Y3**	**Y4**	**Y5**
0.001	0	0	0	39.583	No mixing
0.01	0	0	0	36.437	130.43
0.1	0	0	0	12.244	12.37
1	32.258	35.84	56.01	224.53	259.9
2	69.892	56.201	113.636	>>500	>>500
4	140.28	109.259	220.588	>>500	>>500
8	286.971	210.95	425	>>500	>>500

The mass fraction of each species was plotted at their respective inlets, mid-sections and outlet for each models as shown in **Figure A1.16 & A1.17**. The mass fractions were only recorded at the inlets, mid-sections and outlet for each model and species. In between inlet and the mid-sections, a steep gradient change in mass fraction of each species was observed for each species and in each model between the lines joining inlet to mid-section and mid-section to outlet. **Figure A1.15, A1.16 & A1.17**) agree to each other as it is observed that the mixing process was still ongoing at 8 m/s inlet velocity.. The slope lines from mid-section to outlet in each of the species and models for velocity 8m/s agree to results shown in **Figure A1.15**.

For low velocity inlet of 0.001m/s where the mixing is due to diffusion, it may be perhaps that the mixing is a function of mixing length also.

CHAPTER 4
DESIGN OF AN EFFICIENT ELECTROOSMOTIC MIXER*

Micro-bio/chemical applications often require rapid and uniform mixing of a number of fluid streams that carries bio/chemical species in the solution. Micromixers have been used over a decade for wide varieties of applications in microfluidics. Different types of common geometrical arrangements like T,Y, and circular, etc. were experimented to test rapid mixing effect of species. At microscale, fluid flow is usually laminar with low Reynolds number, fluids mixing mechanism is primarily due to diffusion and free from any turbulence. Demand for highly efficient micromixers for microfluidic networks is due to slower mixing process for larger bio-molecules such as peptides, proteins, and nucleic acids compared to micro-scale molecules. Passive and active mixers are two basic mixers that are currently in use for these applications. Passive mixers often require very long mixing channels unlike most active mixers require bulky moving parts to stir the fluids. Though the high voltage favors good mixing quality, it is often inconvenient for μTAS. Electroosmotic effects orthogonally aligned with the fluid flowstream are utilized for optimum mixing effect in various micromixers. Numerical solution obtained from COMSOL, a finite element software, was used to see the effectiveness in different geometries by varying vital parameters of micromixing. Circular, square and elliptical

* Partial contents of this chapter was presented at 2011 American Society of Mechanical Engineers Summer Bioengineering conference (ASME-SBC 2011), Farmington, PA, USA, 2012 American Society of Mechanical Engineers Summer Bioengineering conference (ASME-SBC 2012), Fajardo, Puerto Rico, and in progress to be published on Open Journal of Fluid Dynamics.

models were designed to see the variation in the mixing keeping the mixing area fairly constant. Mixing process was parametrically analyzed by varying the mixing shape, concentration, mixing area and electrode positions. Edges in the design were filleted, additional obstacles were introduced and electrode positions were also varied to see the enhancement of mixing in one of the effective mixers. Cross-dependencies among several geometrical, electrical, and fluid parameters were studied in order to achieve an optimum mixing effect. A discussion has been made on the basis of the results obtained in different cases using the surface concentration through time. Study of particle traces shows folding and stretching of flow streamlines which are discussed here.

Keywords: Electroosmosis, Mixing, Geometric shape, Numerical Solution, COMSOL

4.1 Introduction

μTAS is integrated system applied for Bio-MEMS where micromixing is one of the basic tasks required for micro biochemical analysis, protein folding, polymer chain reaction, DNA hybridization, and so on. The fluid flow in microfluidic devices is generally laminar where the majority of mixing is primarily by diffusion mode. Low Reynolds number and high Peclet number flow signifies the long mixing length and extended retention time requirement to ensure satisfactory mixing results. As this passive mixing did not prove practical enough for the analysis of large scale molecules, active mixing evolved. Apart from micro mechanical means to improve the active mixing process by using moving parts, an efficient design is being actively researched upon by using electro-magnetic fields to optimize the mixing process. A low voltage operated electroosmotic mixer of specific geometry, consequently, holds a promising solution for this purpose.

There has been a long history of microfluidics researchers to build a lab on a chip for over decades (Knight, 2002). The dynamic field of academic research offers great new capabilities for the future (Whitesides, 2006). Technological breakthroughs in research laboratories around the world are happening and being bridged commercially for practical use (Mark, et al., 2010). The microfluidic mixing enhancement, therefore, is one of the key in setting the milestone for the development of lab-on-a-chip. Several passive mixers such as the T-type (Gobby, et al., 2001), L-shaped (Bau & Yi, 2000), serpentine pipe (Kim, et al., 2005), flow splitting (deMello, et al., 1999), ridged-floor mixer (Stroock, et al., 2002), staggered herringbone mixer (SHM) (Camesasca, et al., 2006), zigzag/wave-like configuration mixer (Mengeaud, et al., 2002) and so on were

studied and developed. The split-up of the fluid streams into lamellae and subsequent recombination, so-called multilamination, was also tested (Hardt & Schönfeld, 2003). Most of these designs implemented chaotic advection or introduced secondary transverse flows to induce chaotic stirring (Meisel & Ehrhard, 2006). However, they did not improve mixing significantly, and needed to be fabricated delicately (Chen, et al., 2003). These micro mixers enhanced the species mixing by using specific channel geometry configurations to increase the interfacial contact area between the mixing species (Chen & Cho, 2008).

Active micro mixers are being developed to cope with the passive mixers. A mixing chamber mimicking a source/sink system (Evans, et al., 1997) was designed to stir fluids effectively using micro fabricated valves and phase-change liquid micro pumps. Pressure disturbances from side channels were also added in micro channel flows to enhance mixing (Lee, et al., 2001). An active micro mixer comprising of a main channel and multiple pairs of side channels generated chaotic mixing effects by pulsing at appropriate amplitude and frequency (Niu & Lee, 2003). The mixing of two reagents by time-pulsing their respective flow rates in the two inlet channels was also demonstrated (Glasgow & Aubry, 2003). Later on, the influence of various dimensionless parameters on the mixing efficiency of the pulse-flow was examined to optimize the mixing performance (Glasgow, et al., 2004). A significant technique for the electroosmotic mixing of two aqueous solutions, via the application of periodically varying electric fields at the two inlet channels was developed. The results indicated that mixing could be enhanced at an appropriate Strouhal number (St = fL/V, f=frequency of applied field, L= characteristic length, and V=velocity of fluid). The efficient mixing of two species

via the electrokinetic instability effects induced by a time-periodic electric field was also studied (Shin, et al., 2005). External oscillatory electric fields to excite secondary flows in fluids passing around internal obstacles in a microchannel or flowing along meandering micro channels was also experimented (Meisel & Ehrhard, 2006). The results confirmed that these secondary flows greatly enhanced the mixing efficiency within the micro channel. Coupling of magnetic and electric fields (Bau, et al., 2001) as well as micro-magnetic stir-bar by the application of external rotating bar (Lu, et al., 2002) was also demonstrated.

It was pointed out that a specific geometry can be used to enhance the mixing process further (Brian, 2010). This thesis work deals with designing models of various shapes and number of electrode pairs, mixing channel width, frequency of the applied voltage in electrodes and concentration to investigate and optimize the mixing process in COMSOL (COMSOL, 2011). Models are later shown in this chapter. A considerable enhancement has been seen while placing several obstacles in the mixing zone of circular electroosmotic mixer. Concentration variance(S) at the outlet was calculated over time for each model to determine the uniformity of mixing.

$$S = \int_0^y (c - \bar{c})^2 \, dy \qquad \text{.....(4.1)}$$

Where c is the concentration at any point at outlet and $\bar{c}$ is the mean concentration

4.2 Mathematical Modeling

The fluid motion is governed by the incompressible Navier Stokes equation

$$\rho\left[\frac{\partial \mathbf{V}}{\partial t}+(\nabla.\mathbf{V})\mathbf{V}\right]=-\nabla p+\mu\nabla^2\mathbf{V}+\rho_e\mathbf{E} \qquad \text{.....} \quad (4.2)$$

Where ρ_e is charge density, **E** is electric field intensity, **V** is velocity vector and μ is dynamic viscosity.

Due to the electric double layer (EDL) formation at the walls, slip velocity boundary conditions will be used.

The slip velocity at the edge of the electric double layer,

$$U_{slip}=-\frac{\varepsilon\zeta\mathbf{E}_x}{\mu} \qquad \text{.....(4.3)}$$

Where ε is permittivity of medium, ζ is potential (0.1V), $\mathbf{E}_x$ is electric field intensity in the x-direction.

The velocity slips at the wall, and the fluid moves just like a plug flow, assuming the double layer thickness is negligible compared with the characteristic length, say $d/\lambda_d >> 100$.

Where λ_d is electric double layer thickness also called, the Debye length.

In the bulk of flow (outside the electric double layer), the fluid motion is governed by the Navier Stokes equation

$$\rho\left[\frac{\partial \mathbf{V}}{\partial t}+(\nabla.\mathbf{V})\mathbf{V}\right]=-\nabla p+\mu\nabla^2\mathbf{V} \qquad \text{....(4.4)}$$

The model setup contains a primary circular electro osmotic mixer contains an area enclosed within the 5μm and 15μm radius. The distance between the inlet and outlet extremities is 80μm. Inlet, outlet and mixing channel width are maintained to be 10μm as in the original COMSOL model (Chen, et al., 2003). All other shape modifications were obtained by taking the same mixing width and area except for the particular cases when mixing area, electrode pairs, electrode locations and obstacles were varied (**Figure 4.1**). An electrolytic fluid of 1 mol/m^3 concentration is fed with non-concentrated species separated at the midpoint along the longitudinal line of the inlet under the entrance length 1 m with velocity of 0.1mm/s. The electrodes are placed at angular positions of 45, 135, -45 and -135 degrees respectively as the farthest placed electrode pairs. All other electrode pairs are patterned at angles 22.5 degrees on each side of the vertical line through center of the mixer and at the vertical line itself preserving the symmetry for required electrode pairs. The models were then meshed as free triangular with extra fine elemental size. The boundaries at electrode positions and the point of separation of two incoming fluids are custom meshed per maximum element size of 0.2 and 0.1 respectively for maximum element growth rate of 1.1 each. The no slip boundary conditions are applied at the walls. The sinusoidal voltage of 0.1V is applied on electrodes over time but with alternate polarity. Other physical parameters are: Conductivity of solution = 0.11845 S/m , Frequency of ac potential = 8 Hz, Diffusion coefficient of the solution = $1\times10^{-11}m^2/s$, and relative permittivity of fluid = 80.2. These were the default conditions used in modeling unless otherwise stated.

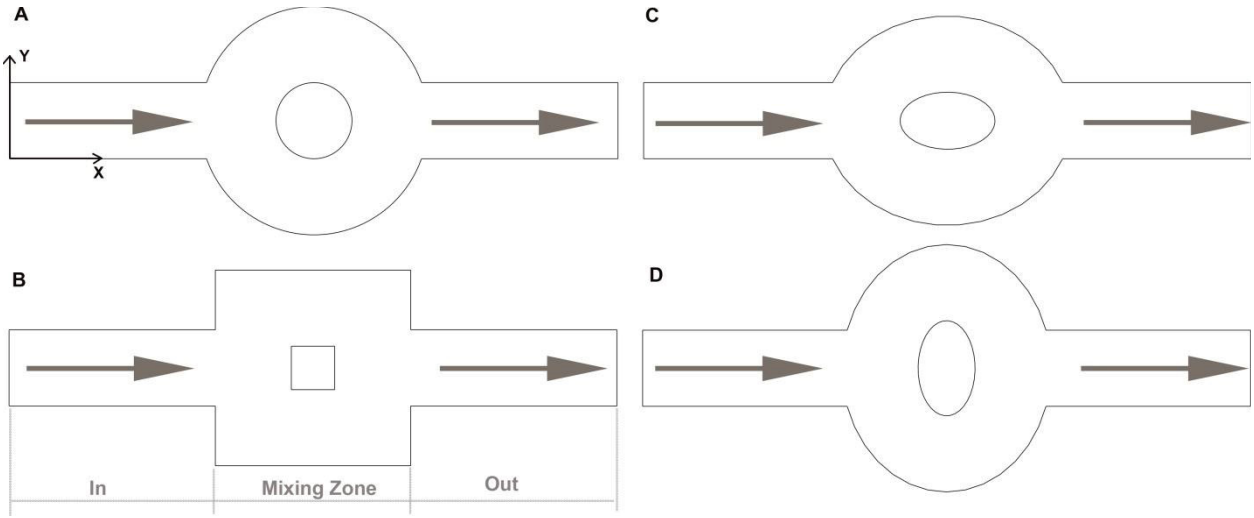

Figure 4.1 Models of various electroosmotic micromixers: (A) circular, (B) square, (C) elliptic-I and (D) elliptic-II

4.3 Results and Discussion

The applied electric field perturbed the flow streamlines over time. **Figure 4.2** shows the perturbation in streamlines at 0.27 second of the applied electric field.

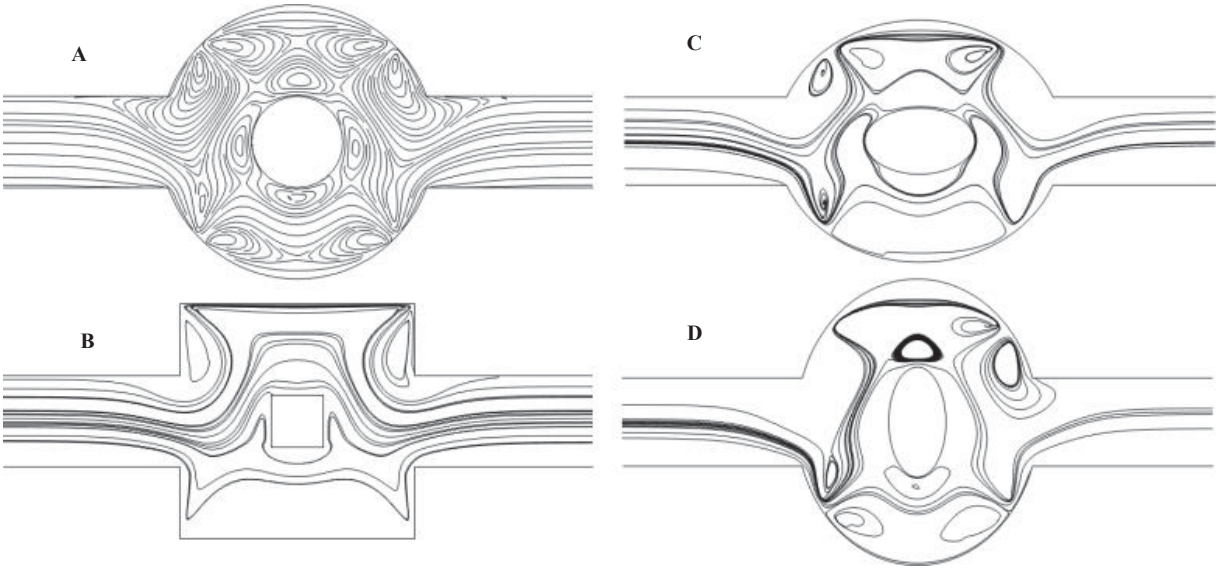

Figure 4.2 Streamlines of velocity field at time 0.27s with two electrode pairs of various shape: (A)circular, (B)square, (C)elliptic-I and (D)elliptic-II

Effect of shape

The circular shaped micromixer was the most effective one when the two electrode pairs were used in each model. The concentration variance indicated to be practically constant for the square shaped mixer. The elliptical micro mixer with the longer longitudinal axis was a better mixer than the longer transverse axis (**Figure 4.3**). The streamlines in **Figure 4.2** along with **Fig. 4.3** suggests that more material lines are interfering one over another in circular mixer over time. The velocity magnitude noted at the instant of 0.27 sec was higher around the electrodes (**Figure A2.1**). The direction of which could be noted from the respective velocity vectors (**Figure A2.2**). The maximum of the highest velocity at the very instant for the individual domains was found in model A while the minimum was found in model B at the very instant. For the given micromixer models, the maximum velocity reached beyond the dark red color of contour at 0.27 sec for circular(A), square(B), elliptic-I(C) and elliptic-II(D) were 5.8255 mm/s, 4.8611 mm/s, 5.0482 mm/s and 5.5973 mm/s respectively. The lowest velocity of 3.822E-17 mm/s was found to be in square shaped micro mixer model. The surface concentration profile at the very instant (0.27s) is shown in **Figure A2.3**. Streamlines in other models B, C and D were lesser in number as compared to the model A (**Figure 4.2**). The geometry in the circular mixing zone has been able to produce higher stretching and folding of material lines which have significantly decreased the concentration variance over time.

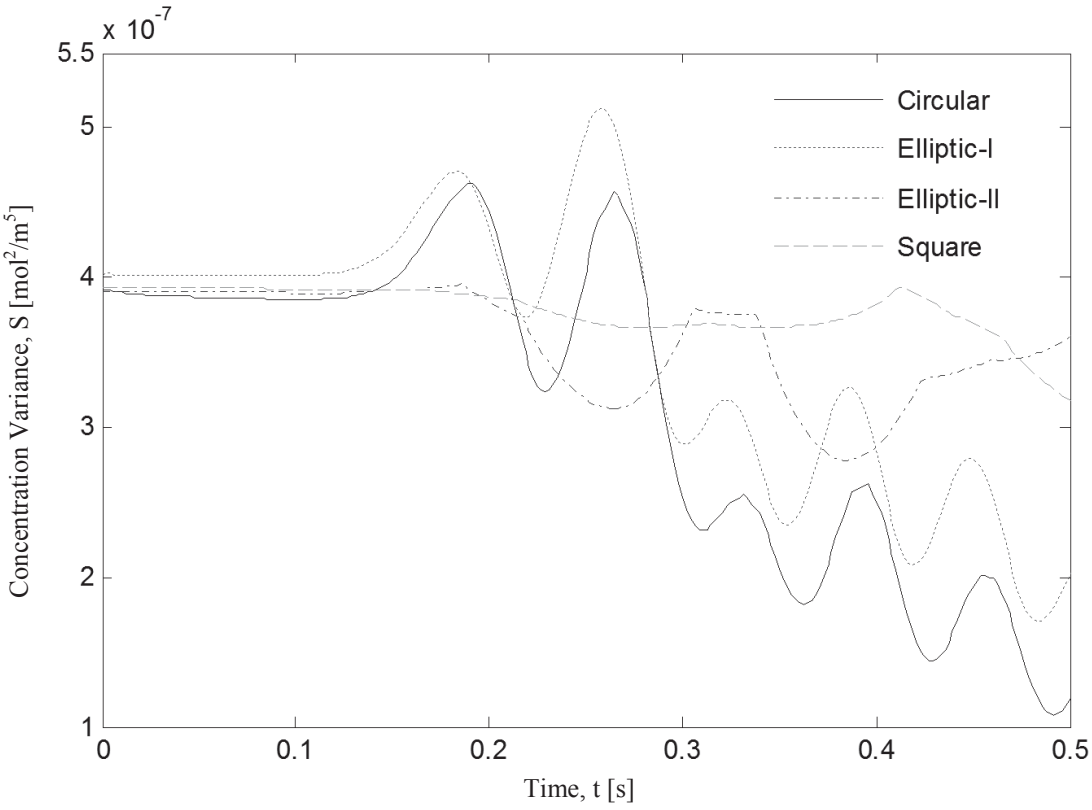

Figure 4.3 Effect of various mixing shapes showing Concentration Variance Vs. Time

Effect of mixing channel width and electrode pairs

In case of mixing area, the smaller channel width favored in elliptic-I and elliptic-II mixers. The increase in channel width did not improve mixing over time in square shaped mixer and elliptic-II mixer. Increase of channel width did not show significant effect on circular mixer (**Figure 4.4 A-D**). The use of four pair electrodes implied better mixing capabilities in each of the models for shapes except the one which has square shaped mixing zone (**Figure 4.4 E-H**).

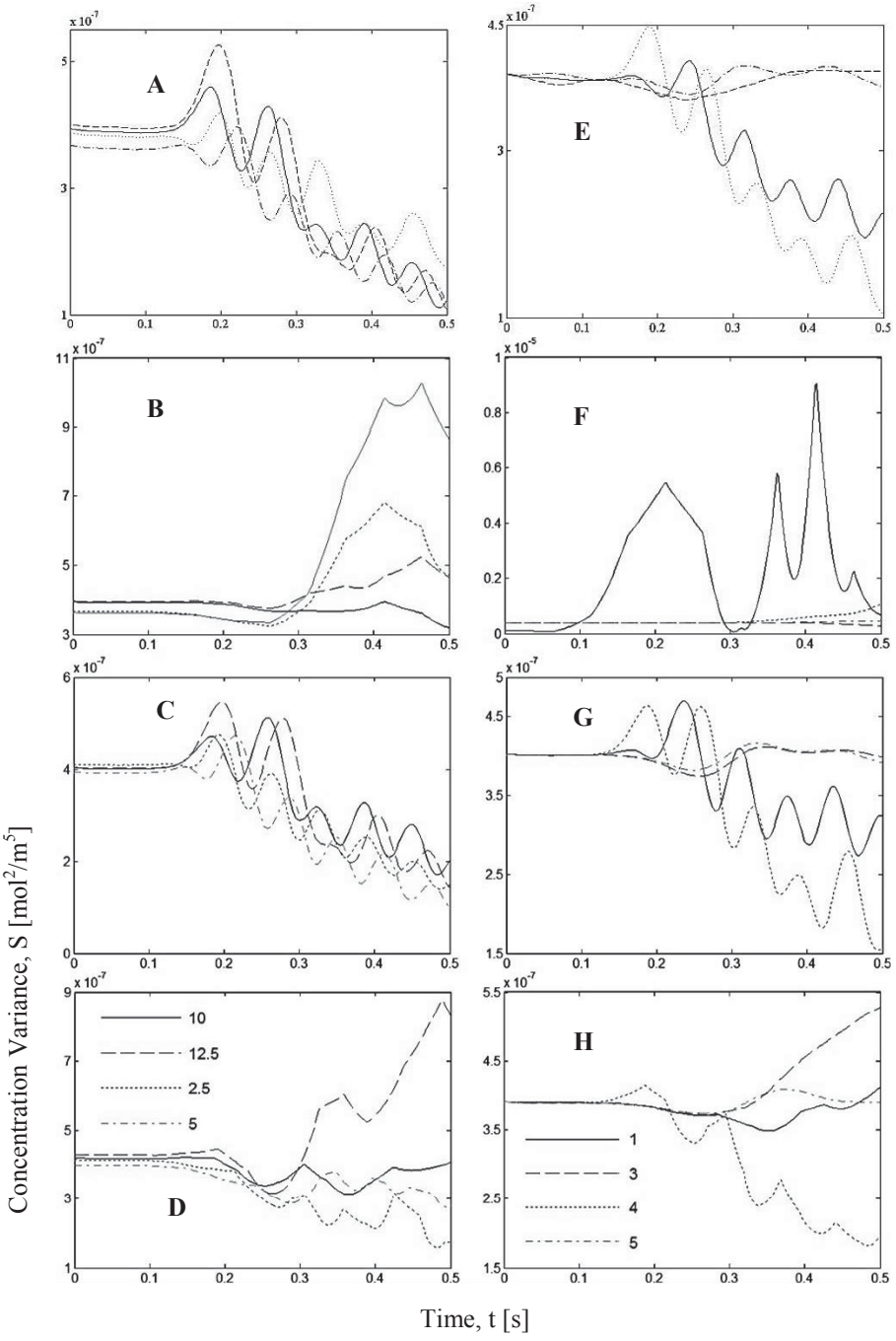

Figure 4.4 Concentration variance at outlet vs. time(s) for different mixing channel widths in μm(A-circular, B-square, C-elliptic-I, D-elliptic-II) and number of electrode pairs in E-circular, F-square, G-elliptic-I, H-elliptic-II)

Effect of voltage frequency in electrodes

The circular electroosmotic mixer showed the best mixing capability over time at 8Hz. The frequency as low as 1 Hz had an initial perturbation unfavorable to the desired output though it falls later in concentration variance. Square mixer did not show any effect on frequency variation. Elliptic-I mixer showed a better mixing over time at 8Hz whereas the 1Hz has the same effect as in circular mixer. Though the 12Hz showed less initial overshoot, it took more time to decrease. In case of Elliptic-II mixer, the 1 Hz showed better mixing effect except that it showed an initial overshoot for a longer duration (**Figure 4.5**).

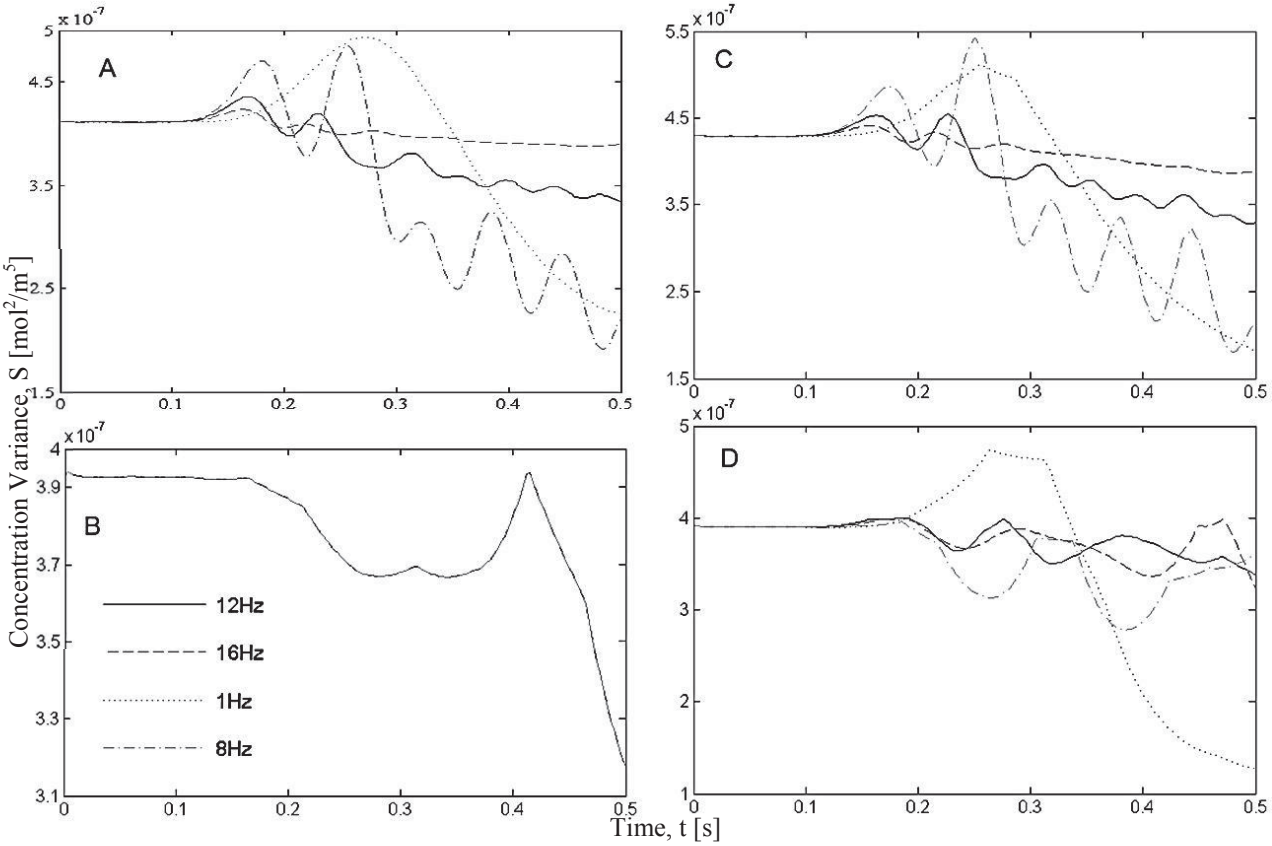

Figure 4.5 Frequency variation in (A)circular, (B) square, (C) elliptic-I and (D) elliptic-II mixers over time

Effect of streamlined input and output at mixing zone

The streamlining at the inlet and outlet corners of the mixing zone created by a fillet radius of 7 μm showed the following behavior of mixing. A considerable fall of concentration variance through time for elliptic-I mixer was observed (**Figure 4.6**).

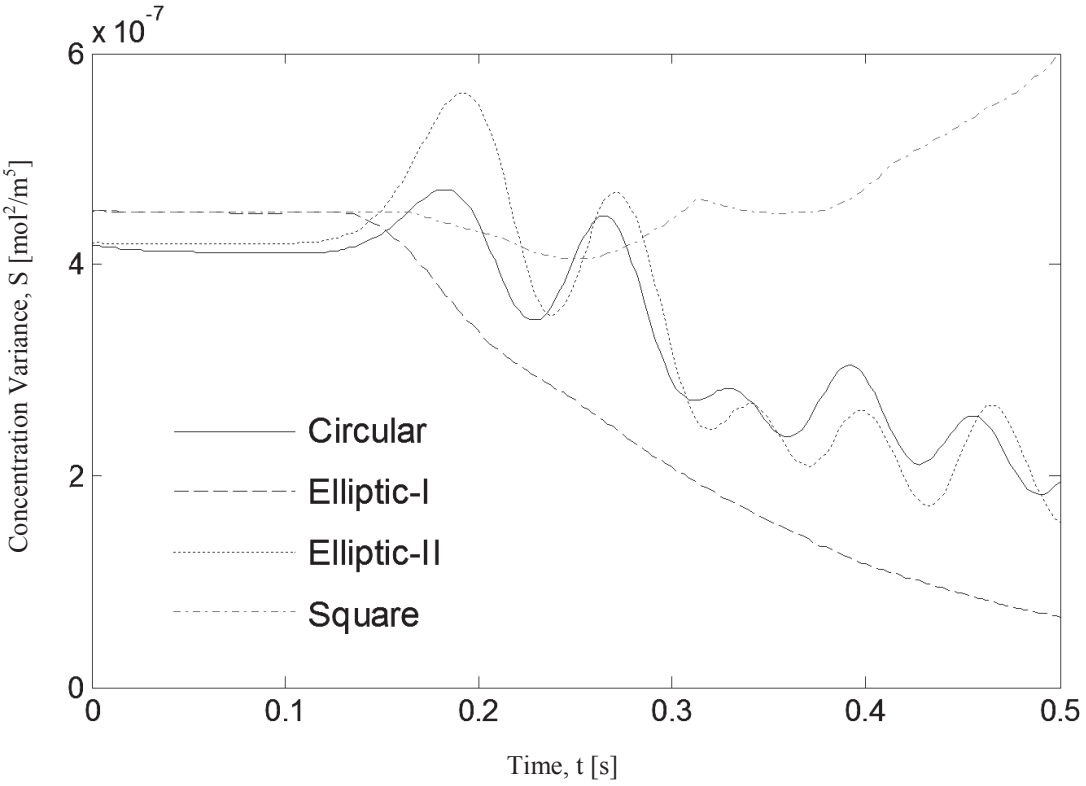

Figure 4.6 Concentration variance at outlet Vs. time, on Effect of Streamlined input and output in mixing zone for different shapes

Effect of circular obstacles

The circular obstacles of 5μm radius were placed at different positions and named as shown in **Figure 4.7** and the resulting mixing plot was noted in **Figure 4.8**. The

electrode voltage, frequency, electrode positions and all other parameters were kept the same as in control model described previously in **Mathematical Modeling 4.2**.

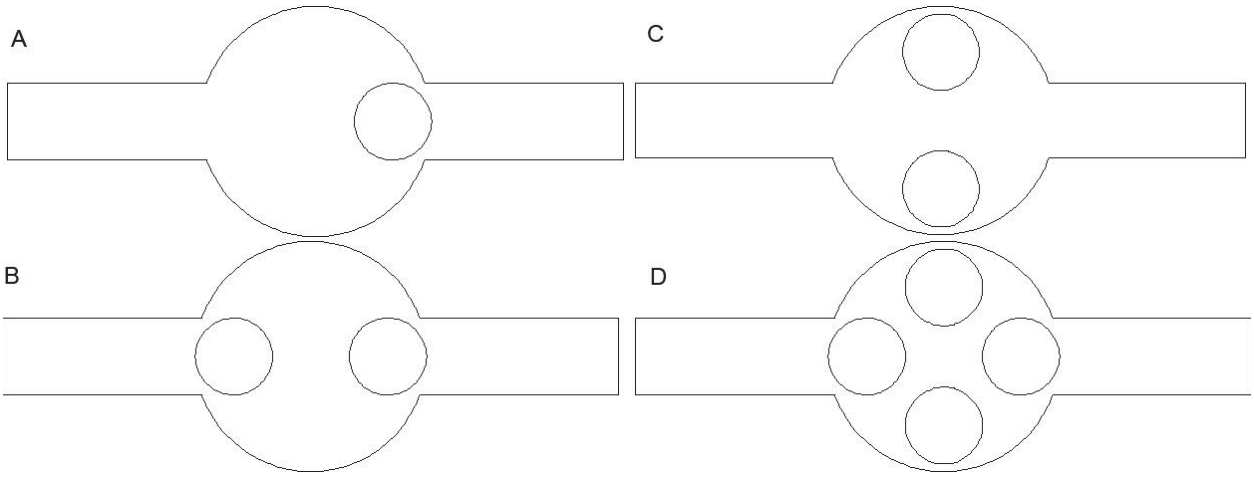

Figure 4.7 Different positions of obstacles in a circular mixer model

The resulting concentration variance over time for these respective micromixers was obtained as shown in the **Figure 4.8**. The four circular obstacles model D (**Figure 4.7** and **4.8**) in mixing zone showed a considerable decrease in concentration variance over time.

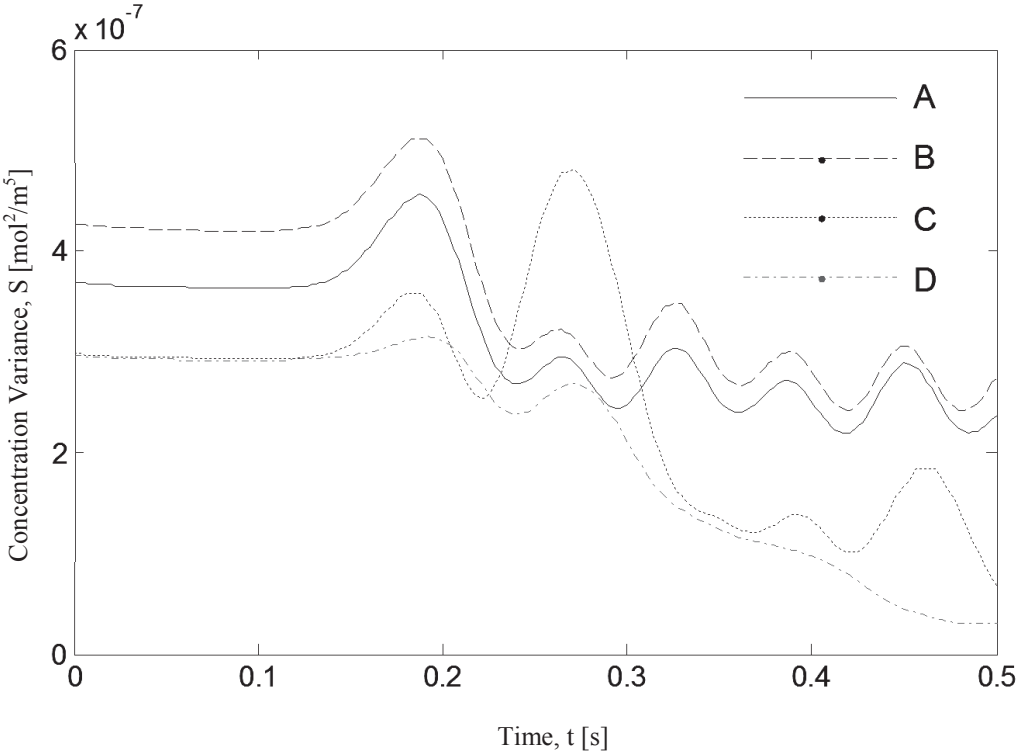

Figure 4.8 Concentration variance at outlet vs. time showing effect of respective obstacles in circular mixer

Effect of electrode positions on circular obstacles

The electrode positions were varied as shown in **Figure 4.9**. The model A with electrodes as shown performed a better mixing over time. Model B also mixed well without overshoots but did not comparatively mix as model A (**Figure 4.10**).

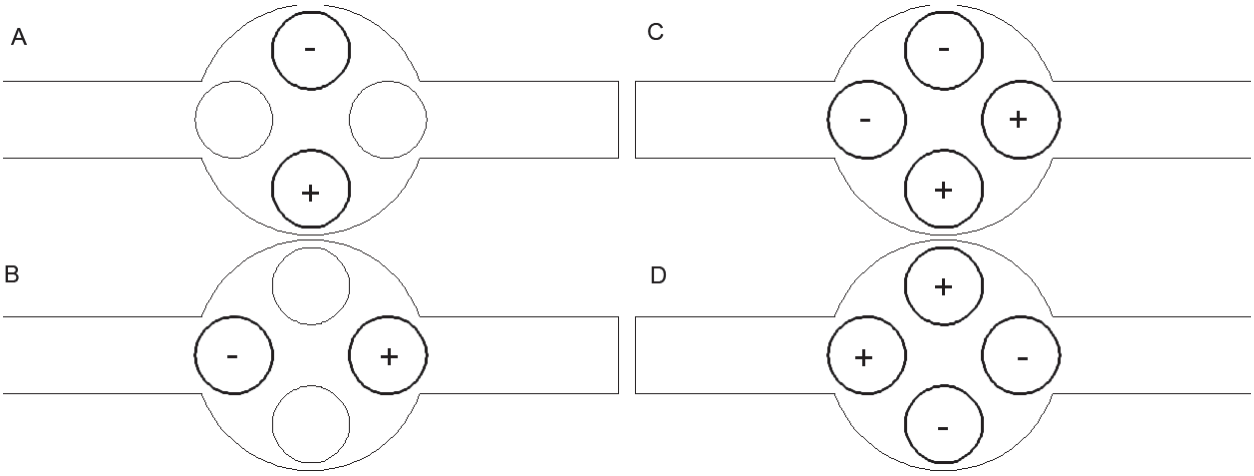

Figure 4.9 Different electrode positions in obstacles of a circular mixer model

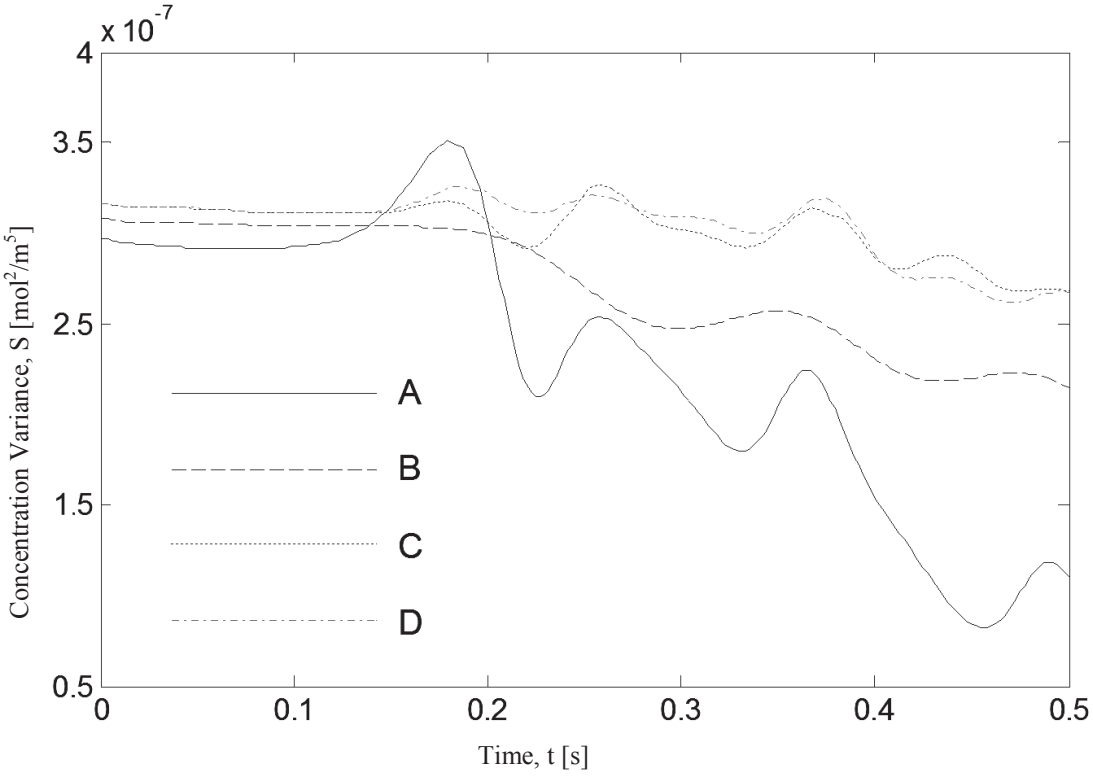

Figure 4.10 Concentration variance at outlet vs. time showing effect of different electrode positions in obstacles of circular mixer

Effect of varying electrode positions from the modeled mixers

The electrode positions were varied as shown in **Figure 4.11** to determine an effective micromixer. The model C showed to mix better than any other models over time in this case. The particular arrangement of electrodes and obstacles in model C in this case showed better mixing characteristic over time (**Figure 4. 12**).

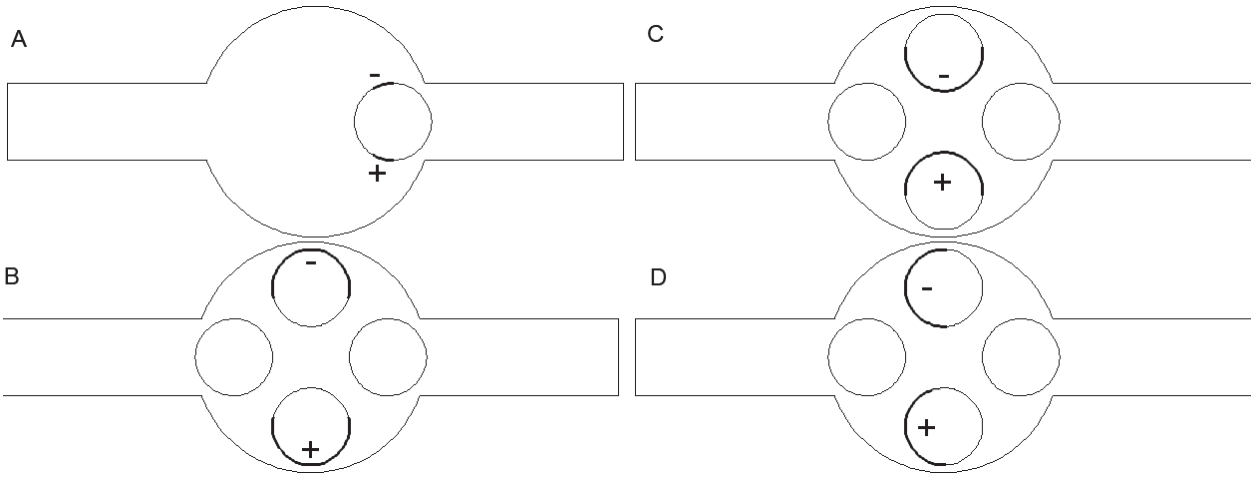

Figure 4.11 Various electrode positions in modeled circular mixers with obstacles as shown

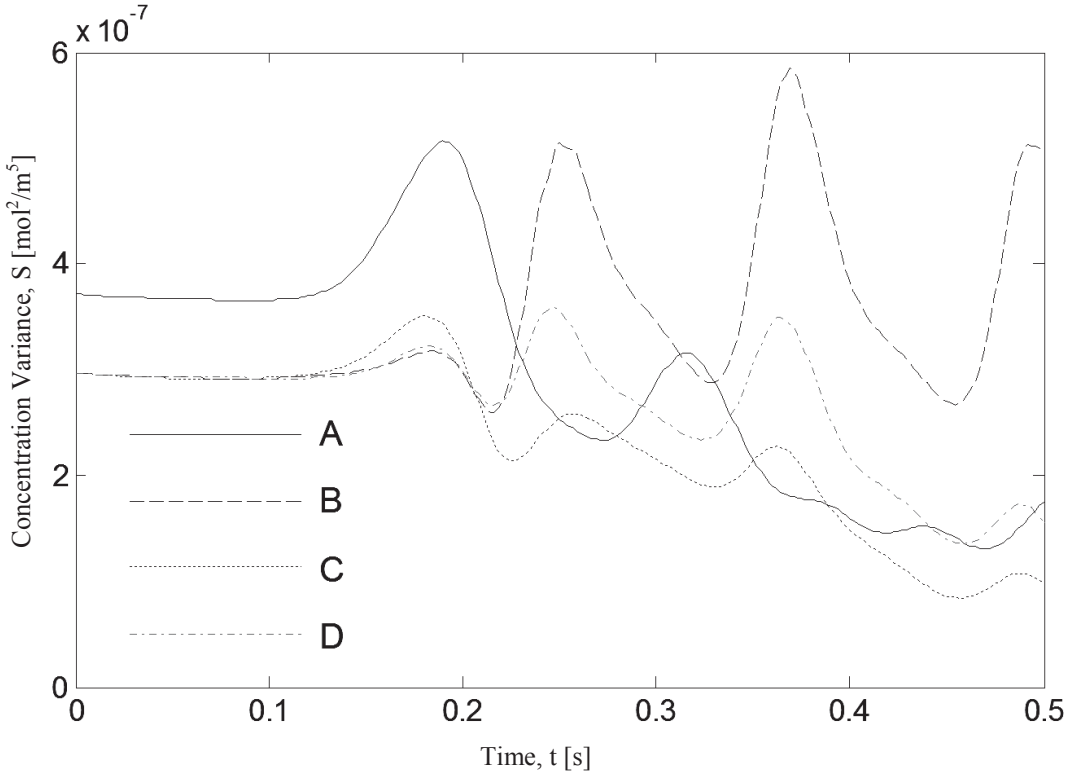

Figure 4.12 Concentration variance at outlet vs. time showing effect of various electrode positions in modeled circular mixers with obstacles

Effect of converging inlet and diverging outlet on current the mixing enhancement

The models were setup as shown in **Figure. 4.13** with corresponding streamlines at 0.3 seconds. The electrode voltage, frequency, and all other parameters were kept the same as in control model described in **Mathematical Modeling 4.2** except the electrode positions which are shown in the boldfaced lines. The two best mixing models studied previously were compared with the converging inlet and diverging outlet. Both the average concentration over time and the concentration variance over time were shown. Compared to our control model described in **Mathematical Modeling 4.2**, the new designs yielded a notable fall in concentration variance down by a factor of at least 10. Though the

average concentration did not show much variation (**Figure 4.14**), the concentration variation over time for models C and D show remarkable improvement on mixing process compared to the performances of all other existing micromixers (**Figure 4.15**).

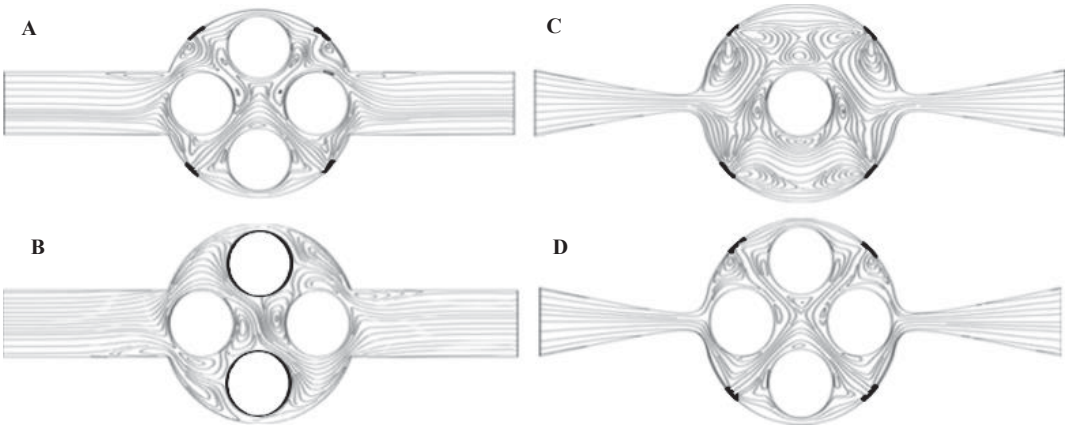

Figure 4.13 Electro-osmotic mixer models under study with streamlines at 0.3 s

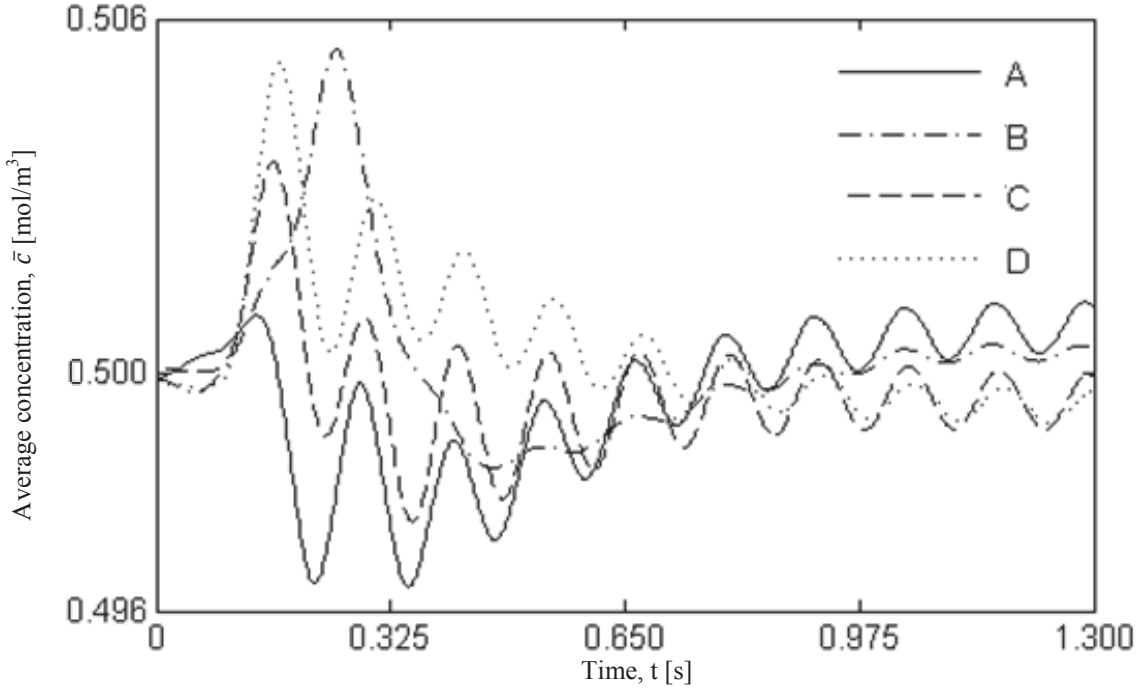

Figure 4.14 Average concentration vs. time, showing effect of converging inlet and diverging outlet on mixing enhancement

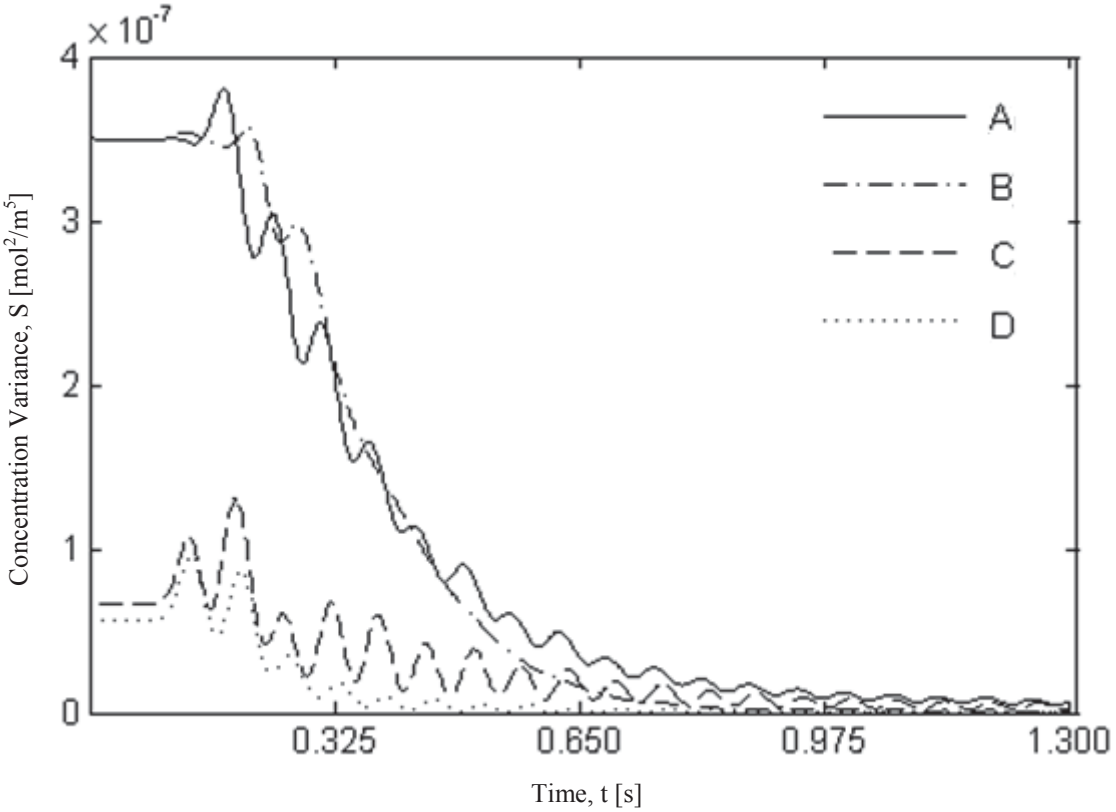

Figure 4.15 Concentration variance vs. time, showing effect of converging inlet and diverging outlet on mixing enhancement

Conclusions are future works related to this chapter are further discussed in **Chapter 5**.

CHAPTER 5
CONCLUSIONS AND RECOMMENDATIONS

Passive mixing in microchannels was studied on various models including T, Y and a number of other designs with combination of these two geometries. From the results and discussion, it could be noticed that the Reynolds and Peclet numbers are the functions of velocity, and comparatively higher at higher velocities, thereby promoting the tendency of mass diffusion over one another. However, a given length of mixing channel was not seen sufficient enough to effectively mix the entire number of species over its length for this increased inlet velocities. Only the convective mixing was attained. Though the concentration distributions were more uniform at outlet, the species did not diffuse completely over one another. This resulted in higher mixing length requirements particularly the Y4 and Y5 designs at 2, 4 and 8 m/s of inlet velocities for each species to mix uniformly. In other words, the higher velocities shorten the diffusion length scale. It is recommended to simulate the presented mixing work on a three dimensional geometry as there may be three dimensional effects. Further study on the passive mixing would be to study these mixing length requirements at a higher resolution and the use of serpentine and zigzag mixing channels as reported in the literature. The introduction of secondary flows in these particular geometries needs to be studied to meet higher diffusion length for adequate and uniform mixing. These unique geometries introduce the components of velocities which can be utilized for optimum mixing. This would increase the actual mixing length requirement with a compromise in the usage of higher volume of fluids.

Special care should be equally taken in increased pressure drop over the whole or part of the intended microchannel to avoid additional micro pumps.

Active mixing phenomenon in micromixers was studied on various designs. It was found that the electro-osmotic mixing is largely dependent on the geometry and the usage of the electrodes. The mixing channel width has also shown significant variations in the mixing process. A better mixing capability in circular mixer was noted while using four electrode pairs. Though the vortices were formed due to electric field, the sudden geometric modifications at its sharp corners render the stretching and folding of material lines unavailable to the non-concentrated species for the diffusive mixing in case of square shaped mixers. It has also proven that the particular geometries of micromixer including mixing, inlet and outlet zones have significant influences on the degree of mixing. A rapid and uniform mixing capability was found in a circular mixer with circular intermediate obstacles. A converging inlet and a diverging outlet has shown even more remarkable improvements in the extent of mixing over other designs. The four circular obstacles positioned in the mixing zone generated a flow separation and recirculation passing over them resulting better mixing along with electric perturbation. Thus, the vortices made the stretching and folding of flow lines yielding the intensified uniform mixing process. Based on several literatures, an external magnetic field can be used along with electric field to optimize the mixing process at lower voltages. Future work is encouraged to correlate mixing effectiveness with geometric, electric and magnetic parameters.

REFERENCES

Adeosun, J. T. & Lawal, A., 2009. Numerical and experimental mixing studies in a MEMS-based multilaminated/elongational flow micromixer. *Sensors and Actuators B: Chemical,* Volume 139, pp. 637-647.

Auroux, P. A., Iossifidis, D., Reyes, D. R. & Manz, A., 2002. Micro total analysis systems. 2. Analytical standard operations and applications. *Anal Chem,* 74(12), pp. 2637-52.

Bau, H. H., Zhong, J. & Yi, M., 2001. A minute magneto hydro dynamic (MHD) mixer. *Sensors and Actuators B: Chemical,* 15 October, 79(2-3), pp. 207-215.

Bau, H. & Yi, M., 2000. *The kinematics of bend-induced stirring in micro-conduits.* IMECE 2000, Proc. ASME Intl. Mechanical Engineering Congress and Exposition, MEMS 2000 Symposium Proceedings, pp. 489-496.

Beebe, D. J. et al., 2001. Passive mixing in microchannels: Fabrication and flow experiments. *Mécanique & Industries,* July-August, 2(4), pp. 343-348.

Blow, N., 2009. Microfluidics: the great divide. *Nature Methods*, September, 6(9), p. 683.

Bökenkamp, D. et al., 1998. Microfabricated Silicon Mixers for Submillisecond Quench-Flow Analysis. *Analytical Chemistry,* 70(2), pp. 232-236.

Bothe, D., Stemich, C. & Warnecke, H.-J., 2006. Fluid mixing in a T-shaped micro-mixer. *Chemical Engineering Science,* May, 61(9), pp. 2950-58.

Brian, K., 2010. *Micro- and Nanoscale Fluid Mechanics: Transport in Microfluidic Devices.* 1 ed. New York: Cambridge University Press.

Camesasca, M., Kaufman, M. & Manas-Zloczower, I., 2006. Staggered passive micromixers with fractal surface patterning. *Journal of Micromechanics and Microengineering,* 16(11), p. 2298.

Chapman, D., 1913. *Philosophical Magazine,* Volume 25, pp. 475-481.

Chen, C.-K. & Cho, C.-C., 2008. Electrokinetically driven flow mixing utilizing chaotic electric fields. *Microfluidics and Nanofluidics,* 5(6), pp. 785-793.

Chen, C. K. & Cho, C. C., 2007. Electrokinetically-driven flow mixing in microchannels with wavy surface. *Journal of Colloid and Interface Science,* 15 August, 312(2), pp. 470-480.

Chen, H. et al., 2003. *Numerical simulation of an electroosmotic micromixer.* Washington, D.C., 2003 ASME IMECE.

COMSOL, 2011. *Multiphysics Modeling and Simulation Software.* [Online]
Available at: http://www.comsol.com
[Accessed 15 01 2011].

deMello, A., Manz, A. & Bessoth, F. G., 1999. Microstructure for efficient continuous flow mixing. *Anal. Commun.,* Volume 36, pp. 213-215.

Ehlers, S., Elgeti, k., Menzel, T. & Wießmeier, G., 2000. Mixing in the offstream of a microchannel system. *Chemical Engineering and Processing: Process Intensification,* July, 39(4), pp. 291-298.

Evans, J. D., Liepmann, D. & Pisano, A. P., 1997. *Planar Laminar Mixer.* Nagoya, Japan, MEMS97 (The Tenth Annual International Workshop on Micro Electro Mechanical Systems), pp. 96-101.

Falk, L. & Commenge, J. M., 2010. Performance comparison of micromixers. *Chemical Engineering Science,* 1 January, 65(1), pp. 405-411.

Fu, L.-M., Yang, R.-J., Lin, C.-H. & Chien, Y.-S., 2005. A novel microfluidic mixer utilizing electrokinetic driving forces under low switching frequency. *ELECTROPHORESIS,* 26(9), pp. 1814-1824.

Gass, V., Vanderschoot, B. H., Jeanneret, S. & Derooij, N. F., 1994. Integrated Flow-Regulated Silicon Micropump. *Sensors and Actuators A-Physical,* 43(1-3), pp. 335-338.

Glasgow, I. & Aubry, N., 2003. Enhancement of microfluidic mixing using time pulsing. *Lab Chip,* 3(2), pp. 114-120.

Glasgow, I., Batton, J. & Aubry, N., 2004. Electroosmotic mixing in microchannels. *Lab Chip,* 4(6), pp. 558-562.

Glasgow, I., Lieber, S. & Aubry, N., 2004. Parameters Influencing Pulsed Flow Mixing in Microchannels. *Analytical Chemistry,* 76(16), pp. 4825-4832.

Gobby, D., Angeli, P. & Gavriilidis, A., 2001. Mixing characteristics of T-type microfluidic mixers. *Journal of Micormechanics and Microengineering,* 11(2), pp. 126-32.

Goullet, A., Glasgow, I. & Aubry, N., 2006. Effects of microchannel geometry on pulsed flow mixing. *Mechanics Research Communications,* September-October, 33(5), pp. 739-746.

Gouy, M., 1910. *Journal de Physique,* Volume 9, pp. 457-468.

Gulliver, J. S. & Halverson, M. J., 1987. Measurements of Large Streamwise Vortices in an Open-Channel Flow. *WATER RESOURCES RESEARCH,* January, 23(1), pp. 115-123.

Haas-Santo, K. et al., 2002. *A Microstructure Reactor System for the Controlled Oxidation of Hydrogen for Possible Application in Space.* In Microreaction Technology: IMRET 5: Proceedings of the Fifth International Conference on Microreaction Technology, Springer Verlag, p. 313.

Hardt, S. & Schönfeld, F., 2003. Laminar mixing in different interdigital micromixers: II. Numerical simulations. *AIChE Journal,* 49(3), pp. 578-584.

Hessel, V., Hardt, S. & Löwe, H., 2004. *Chemical Micro Process Engineering: Fundamentals, Modelling and Reactions.* 1 ed. Weinheim: Wiley-VCH Verlag GmbH & Co. KGaA.

Hessel, V., Hardt, S., Löwe, H. & Schönfeld, F., 2003. Laminar mixing in different interdigital micromixers: I. Experimental characterization. *AIChE Journal,* 16 April, 49(3), pp. 566-577.

Hessel, V., Löwe, H. & Schönfeld, F., 2005. Micromixers—a review on passive and active mixing principles. *Chemical Engineering Science,* April-May, 60(8-9), pp. 2479-2501.

Hossain, S., Ansari, M. A. & Kim, K. Y., 2009. Evaluation of the mixing performance of three passive micromixers. *Chemical Engineering Journal,* 1 August, 150(2-3), pp. 492-501.

Jeon, W. & Shin, C. B., 2009. Design and simulation of passive mixing in microfluidic systems with geometric variations. *Chemical Engineering Journal,* 152(2-3), pp. 575-582.

Kim, D. S., Lee, S. H., Kwon, T. H. & Ahn, C. H., 2005. A serpentine laminating micromixer combining splitting/recombination and advection. *Lab Chip,* Volume 5, pp. 739-747.

Knight, J., 2002. Honey, I shrunk the lab. *Nature*, August, Volume 418.

Kockmann, N., Kiefer, T., Engler, M. & Woias, P., 2006. Convective mixing and chemical reactions in microchannels with high flow rates. *Sensors and Actuators B: Chemical,* 12 October, 117(2), pp. 495-508.

Lee, Y.-K., Deval, J., Tabeling, P. & Chih-ming, H., 2001. *Chaotic mixing in electrokinetically and pressure driven micro flows.* Interlaken, The 14th IEEE International Conference on Micro Electro Mechanical Systems, pp. 483-486.

Le, H. P., 1998. Progress and trends in ink-jet printing technology. *Journal of Imaging Science and Technology,* January, 42(1), pp. 49-62.

Lin, C.-H., Fu, L.-M. & Chien, Y.-S., 2004. Microfluidic T-Form Mixer Utilizing Switching Electroosmotic Flow. *Analytical Chemistry,* 76(18), pp. 5265-5272.

Lintel, H. V., Vandepol, F. & Bouwstra, S., 1988. A Piezoelectric Micropump Based on Micromachining of Silicon. *Sensors and Actuators,* 15(2), pp. 153-167.

Liu, R. et al., 2000. Passive Mixing in Three-Dimensional Serpentine Micro-channel. *Journal of Micro-electromechanical Systems,* Volume 9, pp. 190-197.

Lu, L.-H., Ryu, K. S. & Liu, C., 2002. A magnetic microstirrer and array for microfluidic mixing. *Microelectromechanical Systems, Journal of,* October, 11(5), pp. 462- 469.

Lyklema, J., 1995. *Fundamentals of Interface and Colloid Science: Volume II: Solid-Liquid Interfaces,* Volume 2, p. 3.208.

Manz, A. et al., 1990. Design of An Open-Tubular Column Liquid Chromatograph Using Silicon Chip Technology. *Sensors and Actuators B-Chemical,* January, 1(1-6), pp. 249-255.

Mark, D. et al., 2010. Microfluidic lab-on-a-chip platforms: requirements, characteristics and applications. *Chemical Society Review,* Volume 39, pp. 1153-1182.

Meisel, I. & Ehrhard, P., 2006. Electrically-excited (electroosmotic) flows in microchannels for mixing applications. *European Journal of Mechanics - B/Fluids,* 4 July-August, 25(4), pp. 491-504.

Meisel, I. & Ehrhard, P., 2006. Electrically-excited (electroosmotic) flows in microchannels for mixing applications. *European Journal of Mechanics - B/Fluids,* 25(4), pp. 491-504.

Mengeaud, V., Josserand, J. & Girault, H. H., 2002. Mixing Processes in a Zigzag Microchannel: Finite Element Simulations and Optical Study. *Analytical Chemistry,* 74(16), pp. 4279-4286.

Nguyen, N.-T. & Wu, Z., 2005. Micromixers—a review. *Journal of Micromechanics and Microengineering,* 15(2), p. R1.

Niu, X. & Lee, Y.-K., 2003. Efficient spatial-temporal chaotic mixing in microchannels. *Journal of Micromechanics and Microengineering,* 13(3), p. 454.

Oddy, M. H., Santiago, J. G. & Mikkelsen, J. C., 2001. Electrokinetic Instability Micromixing. *Analytical Chemistry,* 73(24), pp. 5822-5832.

Panta, Y. et al., 2009. Ultrasensitive detection of mercury(II) ions using electrochemical surface plasmon resonance with magnetohydrodynamic convection. *J Colloid Interface Sci,* 15 May, 333(2), pp. 485-90.

Ryu, K. S. et al., 2004. Micro magnetic stir-bar mixer integrated with parylene microfluidic channels. *Lab Chip,* December, 4(6), pp. 608-13.

Sheu, T. S., Chen, S. J. & Chen, J. J., 2012. Mixing of a split and recombine micromixer with tapered curved microchannels. *Chemical Engineering Science,* Volume 71, pp. 321-332.

Shin, S. M., Kang, I. S. & Cho, Y. K., 2005. Mixing enhancement by using electrokinetic instability under time-periodic electric field. *Journal of Micromechanics and Microengineering,* 15(3), p. 455.

Shoji, S., Esashi, M. & Matsuo, T., 1988. Prototype Miniature Blood-Gas Analyzer Fabricated on A Silicon-Wafer. *Sensors and Actuators,* 14(2), pp. 101-107.

Stroock, A. D. et al., 2002. Chaotic Mixer for Microchannels. *Science,* Volume 295, pp. 647-651.

Stroock, A. D., Dertinger, S. K., Whitesides, G. M. & Ajdari, A., 2002. Patterning Flows Using Grooved Surfaces. *Analytical Chemistry,* 74(20), pp. 5306-5312.

Tsai, T.-H., Liou, D.-S., Kuo, L.-S. & Chen, P.-H., 2009. Rapid mixing between ferro-nanofluid and water in a semi-active Y-type micromixer. *Sensors and Actuators A: Physical,* 3 August, 153(2), pp. 267-273.

Vesser, G., 2001. Experimental and theoretical investigation of H2 oxidation in a high-temperature catalytic microreactor. *Chemical Engineering Science,,* February, 56(4), pp. 1265-1273.

Volpert, M., Meinhart, C., Mezic, I. & Dahleh, M., 1999. *An actively controlled micromixer.* New Orleans, American Physical Society, Division of Fluid Dynamics Meeting.

Wang, Y., Suh, Y. K. & Kang, S., 2009. A study on the slip velocity on a pair of asymmetric electrodes for AC-electroosmosis in a microchannel. *Journal of Mechanical Science and Technology,* Volume 23, pp. 874-884.

Wei, X. & Joshi, Y., 2007. Experimental and numerical study of sidewall profile effects on flow and heat transfer inside microchannels. *International Journal of Heat and Mass Transfer,* 50(23-24), pp. 4640-4651.

Whitesides, G. M., 2006. The origins and the future of microfluidics. *Nature*, 27 July, Volume 442.

Wong, S. H., Ward, M. C. & Wharton, C. W., 2004. Micro T-mixer as a rapid mixing micromixer. *Sensors and Actuators B: Chemical,* 15 May, 100(3), pp. 359-379.

www.azonano.com, 2013. *What is Lab-on-a-Chip?*. [Online]
Available at: http://www.azonano.com/article.aspx?ArticleID=3081
[Accessed 1 Feb 2013].

www.thinxxs.com, 2012. *thinxxs.de: thin XXS.* [Online]
Available at: http://www.thinxxs.com/
[Accessed 15 December 2012].

Zhang, Y. T. et al., 2004. *SOI processing of a ring electrokinetic chaotic micromixer.* Boston, Technical Proceedings of the 2004 NSTI Nanotechnology Conference and Trade Show, pp. 292-295.

Zhang, Z. et al., 2008. Focusing-enhanced mixing in microfluidic channels. *Biomicrofluidics,* 2(1), p. 014101.

APPENDIX

A.1 FIGURES FOR PASSIVE MIXING

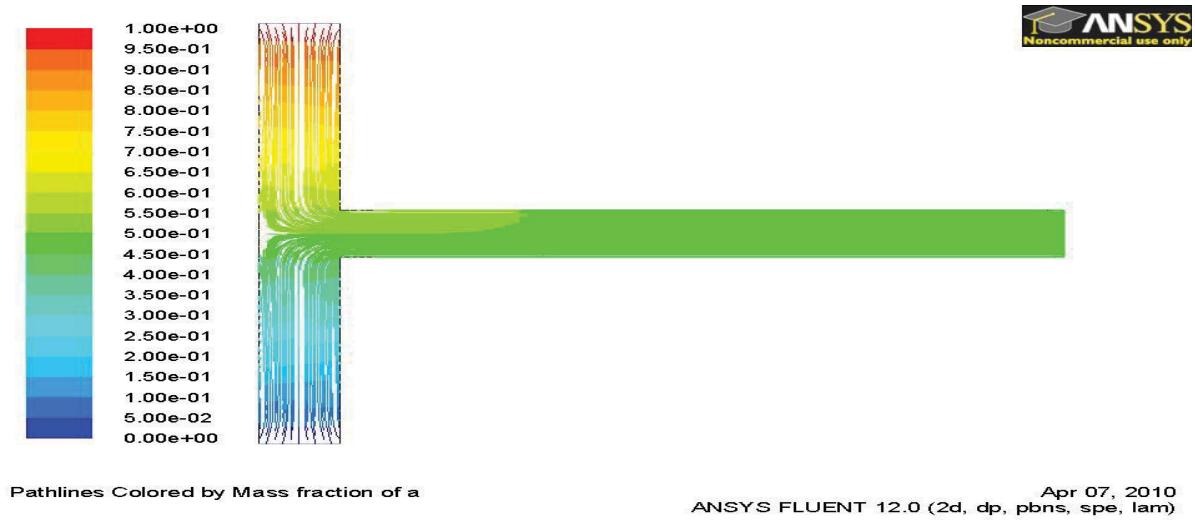

Figure A1.1 Mass fraction of species "a" at 0.001m/s inlet velocities in a T-micromixer

Figure A1.2 Velocity path lines at 0.001m/s inlet velocities in a T-micromixer

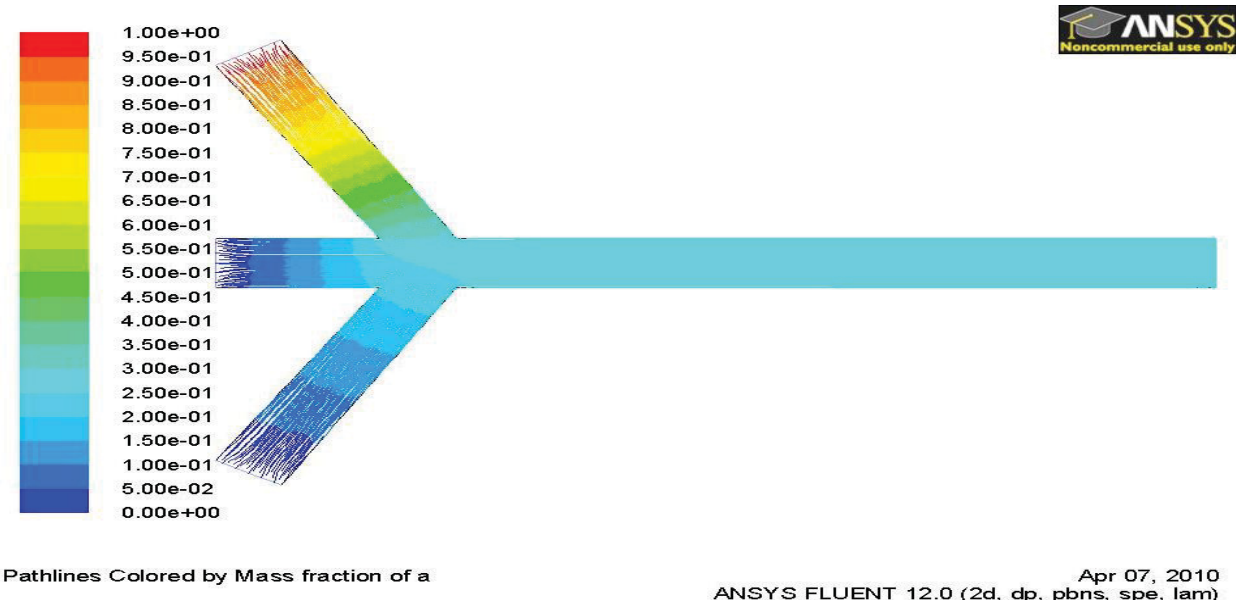

Figure A1.3 Mass fraction of species "a" at 0.001m/s inlet velocities in a Y-micromixer with 3 inlets (Y3).

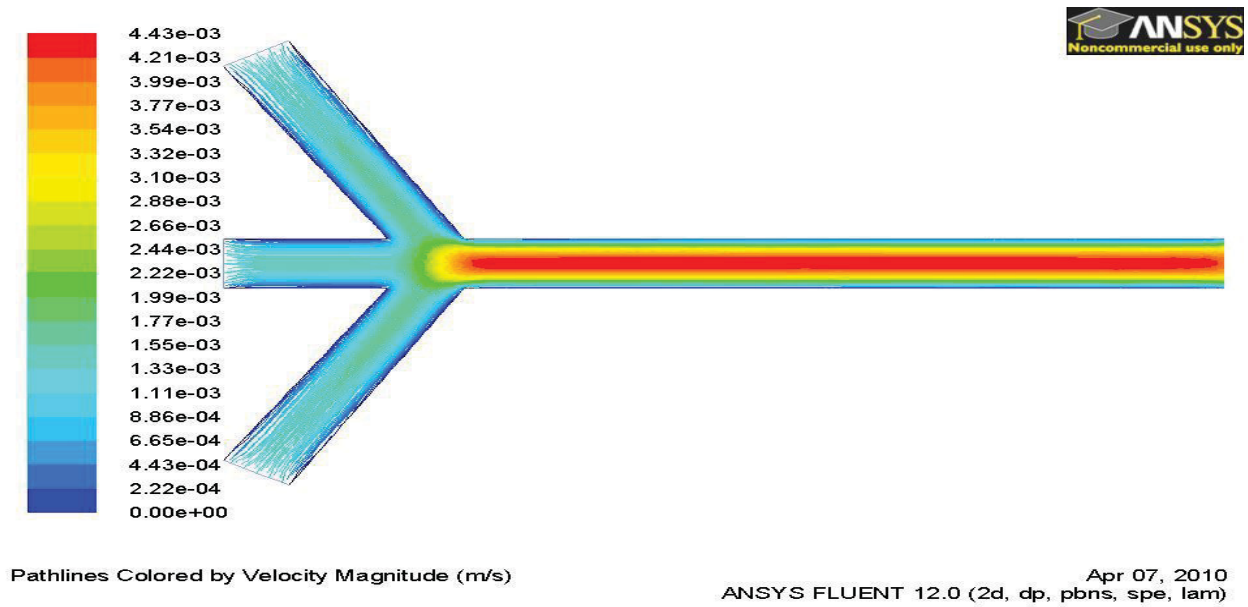

Figure A1.4 Velocity path lines at 0.001 m/s inlet velocities in a Y-micromixer with 3 inlets (Y3)

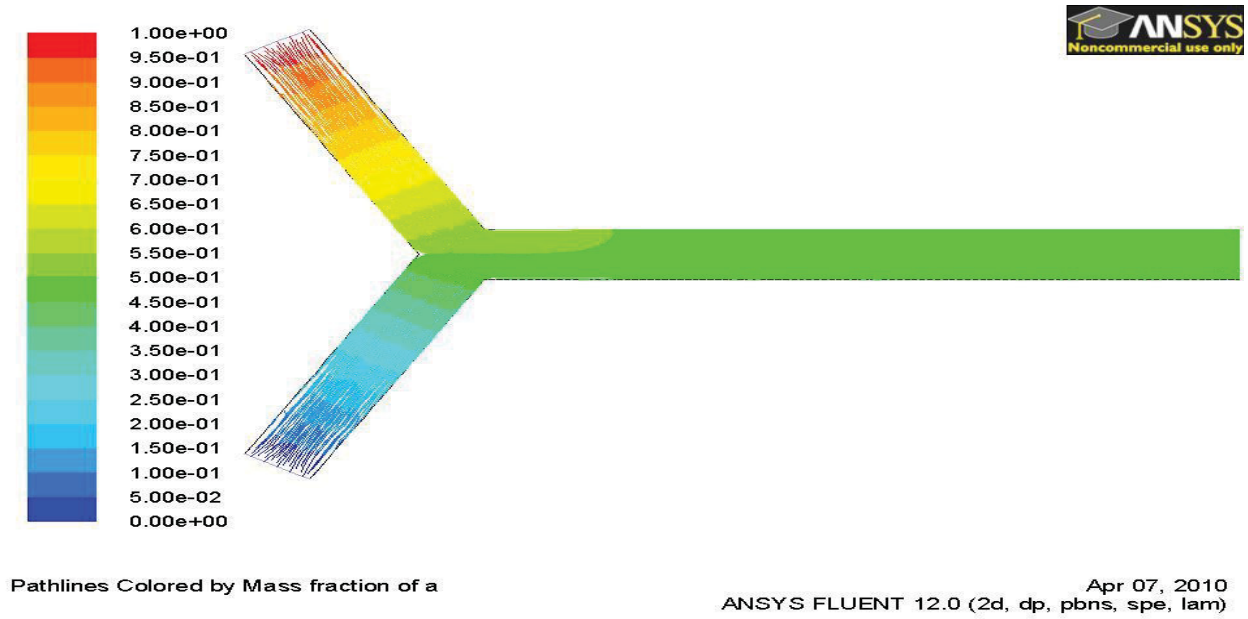

Figure A1.5 Mass fraction of species "a" at 0.01m/s inlet velocities in a Y-micromixer

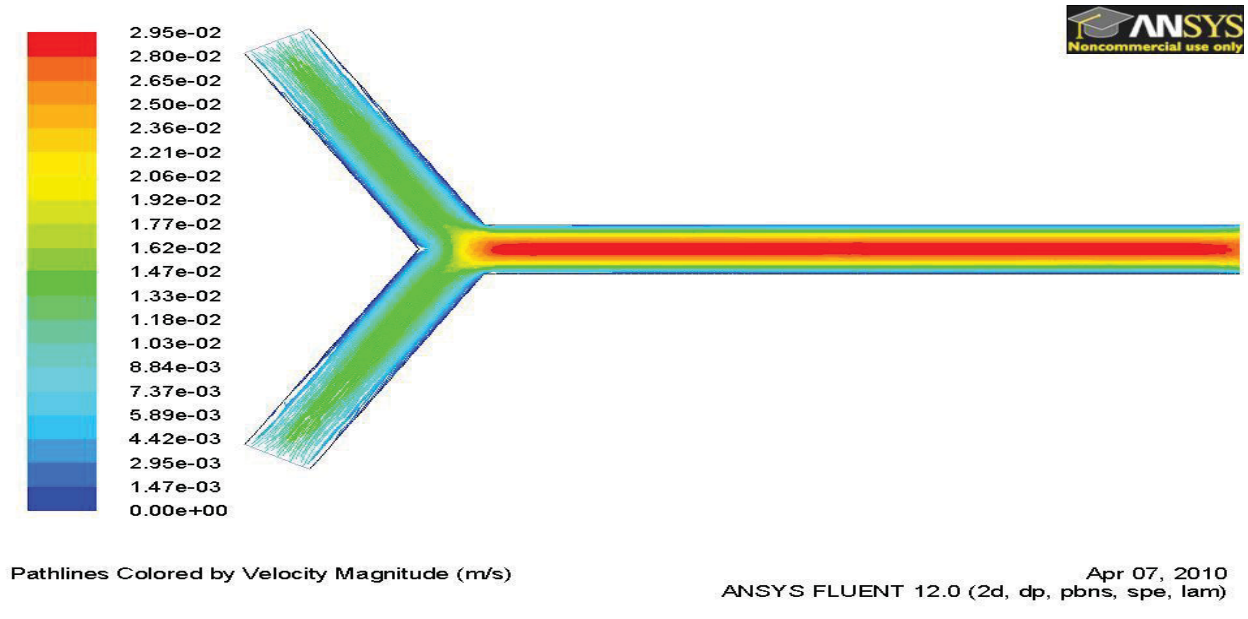

Figure A1.6 Velocity path lines at 0.01 m/s inlet velocities in a Y-micromixer

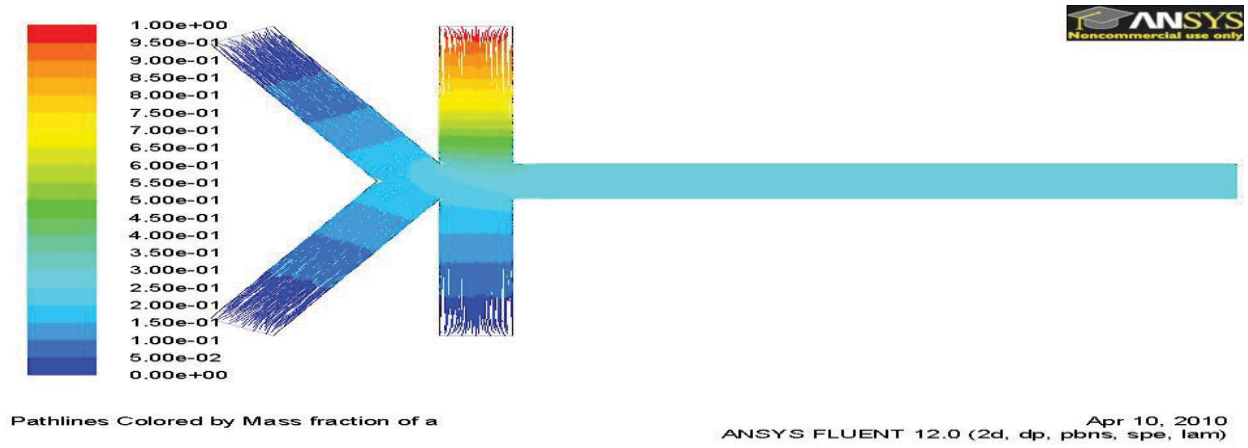

Figure A1.7 Mass fraction of species "a" at 0.1m/s inlet velocities in a Y4-micromixer

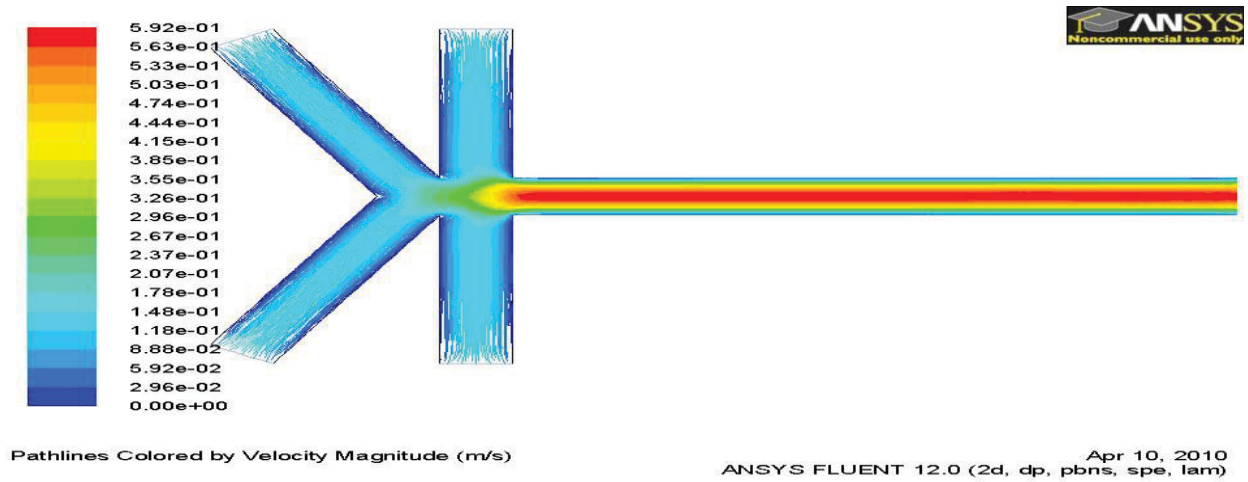

Figure A1.8 Velocity path lines at 0.1 m/s inlet velocities in a Y4-micromixer

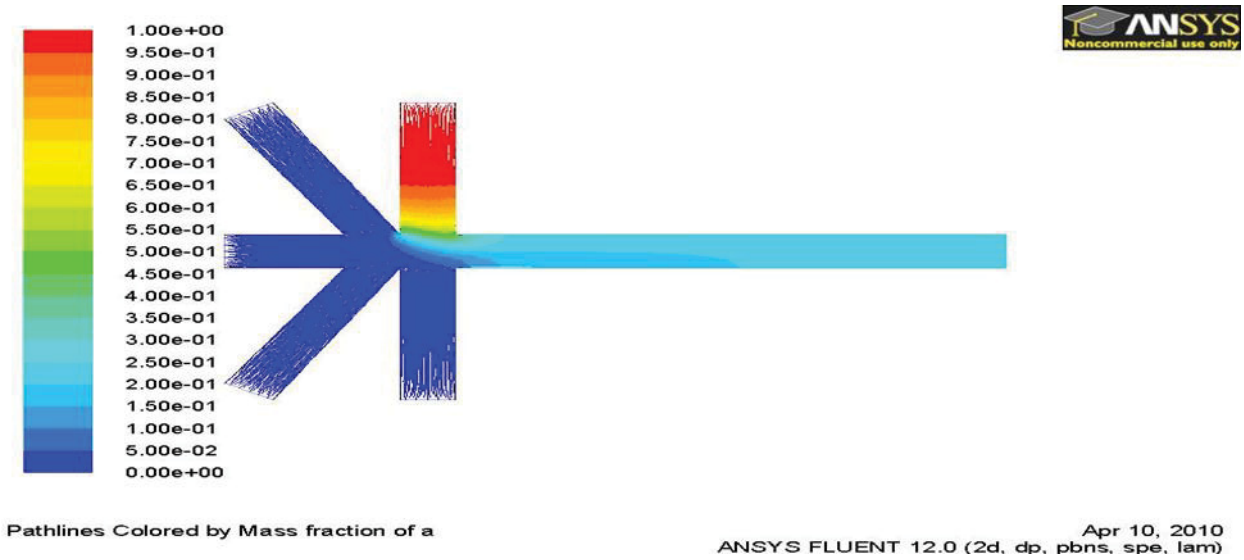

Figure A1.9 Mass fraction of species "a" at 1m/s inlet velocities in a Y5-micromixer

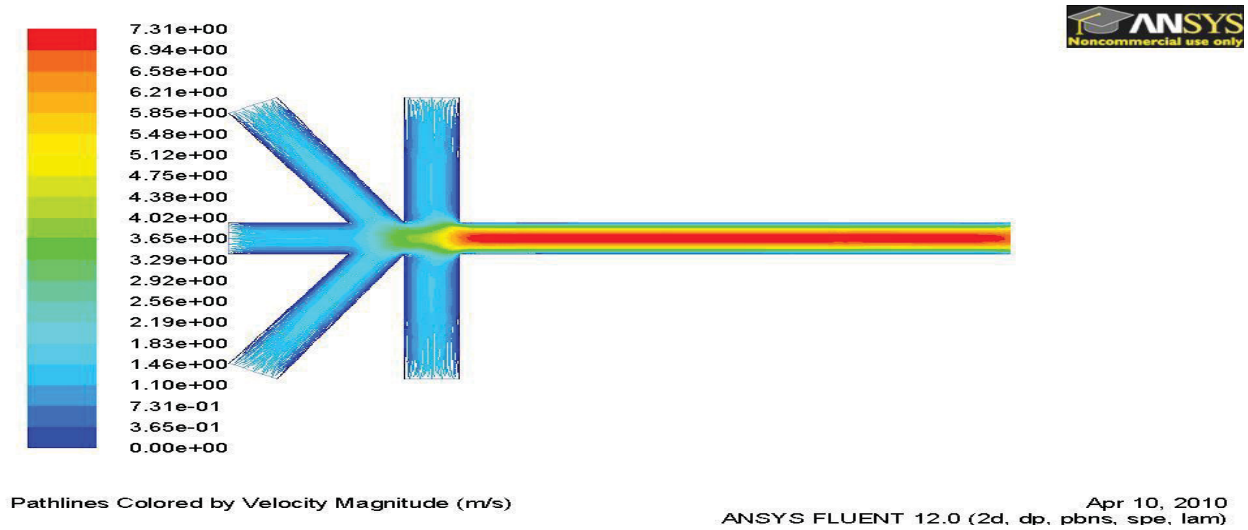

Figure A1.10 Velocity path lines at 1 m/s inlet velocities in a Y5-micromixer

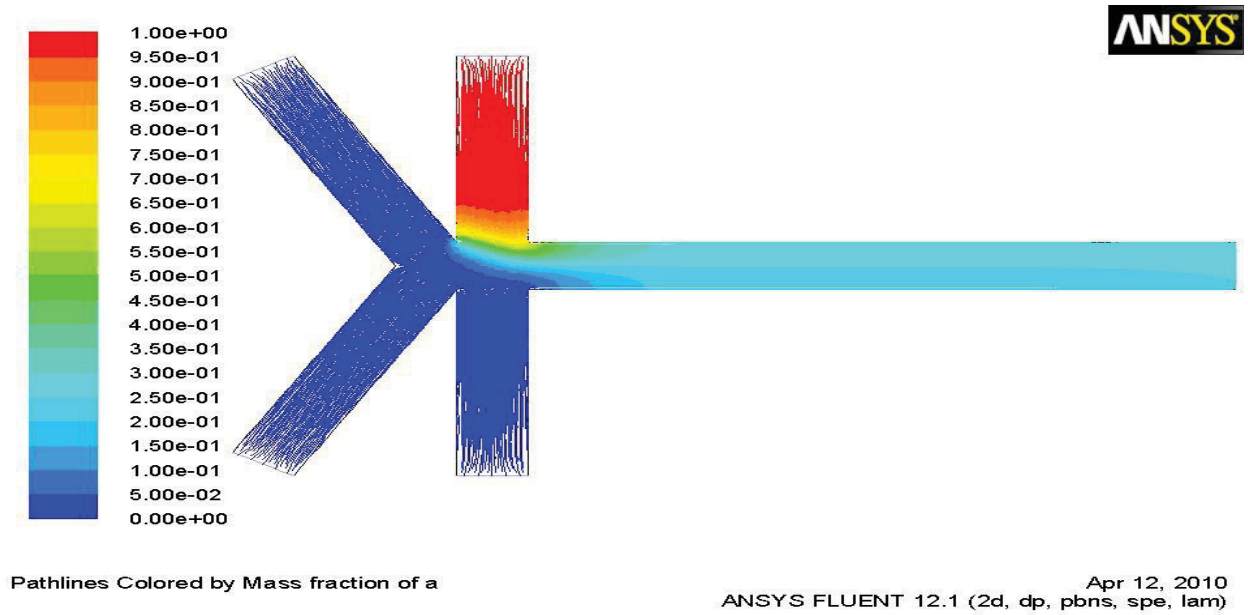

Figure A1.11 Mass fraction of species "a" at 2m/s inlet velocities in a Y4-micromixer

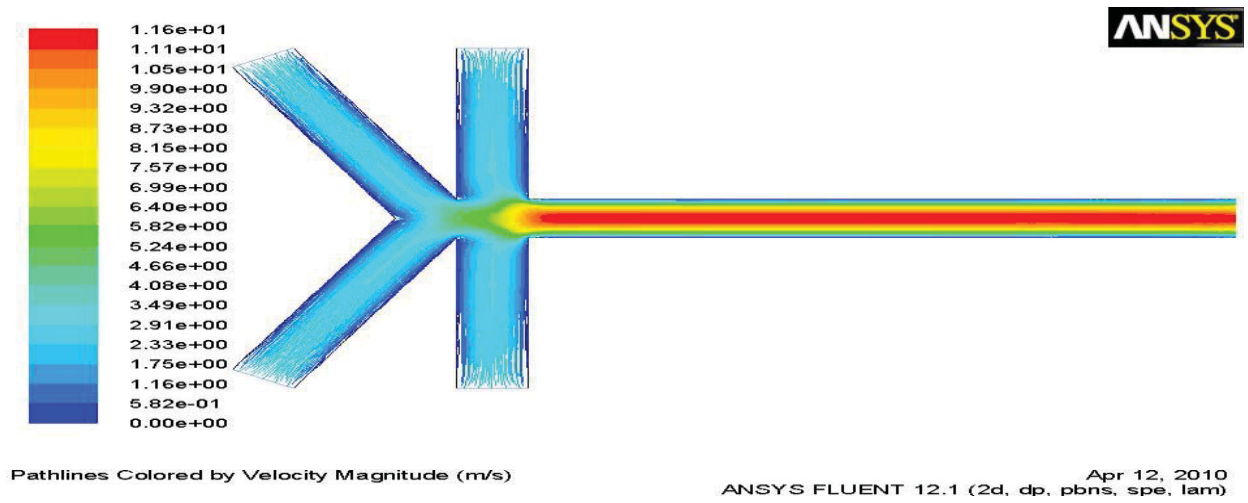

Figure A1.12 Velocity path lines at 2 m/s inlet velocities in a Y4-micromixer

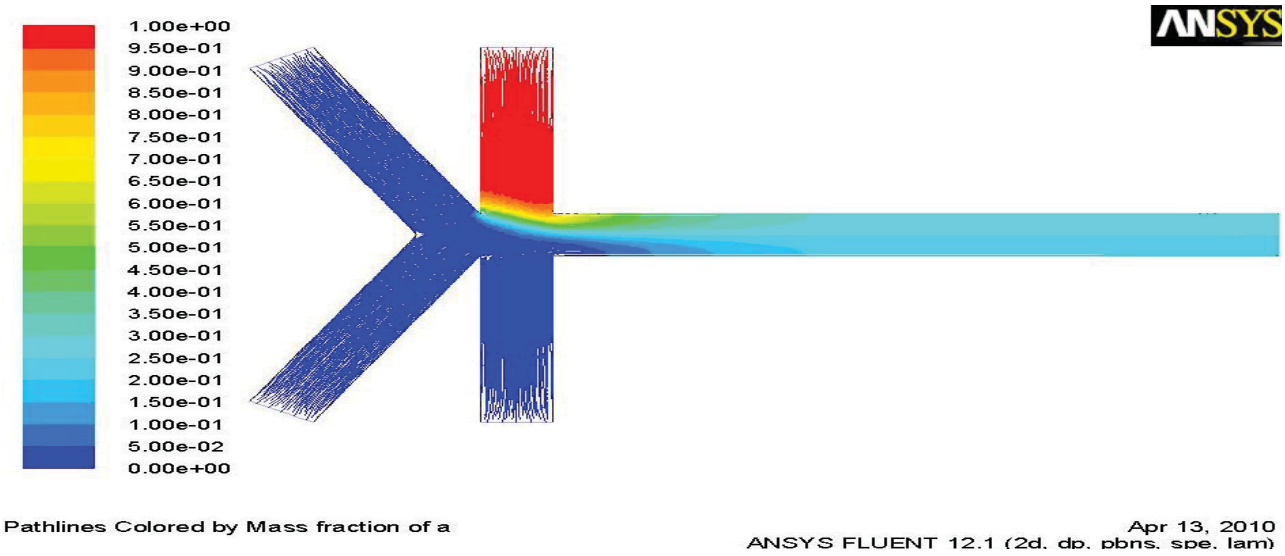

Figure A1.13 Mass fraction of species "a" at 4m/s inlet velocities in a Y4-micromixer

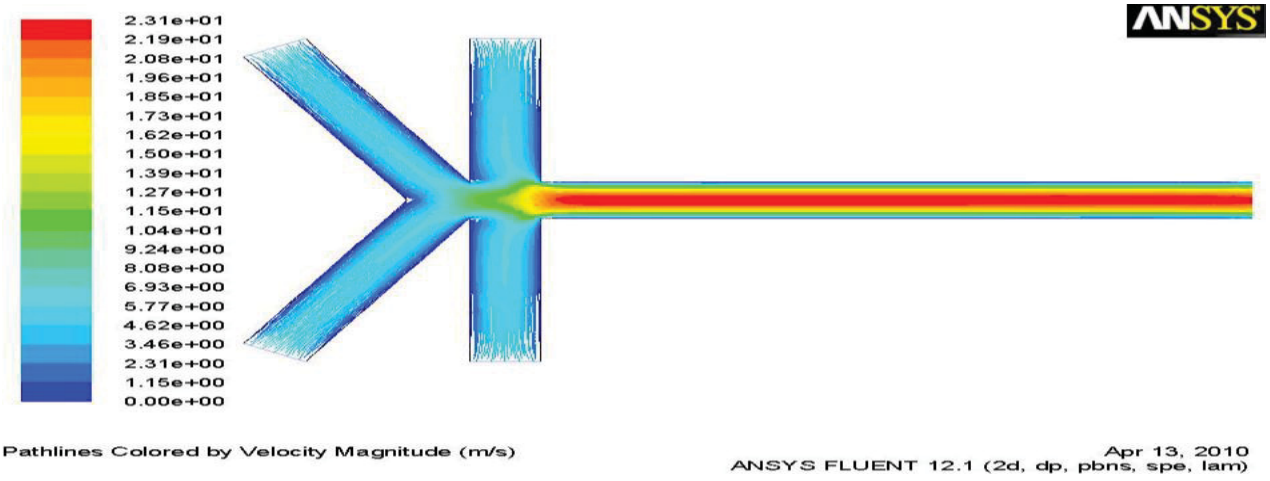

Figure A1.14 Velocity path lines at 4 m/s inlet velocities in a Y4-micromixer

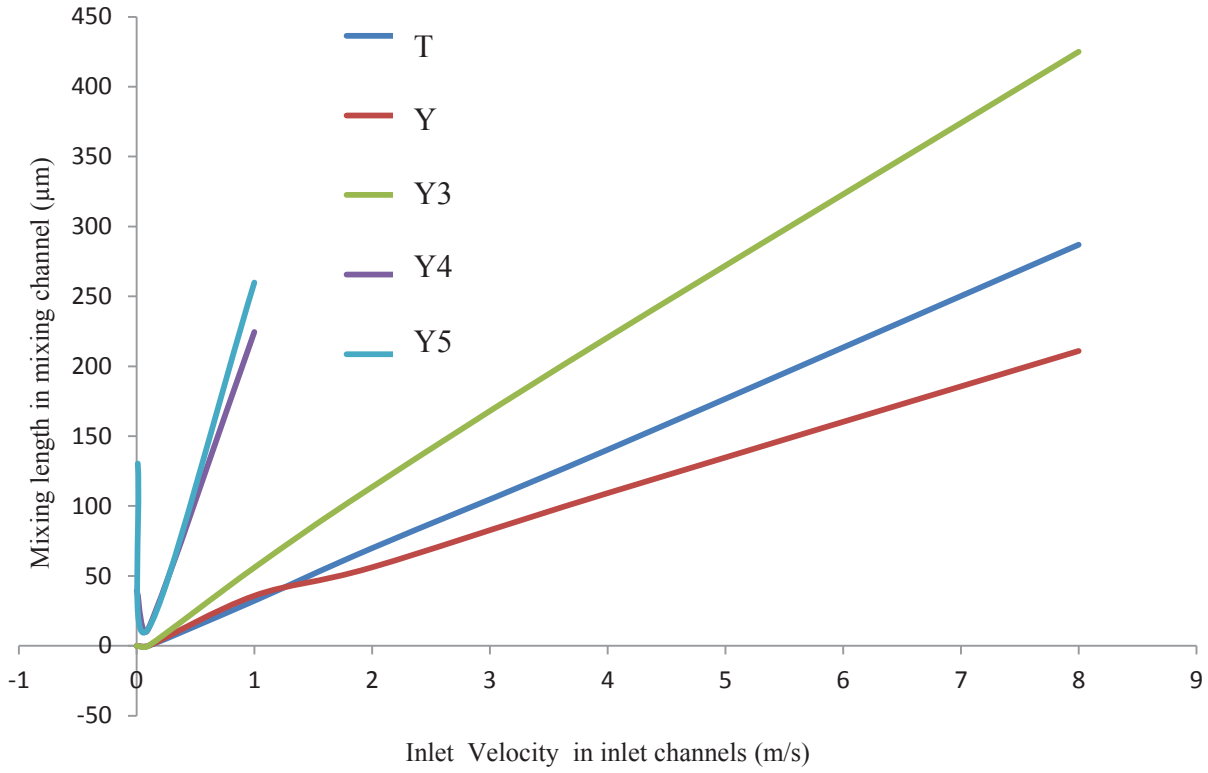

Figure A1.15 Mixing length vs. Inlet velocity in mixing channel

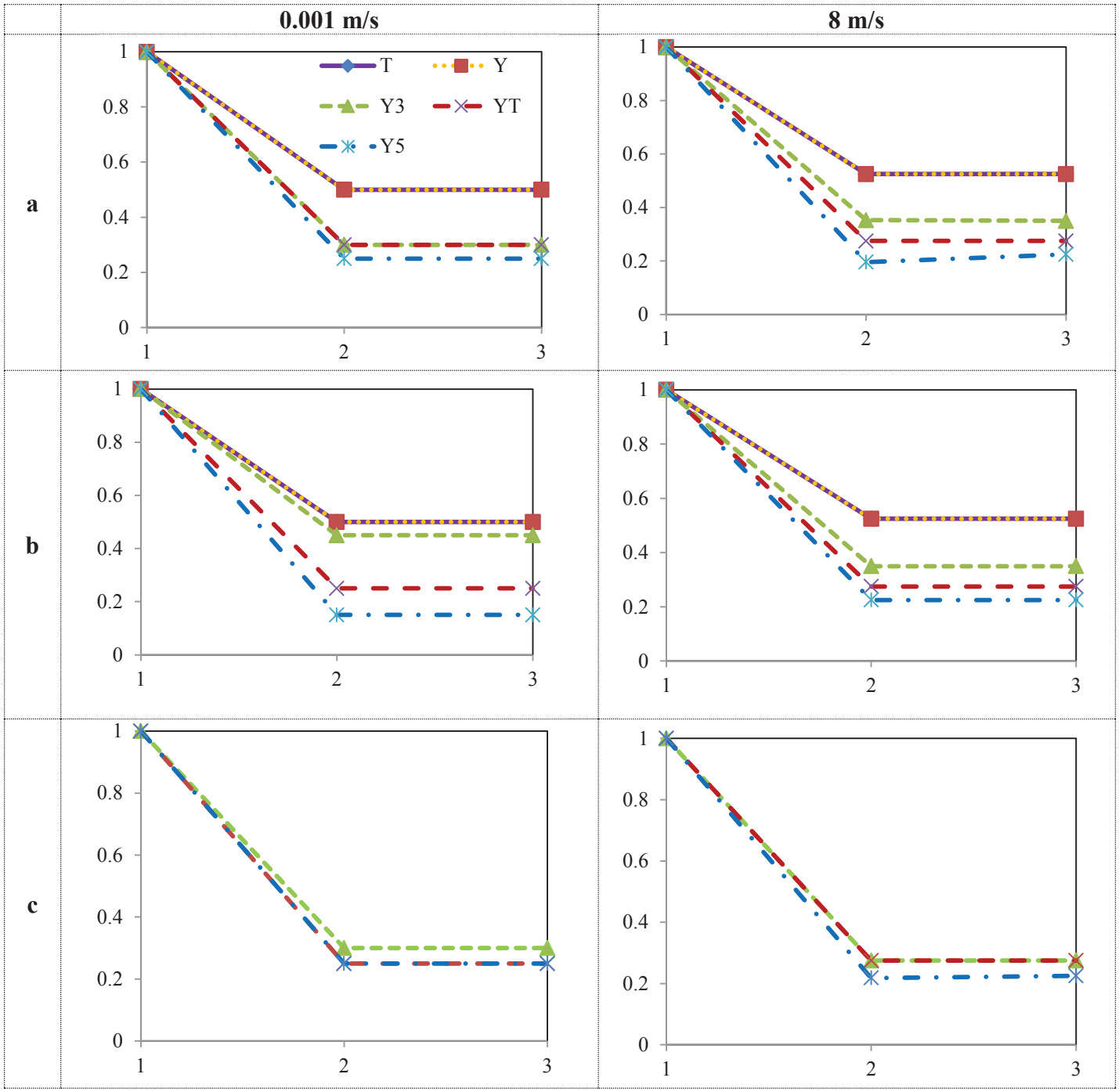

Figure A1.16 Comparison of mixing trend of species (a, b and c) in respective models at 0.001m/s and 8 m/s (Note: Y4 is referred as YT)

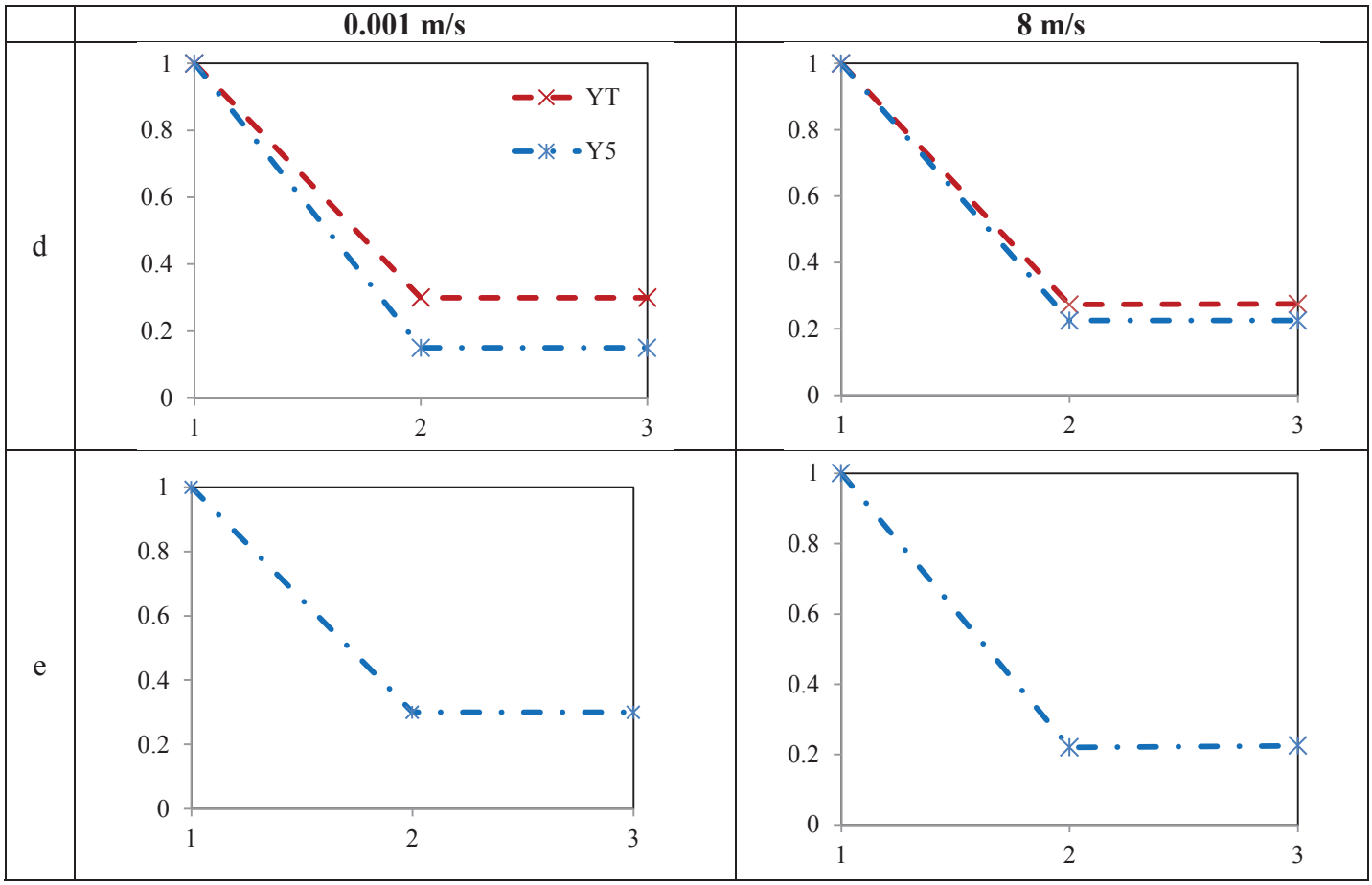

Figure A1.17 Comparison of mixing trend of species (d and e) in respective models at 0.001m/s and 8 m/s (Note: Y4 is referred as YT)

A.2 FIGURES FOR ACTIVE MIXING

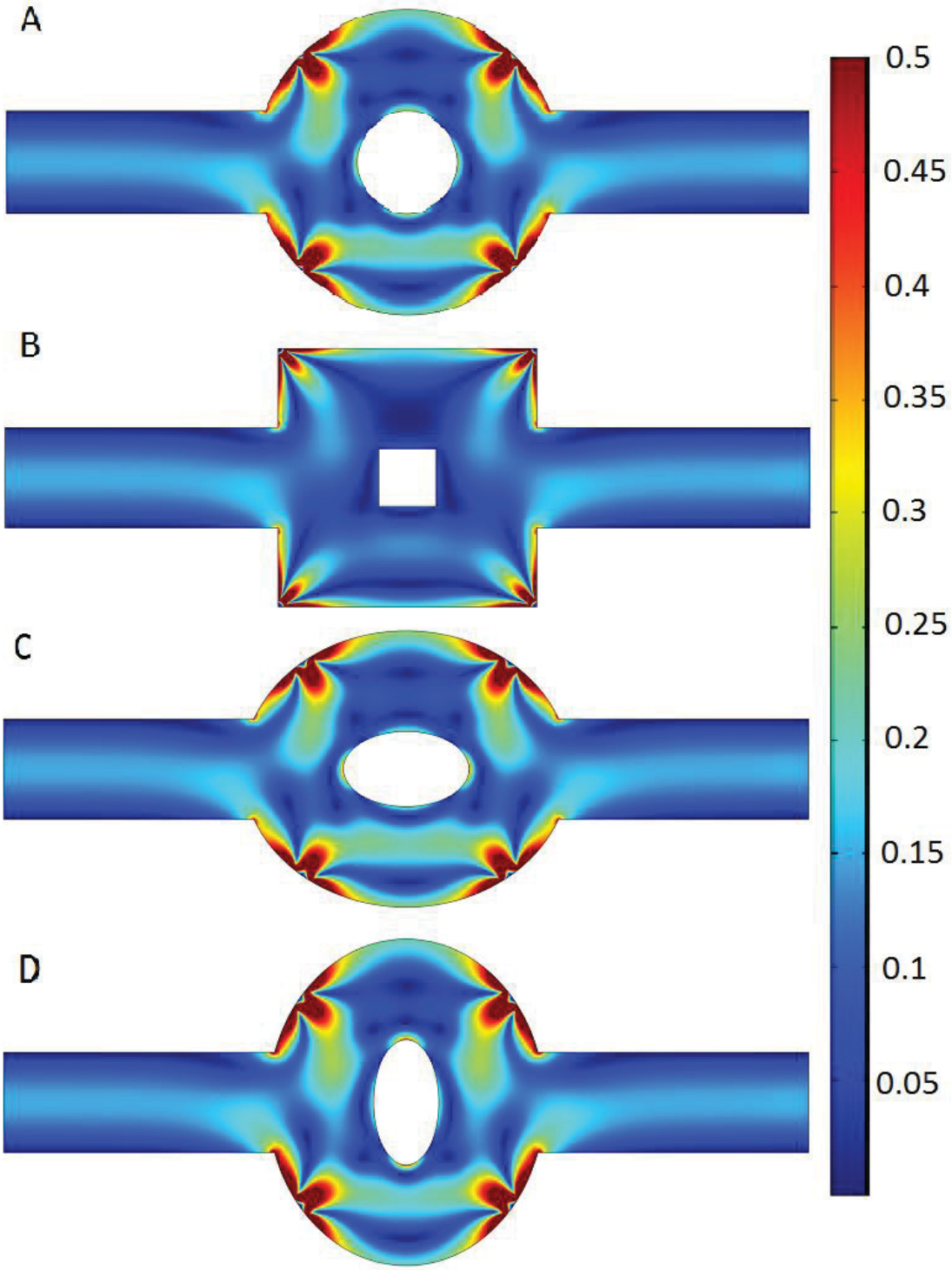

Figure A2.1 Velocity magnitude contours capped at 0.5 mm/s at 0.27 sec

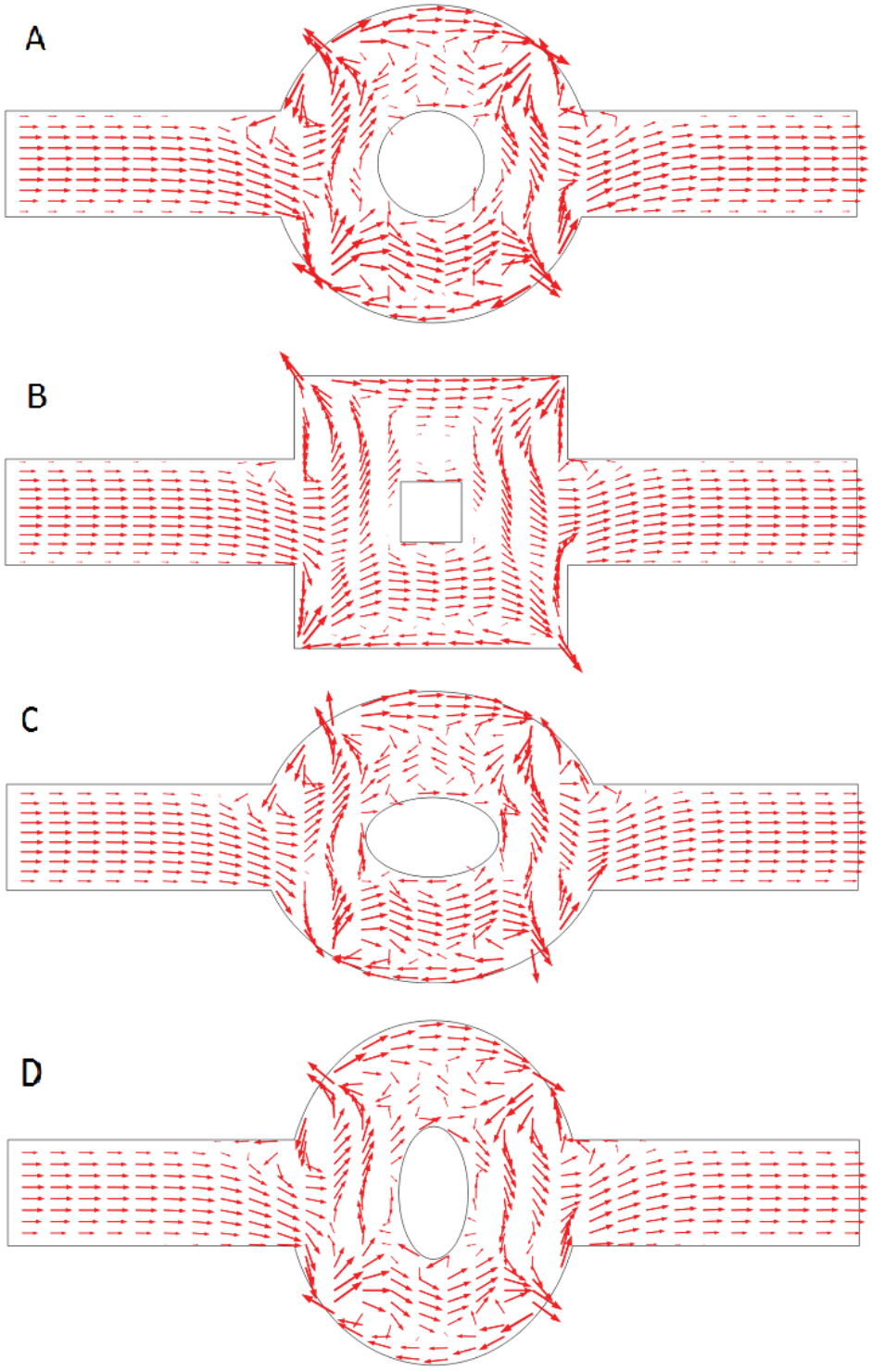

Figure A2.2 Velocity vectors of respective micromixers at 0.27 secs. (Arrow lengths are logarithmically scaled to a range quotient of 100 and scaled to a factor of 3800 for models ‘A &D’ and to a factor of 4500 for models ‘B & C’

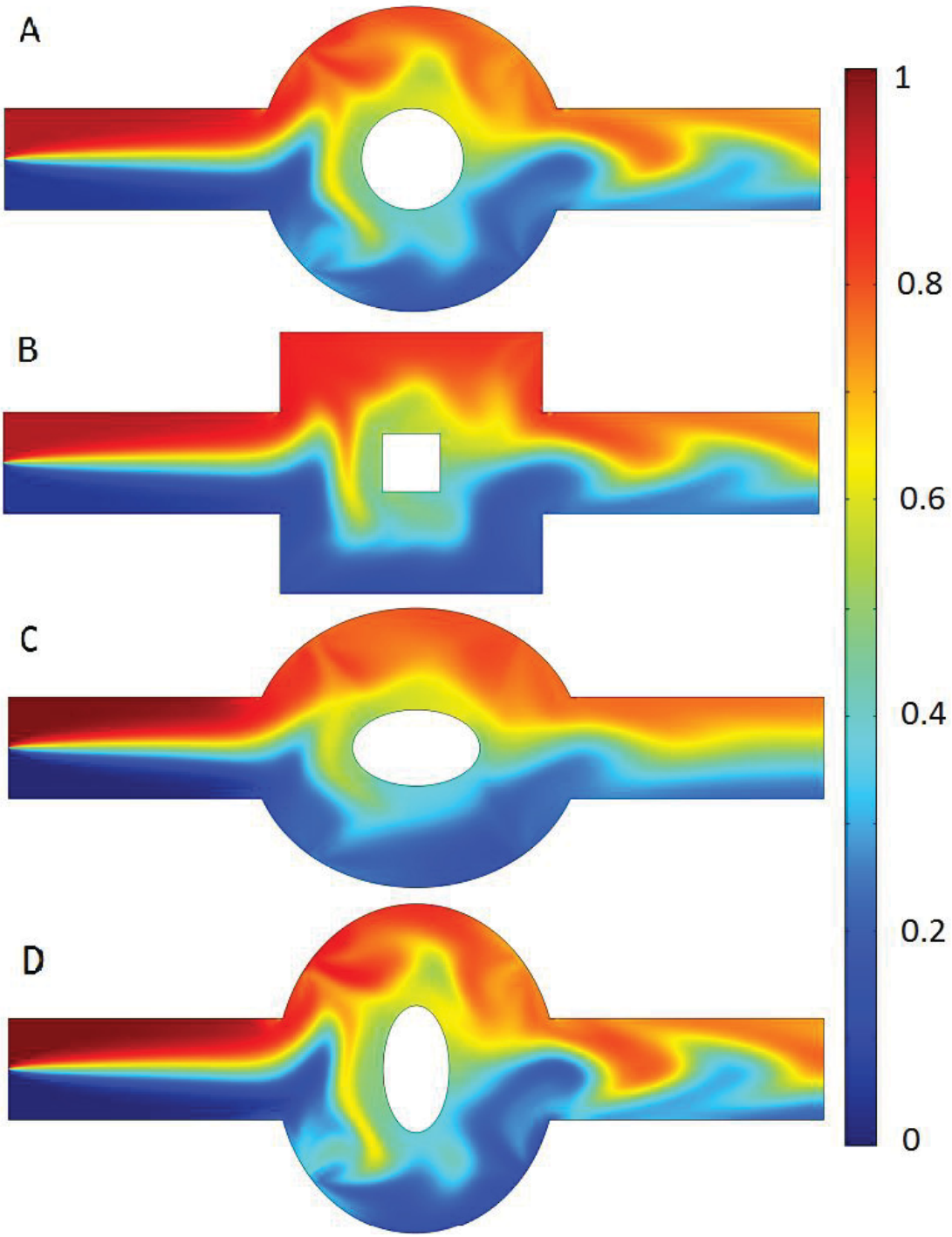

Figure A2.3 Surface Concentration at time 0.27 sec for each model (A = Circular, B= Square, C= Elliptic-I, and D=Elliptic-II)